SYNTHESIS AND SHAPE CONTROL OF FUNCTIONALIZED CADMIUM TELLURIDE NANOPARTICLES

Submitted to the Faculty of Science and Agriculture by

Nhlakanipho Mntungwa

20022499

In fulfilment of the requirement for the award of the degree of

Master of Science

in the Department of Chemistry

University of Zululand

Supervisor: Prof. N. Revaprasadu

Department of Chemistry

University of Zululand

Private bag X1001

KwaDlangezwa

3886

November 2010

DECLARATION STATEMENT

''I hereby declare that the work on the synthesis and shape control of functionalized cadmium telluride nanoparticles is my own work and that all the sources I have quoted have been indicated and acknowledged by means of complete references.''

.....
N. MNTUNGWA (20022499)

TABLE OF CONTENTS

ACKNOWLEDGEMENTS

I want first to thank my supervisor Prof. Neerish Revaprasadu for believing in me before I could do any research at all and allowing me to work in his group. Thank you Prof. for financial support and your forgiveness in all the mistakes I have made. Prof you are the one who gave me research topics for my honours and masters degree and have taught me the basics of nanotechnology, showing me how to prepare presentation slides and to present them. I appreciate you for all that you have taught me in research for all the years I have been postgraduate student.

A special thanks goes to Dr. Rajaserkhar Pullabhotla who have analysed all my samples using the TEM and HRTEM techniques. Dr. Raj has been a friend and mentor since his arrival in the group and has been forgiving. He taught me how to write articles, brought out good ideas in me and I have been able to write this dissertation because of him. More importantly he taught me how to work hard and swiftly without any waste of time. Dr Raj has been different from other researchers that I have met because he was helpful and shared information. Thank you for helping me out in times of confusion where I did not know what to do.

I also thank Prof. Kolawole, Prof. Bola Oyedeji and Mr. Peckham for allowing me to study my honours degree in spite of the challenges I was facing. I thank them for trusting me that I could pass and be promoted to another level in life. Prof. Kolawole thank you for speaking well about me even to the Dean of Students and putting pressure on me by always asking me when am I going to finish writing this

dissertation. I am aware of the situation I put you through with the manangement of the university in 2007, thank you Prof.

I would also like to thank all the staff members and postgraduate students of the department of chemistry at Unizul for being there for me. I thank Dr. Nejo for teaching me how to use the FT-IR, Dr Hlabangani and Dr Segapelo for their support, Sister Lucy for being a good secretary in our group, and the following people who have also made contributions to my work the two Mpumis, Ziningi, Sbu, Norman, Sanjay and Ben.

I thank the most special people in my life for their understanding and allowing me to pursue my goals in life, my family members Gogo Hilda Mntungwa, Gogo waka Mahlaba, My late father and mother, father Bhi, mother Jabulile, Muzi, Sandile, Ntshewu, father Moses and his wife, uncle Mali, cousin Ben, Zimbili, my sister Nomfundo, Nomalungelo, Belo, Zakhele, Ndabenhle, Nomvula, Nhlo, Martin, Bafee, my friend Maqumbane, aunt Ntombi and Babaka Mandoba and manqoba, Busi and Xolani, Mamnyo and Nosipho.

My special thanks to the Pastor of Christ Embassy Zululand, Pastor Pat Dlamini and his wife. Thanks to all the church members, keep up the good work of soul winning.

LIST OF FIGURES

LIST OF SCHEMES

LIST OF ABBREVIATIONS AND SYMBOLS

Chemical reagents

$Cd(CH_3COO)_2$	cadmium acetate
$CdCl_2$	cadmium chloride
$CdCO_3$	cadmium carbonate
$Cd(NO_3)_2$	cadmium nitrate
HDA	hexadecylamine
$NaBH_4$	sodium borohydride
Te	tellurium
TEA	triethanolamine
TOPO	tri-*n*-octylphosphine oxide
TOP	tri-*n*-octylphosphine

Instrumentation

FT-IR	fourier transform infrared
HRTEM	high resolution transmission electron microscopy
PL	photoluminescence
TEM	transmission electron microscopy
UV/Vis	ultra violet visible
XRD	x-ray diffraction

Symbols and constants

a.u.	arbitrary units
d	diameter
e	elementary charge
e^-	electron
E	energy
E_g	band gap
ε	dielectric coefficient
ħ	Planck's constant
h^+	hole
m	effective mass (e = electron, h = hole)
v	frequency
R	radius
FRET	fluorescence resonance energy transfer
CRET	chemiluminescent resonance energy transfer
HRP	horseradish peroxidase
QD	quantum dot
BSA	bovine serum albumin
TGA	thermogravimetric analysis
NPs	nanoparticles

ABSTRACT

The synthesis of organically and water soluble cadmium telluride nanoparticles by a facile hybrid solution high temperature method is presented. This method involves the reaction by the addition of an aqueous suspension or solution of a cadmium salt (chloride, acetate, nitrate or carbonate) to a freshly prepared NaHTe solution. The nanoparticles were prepared by passivating with organic surfactants such as hexadecylamine (HDA) and tri-*n*-octylphosphine oxide (TOPO) for their solubility and stability in organic solvents. To stabilize and make the nanoparticles water soluble, L-cysteine ethyl ester hydrochloride and triethanolamine were used as capping agents. The absorption and photoluminescence spectroscopy, fourier transform infrared spectroscopy, powder X-ray diffraction, transmission electron microscopy and high resolution transmission electron microscopy techniques were used to confirm the quality of the as-synthesized nanoparticles. All measurements were performed without any post preparative size separation of the nanoparticles.

The dissertation comprises of four chapters. The first chapter is a brief description of the properties of nanomaterials and a literature review on some of the principal routes to synthesize nanomaterials. The mechanisms of particle growth and shape control are also discussed. Finally some key applications of CdTe are described.

The second chapter deals with the synthesis of HDA and TOPO-capped CdTe nanoparticles. The reaction parameters such as reaction time, reduction time of tellurium, Cd:Te ratio, reaction temperature and cadmium source were varied to investigate their influence on the optical properties and morphology of the particles.

Details of the absorption features such as excitonic peaks and band edges are presented. The emission properties are also discussed. The morphology of the particles was investigated by electron microscopy and powder X-ray diffraction techniques. It was found that the cadmium source (chloride, carbonate, acetate and nitrate) had a profound effect on the final morphology of the particles. A detailed mechanism for the particle growth is presented.

The synthesis of cysteine and TEA-capped CdTe nanoparticles are described in Chapter three. A systematic study of the effects of the capping group, pH, reaction time and cadmium source was carried out for the water soluble CdTe nanoparticles. The absorption and emission data for the particles are discussed in detail. The electron microscopy images confirm the nanosize and crystalline nature of the particles. In addition fourier transform infrared spectroscopy was used to confirm the capping of the particles by cysteine and TEA. All the cadmium sources were found to be successful in producing high quality water soluble CdTe particles. The final chapter four is a summary of general conclusions of the study.

CHAPTER ONE

GENERAL INTRODUCTION

1.0 *Background*

The term nanotechnology is employed to describe the creation and manipulation of materials with structural features in between those of atoms and bulk materials, with at least one dimension in the nanometer range (1 nm = 10^{-9} m). These materials are often referred to in the literature as quantum dots (QDs), Q-particles, nanoclusters, nanoparticles or artificial atoms [1-4]. At the nanoscale, the fundamental mechanical, electrical, optical and magnetic properties can significantly differ from their bulk material counterparts.

The novel properties of the nanoparticles are unique for various reasons. The first is that their intrinsic physical sizes are comparable to the critical sizes of many important properties of a given class of functional materials, such as the wavelength of the electron wavefunction, and the diameter of photogenerated excitons [5]. The second reason is their large surface-to-volume atom ratio, which considerably alters the chemical potential of the structural units in comparison to that of the corresponding bulk crystals [6]. The strongly size-dependent solubility of nanocrystals is a direct result of this property. The third reason is the size dependence of the structure in the nanometer regime, which includes electron band configuration, surface structure and reconstruction, and crystal structure, etc [7]. The unique catalytic properties of gold nanocrystals [8] can be considered as an example of the third type.

In the last two decades, research in nanotechnology has grown tremendously with over three hundred thousand publications in the field of nanoscience [9]. The availability of new strategies for the synthesis of nanomaterials and new tools for

characterization and manipulation has fuelled this growth. There are many examples to demonstrate the current achievements in this area. Several methods of synthesizing nanoparticles, nanowires, nanotubes and their assemblies have been reported [10]. Spectroscopic tools, electron microscopy and diffraction methods have been established and scanning probe microscopies have provided powerful tools for studying nanostructures. New methods of fabrication of patterned nanostructures as well as new devices and production concepts are constantly being discovered [11].

1.1 *Electronic and luminescence properties*

1.1.1 *Electronic properties*

The size of the nanoparticles is important in relation to the excitonic radius (electron-hole pair) of the bulk material. The optical spectra of many semiconductor nanocrystals show a blue shift in the absorption edge as the particle size decreases [3,6,7]. Charge carriers in the nanoparticles are confined in three dimensions and as the size of the nanoparticle become comparable to the excitonic radius the quantum size effects occurs. The electron-hole pair is such that the coulomb interaction between electron and hole cannot be neglected and they assume a state of higher kinetic energy than in the bulk solid [1]. This effect causes the continuous band of the solid to split into discrete quantized levels and the band gap to increase (Figure 1.1).

Where E represents energy; charge carriers are h^+, which represents a hole; and e^- which represents an electron, *hv* represents a photon of energy and E_g represents the band gap of the semiconductor.

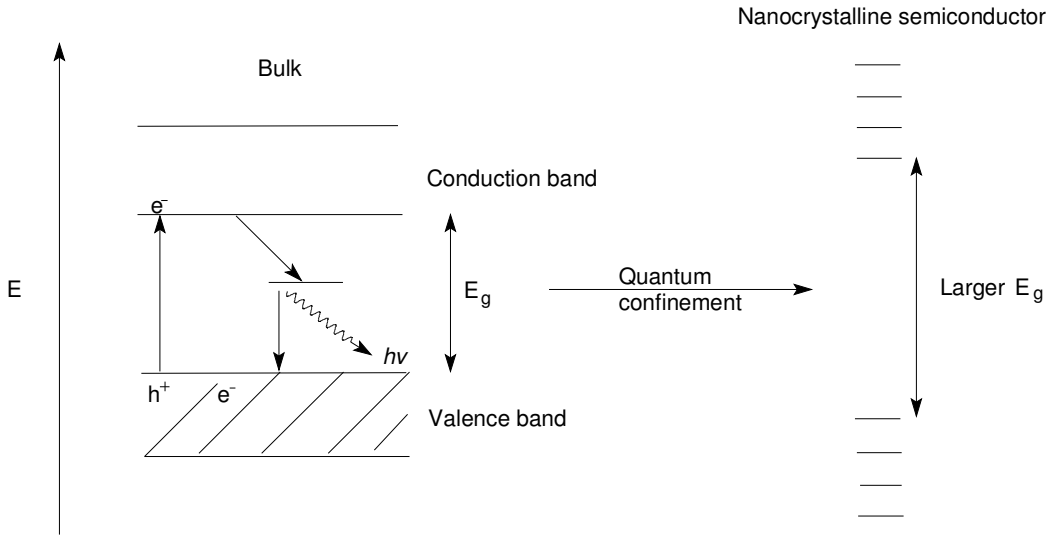

Figure 1.1 Diagram showing the increase in energy and evolution of discrete energy levels in nanocrystalline semiconductors [7].

Brus [5,12] developed the energy levels of the first excited state by considering the coulombic interactions and polarization terms. The size-dependent shifts with respect to the bulk band gap energy (E_g) were approximated by the following equation (1.1).

$$\triangle E = \frac{\hbar^2 \pi^2}{2\,R^2}\left[\frac{1}{m_e} + \frac{1}{m_h}\right] - \frac{1.786\,e^2}{\varepsilon\,R} - 0.248\,E^*_{Ry} \qquad \text{..... (1.1)}$$

Where m_e and m_h are the effective mass of the electron and the hole respectively, ħ represents the Planck's constant, E^*_{Ry} represents the effective Rydberg energy, ε represents the bulk optical dielectric constant, e represents the elementary charge and R represents the radius of the spherical crystallite. From the above equation (1.1), the energy spacing between the quantized levels is inversely proportional to the effective mass and the square of the particle radius. The values used for the effective mass and

dielectric constants were those of macrocrystalline solids and could vary for smaller particles. Even though the model deviates for smaller particles, it is found useful in determining the energy shift for nanocrystalline semiconductors [7]. In addition to a blue shift in the absorption edge, the presence of a peak often described as excitonic is taken as evidence for quantum confinement, i.e. the spectrum starts to resemble a molecule with discrete absorption rather than a solid with continuous bands.

1.1.2 *Luminescence properties*

The general mechanism of luminescence in semiconductors is illustrated in Figure 1.2. When a photon of energy higher than the band gap of the material is absorbed, an electron-hole pair is created. On a very short timescale the energy is thermalized so that the energy separation between the electron and the hole becomes approximately equal to the energy of the gap. Then the pair can radiatively recombine, giving rise to the emission of a photon (luminescence) [13]. As a result, the peak position of the photoluminescence roughly reflects the band gap of the material. In general, the yield of photoluminescence is governed by competition between radiative and non-radiative recombination. The sources of non-radiative recombination are defects in the material (e.g. impurities and disorder sites in a crystal or dangling bonds on the surface). Therefore, the defects are said to quench the photoluminescence [14].

When the size is reduced to the nanometer scale the probability of non-radiative recombination decreases (if we assume that the density of defects remains constant). This is because the probability for the carriers to find a defect in the core is getting smaller. On the other hand, the number of surface atoms relative to the number of volume atoms increases with decreasing particle size [16]. As a result, the problem of

dangling bonds becomes more pronounced for nanoparticles. Since the dangling bonds represent traps for the carriers, the surfaces of nanoparticles must be completely passivated to avoid quenching the photoluminescence. For CdSe nanoparticles this can be achieved by passivating with organic ligands such as tri-*n*-octylphosphine oxide (TOPO), inorganic phases and/or oxidation of surface molecules [7]. In any case, it should be stressed here that non-passivated CdSe nanoparticles will not exhibit photoluminescence (PL).

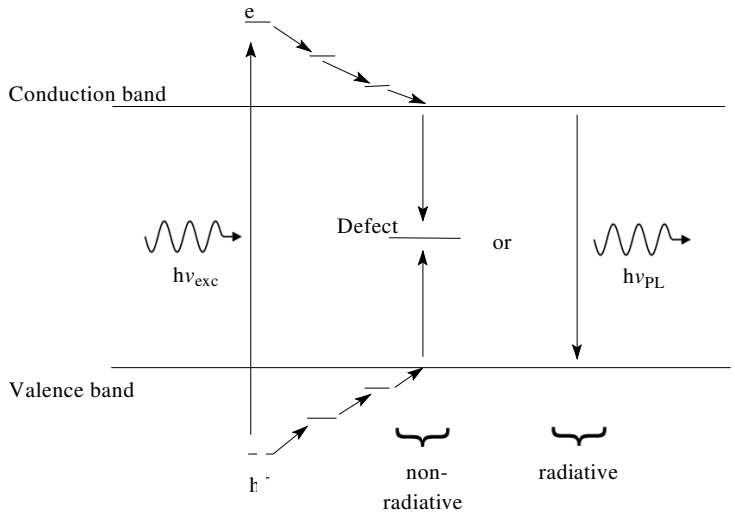

Figure 1.2 Diagram showing luminescence in semiconductors [15].

Another consequence of the spatial confinement of the electronic wave function in nanosized systems is the progressive widening of the band gap as the particle size is reduced. Theoretical studies have shown that, e.g. for CdSe nanoparticles, the band gap increases from 1.7 eV (deep red) to 2.4 eV (green) when the diameter is reduced from 200 to 20 Å [17]. As a result the peaks of photoluminescence spectra of these particles are expected to vary from 602 to 427 nm, respectively. Thus it appears that a single material with well-defined internal structure can give rise to a pronounced spectral variation when the size is changed within a certain range.

Since the radiative recombination takes place between states near the edges of the bands, one of the factors determining the width of the PL curve is the variation of the band gap inside a given sample. As a result the crystals have rather sharp PL response, while amorphous materials exhibit much broader PL bands since they have a distribution of gaps [18]. Thus, it follows that in amorphous materials only those locations can contribute to the PL where the gap is smaller than the energy of the exciting photon. Therefore, it is very important to measure the PL spectra with exciting photons of sufficiently high energy. When the excitation is made with photons that are too low in energy, the PL spectra may not be representative of the material.

1.2 *Preparation methods*

Several synthetic methods for the preparation of semiconductor nanoparticles have been reported [1,7,19]. Colloidal and organometallic routes are the two principal methods in use. An ideal synthetic route should produce nanoparticles that are pure, crystalline, reasonably monodispersed and have a surface which is independently derivatized.

1.2.1 *Colloidal routes*

The colloidal access to nanoparticles is achieved by carrying out a precipitation reaction in a homogenous solution in the presence of stabilizers, whose role is to prevent agglomeration and further growth. Jonson and La Mer [20] explained the synthesis of highly monodispersed colloids by suggesting that if seeds (nuclei) could be made to grow in concert into larger particles, monodispersed sols could be formed. If the nucleation and growth processes were properly controlled, particles with

nanosize dimensions could be reproducibly synthesized. In this process, known as Ostwald ripening, small crystals, which are less stable, dissolve and then recrystallize on larger and more stable crystals. For this method to be effective, the nanoparticles must have low solubility, which can be achieved by the judicious choice of solvents, pH, and passivating agents. Highly monodispersed nanocrystals are obtained if nucleation and growth processes are distinctly separated (i.e., fast nucleation and slow growth) [20]. The colloidal growth stability of the crystals can be improved by using solvents with low dielectric constants or by using stabilizers such as styrene/maleic acid copolymer.

The colloidal method have been used by Brus and co-workers in their studies on CdS and ZnS [21,22], which have led to the tremendous interest in solid samples of semiconductors which show quantum confinement effects. They prepared CdS nanoparticles by a process involving the controlled nucleation of CdS in dilute aqueous solutions of cadmium sulphate and ammonium sulphide. The dynamic equilibrium between solvated ions and solid CdS in acetonitrile as a solvent in the presence of a styrene or maleic anhydride copolymer allowed the preparation of stable CdS nanoparticles, with an average size of 3.4 nm or 4.3 nm, respectively. ZnS and CdS nanocrystallites have also been synthesized from aqueous and methanolic solutions without an organic capping agent [22]. The repulsion of the electrostatic double layer prevented agglomeration and/or sedimentation.

Henglein [4] and Weller [23] made significant progress using CdS colloids prepared by controlled precipitation methods [24-26]. The analysis of the size distribution revealed that a certain size with the greatest oscillator strength was favoured, which

corresponds to the optical transition in the absorption spectrum. This was attributed to the existence of magic agglomeration numbers in the size distribution of the sample. Magic agglomeration numbers, integral multiples N of a large number m_0, arise due to the stability of particles with a certain size or as a result of the kinetics of particle growth. The fast precipitation of the colloids renders a primary size distribution of small particles, peaking at an initial size m_0 (Equation 1.2).

$$m_0Cd^{2+} + m_0S^{2-} \rightarrow (CdS)\ m_0 \quad \text{(1.2)}$$

Growth, via Ostwald ripening, occurs with the initial size (m_0) and is preserved in the form of integer multiples as shown in equations 1.3 and 1.4.

$$(CdS)\ m_0 \rightarrow (CdS)\ m_{0\text{-}l} + Cd^{2+} + S^{2-} \quad \text{(1.3)}$$

$$(CdS)\ m_0 + Cd^{2+} + S^{2-} \rightarrow (CdS)\ m_{0\text{-}l} \quad \text{(1.4)}$$

However, to obtain highly monodispersed nanoparticles, post-preparative separation techniques, such as size exclusion chromatography [21] and gel electrophoresis, have been employed [27]. Gel electrophoresis was found to be superior to the other separation techniques because it is fast and efficient in producing highly monodispersed colloidal nanoparticles.

Hassan and Ali [28] reported a simple route to CdS and ZnS nanoparticles and their respective core/shell nanostructures in aqueous solution containing polyethyleneimine (PEI), a hyperbranched polymer, using cost effective starting materials ($CdCl_2$ or $ZnCl_2$ and Na_2S solutions). The reaction produced homogenous CdS and ZnS

nanoparticles with the sizes of about 7-53 and 4-17 nm respectively, on using different proportions of PEI. The hyperbranched polymer proved to be a suitable capping agent and/or surfactant for the synthesis of nanoparticles of these metal sulfides.

Oluwafemi *et al*. [29] reported a facile one-pot synthetic route to highly water dispersible and potentially biocompatible monodispersed cysteine-capped CdSe nanoparticles. This route involves the reaction of Se powder with $NaBH_4$ to produce Se^{2-} ions, followed by addition of $CdCl_2$ and L-cysteine ethyl ester hydrochloride. The absorption spectra of the nanoparticles exhibit a blue shift in relation to the bulk CdSe, whereas the emission spectrum shows a relatively broad emission peak in the blue region. The resultant nanoparticles were predominantly of the hexagonal phase of CdSe. Using the same synthetic scheme and by tuning the Cd:Se molar ratio Oluwafemi [30] also produced dots and elongated CdSe nanostructures at room temperature using starch as a capping agent. XRD results demonstrated that the nanocrystals have a wurtzite structure regardless of their size and shape. The elongated particles are formed by self-reorganisation occurring via adhesion between the spherical nanoparticles as a result of dipole–dipole interactions.

Pullabhotla and Revaprasadu [31] have extended this work for the synthesis of Au-CdSe hybrid core-shell particles. Very briefly, a solution of $HAuCl_4$, Se powder, and $NaBH_4$ were simultaneously mixed, followed by addition of $CdCl_2$ solution. The absorption spectrum of the hybrid particles displays unique excitonic features that vary from CdSe and Au. The XRD pattern shows peaks attributed to both parent materials.

Singh and Chauhan [32] produced CdS semiconductor QD's in aqueous solution containing $CdSO_4$, $Na_2S_2O_3$ and thioglycerol as the capping agent by using chemical precipitation method. In this method, the pH was adjusted to 7 by adding NH_4OH followed by heat treatment at 50 ^oC. The synthesized CdS nanoparticles have a mixture of cubical and hexagonal crystal symmetry with particle size of 12 nm. PL spectrum exhibits peaks centered at 485 and 515 nm because of band-edge emission and interstitial sulphur sites.

Shang *et al*. [33] reported a new and simple method for creating stable water soluble CdSe QDs by replacing the oleic acid chains on the CdSe QDs with highly water-soluble triethanolamine (TEA). Based on the quenching of fluorescence signals of the functionalized CdSe QDs, a simple and specific method for the reciprocal recognition of mercury (II) and /or iodine (I) ions was proposed with wide linear range, low detection limits and good precision. Meanwhile, the results show that QD systems can be designed as specific sensors for not only various ions but also ionic pairs if functionalized with appropriate ligands as the general organic receptors acted [34].

Very recently colloidal CdS QDs have been synthesized in a low-temperature 3-component synthetic route affording the growth of particles with sizes varying from 3.4 nm to 8.4 nm [35]. Cetyltrimethylammonium bromide (CTAB) acted as a surfactant with Na_2S and $CdCl_2$ as aqueous precursors. Increasing the reaction time and temperature leads to kinetically-controlled growth. The growth kinetics was found to follow a diffusion-controlled process at the initial stage, then shifts to a surface-controlled incorporation of reactants to the crystallite after the particle size becomes comparable to the exciton Bohr radius.

The colloidal route is an efficient one for the preparation of nanosized semiconductor particles. However, certain types of semiconductors such as CdSe, GaAs, InP and InAs cannot be synthesized easily via this route. Annealing of the colloidal particles is not possible as these tend to be low temperature processes. The nanoparticles prepared by the colloidal route are not sufficiently stable at higher temperature and thus makes annealing of the particle difficult, thereby making the material poorly crystalline. As a result of these difficulties, many studies reported to date have also dealt with the exploration of synthetic strategies via the organometallic route.

1.2.2 *Organometallic routes*

The problems associated with the low-temperature colloidal route could be overcome by injecting precursors that undergo pyrolysis at high temperature into a high boiling point coordinating solvent. The routine synthesis of well-defined semiconductor nanocrystals was opened up in a landmark paper by Murray *et al.* [36]. The solutions of dimethylcadmium $(CH_3)_2Cd$ (in tri-*n*-octylphosphine, TOP and tri-*n*-octylphosphine chalcogenide, TOPX, X = Se, S and Te) were reacted in hot tri-*n*-octylphosphine oxide (TOPO) in the temperature range (120-300 ^oC). This reaction produced TOPO-capped nanocrystallites of CdX. Nucleation of the CdSe nanoparticles was achieved by the sudden introduction of the concentrated reagents resulting in the abrupt supersaturation and formation of nuclei, followed by slower growth and annealing, consistent with an Ostwald ripening process. The nanoparticles were passivated by a monolayer of the solvent ligand and hence could be isolated/purified by solvent/non-solvent interactions. Purified nanocrystals undergo size selective precipitation to provide powders of nearly monodispersed nanocrystals

which can be dispersed in a variety of solvents. The particle size can be controlled by varying the temperature and the time of the reaction.

This TOPO method has several advantages, including, producing monodispersity and the ability to produce hundreds of milligrams of materials in a single experiment. The surface nature of CdSe/TOPO nanocrystallites has been studied by nuclear magnetic resonance spectroscopy and X-ray photoelectron spectroscopy [37]. For these methods the surface coverage, the percentage of surface sites bound to TOPO molecules through a metal-oxygen dative bond, increases from 30% to 60% as the particle size decreases. Steric effects can explain variations in surface coverage with particle size. The interaction between surface bound bulky neighbouring capping molecules (TOPO) predominates in larger particles while smaller particles can accommodate higher percentage levels of surface coverage due to less steric hinderance [37]. However, the use of dimethylcadmium, a volatile and highly toxic substance, is a limitation to this method.

The inherent problems associated with the use of toxic and volatile compounds such as metal alkyls at elevated temperatures also led to the development of alternative chemical routes to nanoparticles. The use of single-molecule precursors in which the metal-chalcogenide bond is available has proven to be a very efficient route to high-quality nanoparticles. Trindade and O'Brien first investigated cadmium dithio- and diselenocarbamate complexes as precursors for the synthesis of TOPO-capped II/VI semiconductor nanoparticles [38,39]. The method of nanoparticle synthesis involves the dispersion of the single source precursor in TOP, followed by injection into hot TOPO at 250 ^{o}C. The general scheme of nanoparticle synthesis using single-molecule

precursors is shown in Figure 1.3. In this single molecular source method the formation of nanoparticles is consistent with the La Mer mechanism for colloids [21]. The decomposition of the precursor drives the formation of the nanoparticles with termination of growth occurring when the precursor supply is depleted. After the initial injection there is a rapid burst of nucleation, which is followed by controlled growth of the nuclei by Ostwald ripening. The resultant nanoparticles are passivated by TOPO, which prevents agglomeration. The nanoparticles were isolated by a process whereby a non-solvent (methanol) was added to the reaction mixture, which increases the average polarity of the solution and consequently decreases the energy barrier to flocculation. The flocculant precipitate obtained was separated by centrifugation and redispersed in toluene to give an optically clear solution of TOPO-capped nanoparticles.

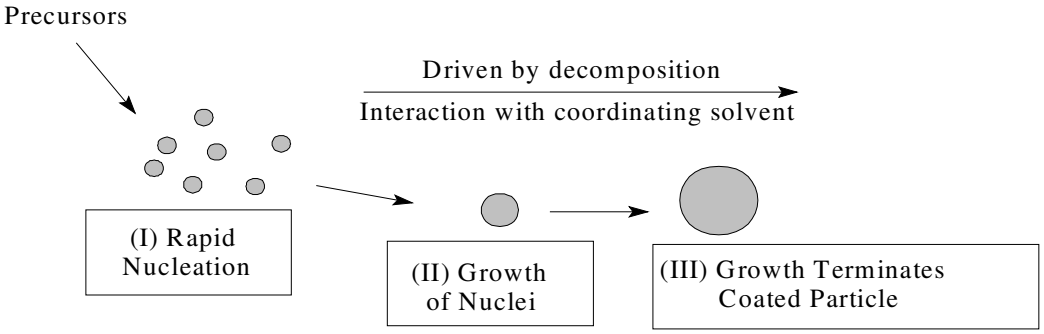

Figure 1.3 Scheme showing the various stages of nanoparticle growth using the one-pot synthetic method [40].

When using oleylamine (OA) as the coordinating solvent instead of TOPO, Geng *et al.* [41] thermolysed cadmium 2-mercaptobenzothiazole complex $Cd(Mer)_2$ (Mer $=C_6H_4NS^-$), [which could be easily obtained from the reaction of mercaptobenzothiolate (Mer) and cadmium ion in aqueous solution] to synthesize CdS nanoparticles of various sizes. Meanwhile, the size of the synthesized CdS

nanocrystals could be easily controlled by adjusting the ratio of OA/$Cd(Mer)_2$ under inert atmosphere. The studies on the optical properties of the nanocrystals displayed an obvious size-dependent photoluminescence characteristic.

Mthethwa *et al*. [42] used heterocyclic cadmium dithiocarbamates, $[Cd(S_2CNC_5H_{10})_2]$ and $[Cd(S_2CNC_9H_{10})_2]$, for the synthesis of CdS nanoparticles. The complexes were thermolysed in HDA to give HDA-capped CdS nanoparticles. A combination of close to spherical, rod, bipods and tripods were obtained by varying the reaction parameters such as precursor concentration and temperature. The optical measurements also supported the presence of anisotropic particles at lower precursor concentrations. The XRD patterns confirmed the hexagonal phase of CdS.

In the search for a greener method to avoid the use of pyrophoric precursors and reduce hazardous materials, Peng and Peng [43] reported the synthesis of high quality CdTe, CdSe and CdS nanocrystals using CdO as a cadmium precursor instead of dimethyl cadmium. In this one pot approach, CdO, TOPO and either hexylphosphonic acid (HPA) or tetradecylphosphonic acid (TDPA) were loaded into a three-necked flask. At temperatures above 270 ^{o}C, the phosphonic acid complexes with CdO and TOPO formed a clear and colourless solution. After the formation of the colourless cadmium phosphonate complex, tributylphosphine (TBP): E (E = S, Se or Te) was then injected to initiate the formation of the nanocrystals. This synthetic scheme produced both quantum-confined dots and rods. The quality of the quantum dots and rods of all cadmium chalcogenides formed in this new method is comparable to that of the best CdSe nanocrystals reported in the literature [36,44,45]. Peng and Peng [43] postulated that CdO works well as a precursor due to its low stability, relative to

phosphonic acid than other precursor candidates, such as $CdCl_2$. This 'green' route proved to be reproducible, involving simple reaction conditions and had potential to be scaled up for industrial applications. Qu *et al.* [46] used other cadmium sources apart from CdO such as $Cd(CH_3COO)_2$, $CdCO_3$, $CdSO_4$ and $CdCl_2$ as an alternative to $Cd(CH_3)_2$ in the presence of different solvents, like fatty acids and amines. Their results proved fatty acids to be excellent solvent for synthesizing relatively large-sized CdSe nanoparticles but not for smaller nanoparticles because of the fast growth rate of the nanocrystals. The use of $CdCl_2$ and $CdSO_4$ generated only bulk-sized CdSe. They attributed this to relatively high stability under acidic conditions of the salt formed by cadmium and a strong acid in comparison to that of CdSe. In trying to avoid the use of additional ligands several adaptation methods to the Peng's route have been reported to address this issue.

Oluwafemi and Revaprasadu [47] reported a novel facile solution based synthesis of nearly monodispersed CdSe nanoparticles whereby Se powder was first reacted with $NaBH_4$ in water to produce Se^{2-} ions, which acted as the source of Se, followed by the addition of $CdCl_2$. The resultant CdSe was dispersed in TOP and this CdSe-TOP mixture was thermolysed in TOPO or HDA to passivate the surface. The nanoparticles showed quantum confinement with characteristic close to band-edge luminescence in their emission spectra. This synthetic procedure offered several important advantages for the synthesis of selenide nanocrystals. The technique is environmentally friendly, inexpensive, involving the use of relatively non-toxic reagents and has short reaction time. The effect of the cadmium source on the shape of the CdSe nanoparticle using the same synthetic route, by varying different cadmium salts was also investigated [48]. When $CdCl_2$ and $CdSO_4$ were used as

cadmium sources, spherical particles were formed; however when cadmium carbonate was used, rod shaped TOPO and HDA-capped CdSe particles were observed.

1.3 *Shape control mechanism*

Several proposals have been made to achieve shape control of nanocrystals. Generally crystal growth starting from nanoparticles can be classified into two different mechanisms:

1) Ostwald ripening

2) Oriented attachment

Both of these growth mechanisms have the merit of facile separation between the nucleation and growth stages, which is a pre-requisite for the shape-controlled nanocrystals fabrication.

1.3.1 *Ostwald ripening*

The nanocrystals growth through colloidal chemistry is a classical model and describes the resultant nanocrystals by the formation of tiny crystalline nuclei in a supersaturated solution followed by crystal growth. The later processes were performed by mass supply of precursor monomers and by surface energy equilibrium on which addition or removal of the individual monomers at sites depends. Within a colloid solution system with particle size distribution, the large particles will grow at the dissolution of the small ones as shown in Figure 1.4. This mechanism is termed Ostwald ripening, which is generally believed to be a main route to crystal growth [49].

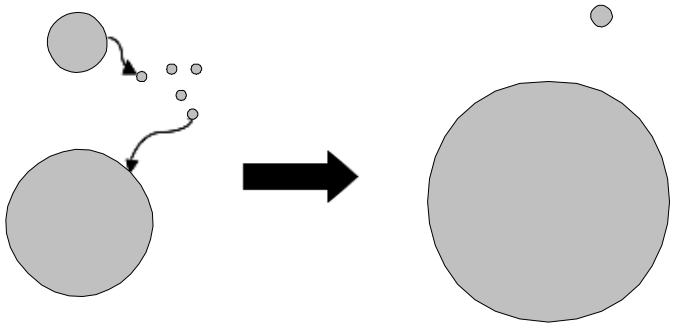

Figure 1.4 Basic schematic of the Ostwald ripening process [50].

This thermodynamically-driven spontaneous process occurs because larger particles are more energetically favoured than smaller particles [51]. This stems from the fact that molecules on the surface of a particle are energetically less stable than the ones already well ordered and packed in the interior. Large particles with their lower surface to volume ratio, results in a lower energy state (and have a lower surface energy). As the system tries to lower its overall energy, molecules on the surface of a small (energetically unfavourable) particle will tend to detach and diffuse through solution and then attach to the surface of larger particle [51]. Therefore, the number of smaller particles continues to shrink, while larger particles continue to grow.

Peng *et al*. [52] demonstrated that by varying the initial concentration of the monomer during the synthesis of CdSe and InAs nanocrystals, the focusing time as well as the focused size changes because of the time for depleting the monomer concentration changes. For example, in the case of CdSe nanocrystals, at a Cd:Se ratio of 1.9:1, after reaching the focused size, the nanocrystals can be maintained at the growth temperature for hours before Ostwald ripening or defocusing occurs. On the other hand, at a ratio of 1.1:1, defocusing is rapid, and the only way to get a tight size distribution is to almost double the concentration of both Cd and Se, which again

reduces the critical size. The effect seen in CdSe and InAs also apply to CdS and InP and presumably to the entire class of II-VI and III-V semiconductors.

The extinction coefficient, concentration, nucleation condition and the growth mechanism were studied by Oluwafemi and Revaprasadu [53] in the synthesis of HDA capped CdSe via a non-organometallic route. Nucleation was very fast and well separated from particle growth under this reaction condition and two distinguishable stages of growth were observed: an early stage 0-10 min characterized by fast growth, with narrow size distribution and the late stage characterized by slow growth with slight defocusing of size distribution and large particle sizes.

1.3.2 *Oriented attachment*

The other emerging view of crystal growth is called 'oriented attachment' as suggested by several reports [54-56]. According to the oriented attachment mechanism, crystal growth views the formation of bigger crystals as a result of pileup and coalescence of smaller particles with sizes of a few nanometers rather than the adhesion of individual monomers, such as ions. At an early stage, the adjacent individual nanoparticles with the same crystal structure join together and perfectly align along the same crystallographic direction. Subsequently, the as-formed aggregates coalesce into larger nanocrystals with a specific shape at the terminal stage. In the formation of oriented-attached rod-shaped nanocrystals, the surface energies of the various crystallographic planes plays an important role, high surface energy at a specific crystallographic plane will promote anisotropic nanoparticles stacking preferentially in the direction perpendicular to the crystallographic plane. For the cubic zinc-blende structure, the surface energy on the (111) plane is higher than

other crystallographic planes such as (100) and (110) due to the high atomic density [57]. The general mechanism of oriented attachment is shown in Figure 1.5.

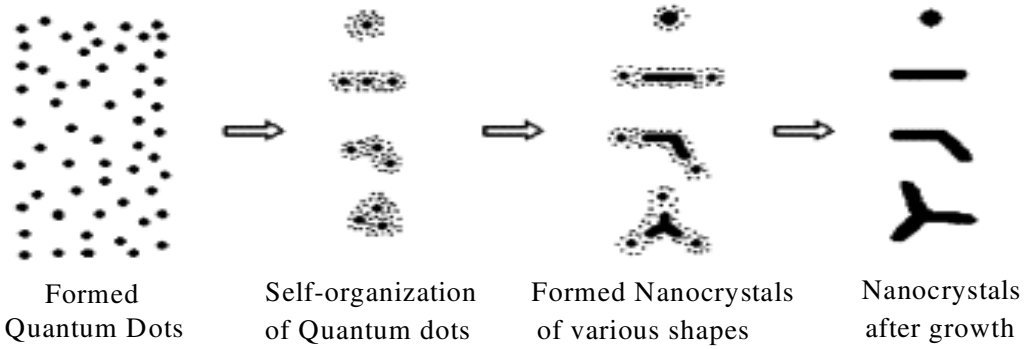

Figure 1.5 Basic scheme of oriented attachment growth [58].

The concept of oriented attachment has been demonstrated by Banfield and co-workers in the hydrolytic synthesis of TiO_2 nanocrystals [59]. Truncated diamond-shaped anatase TiO_2 nanocrystals have three different faces: {011}, {121} and {101}. According to Donnay-Harker rules, the surface energy of the (001) is higher than those of the other surfaces [60]. When there is a sufficient thermal energy in the system, the removal of high-energy surfaces is thermodynamically favourable. Therefore, the fusion of diamond-shaped nanocrystals along the [001] direction is facilitated by the oriented attachment process that results in a necklace-shaped nanocrystals [59].

Deng *et al*. [61] demonstrated a new approach for the controllable growth of Bi_2Te_3 nanorods via oriented attachment of nanoparticles. One of the advantages of the method is that the synthesized Bi_2Te_3 nanoparticles directly serve as building blocks to further form nanorods and the formation of secondary particles are homogeneous single crystals. EDTA molecules play a key role in this process. It is proved that this

synthetic approach could be promising to prepare self-assembled one-dimensional nanocrystals of metals and semiconductors [61].

Quantum-sized ZnS nanocrystals with quasi-spherical and rod shapes have been synthesized by the aging reaction mixtures containing diethylzinc, sulphur and amine [62]. Structural characterizations showed that these nanorods had a cubic zinc blende structure, whereas the fabrication of nanorods with this structure has been known to be difficult to achieve via colloidal chemical synthetic route. High-resolution transmission electron microscopy (HRTEM) images and reaction studies demonstrated that these nanorods were formed from the oriented attachment of quasi-spherical nanocrystals. The photoluminescence spectra of the ZnS nanorods and quasi-spherical nanocrystals showed a well-defined excitonic emission features, size- and shape- dependent quantum confinement effects [62].

Single-crystal PbSe nanowires were synthesized in solution through oriented attachment of nanocrystal building blocks [63]. PbSe nanocrystals bind to each other on either {100}, {110}, or {111} faces, depending on the surfactant molecules present in the reaction solution. While PbSe nanocrystals have the centrosymmetric rock salt lattice, they can lack central symmetry due to a noncentrosymmetric arrangement of Pb- and Se-terminated {111} facets and possess dipole driving one-dimensional oriented attachment of nanocrystals to form nanowires. In addition to straight nanowires, zigzag, helical, branched and tapered nanowires as well as single-crystal nanorings can be controllably prepared in one-pot reactions by careful adjustment of the reaction conditions [63].

CdS nanorods were prepared on a large scale by the thermolysis of the single-source precursor, $\{(Me_4N)_4[S_4Cd_{10}(SPh)_{16}]\}$, in HDA [64]. The influence of reaction conditions on the growth of CdS nanorods demonstrated that high precursor concentration and high reaction temperature (>190 ^oC) were favourable for the formation of CdS nanorods. Under high temperature, the produced particles were aggregated along the (002) plane of its wurzite crystal lattice as demonstrated by the HRTEM. During the formation process, the nanoparticles were produced first and then the particles aggregated with each other to form 'oligomers', which were epitaxially fused together to form nanorods [64].

CdSe nanocrystals with tunable morphologies were prepared by controlling the temperature in the solution reaction route using selenium powder (Se), hydrazine hydrate ($N_2H_4 \cdot H_2O$) and $Cd(CH_3COO)_2$ as reagents [65]. The lower reaction temperature benefited the anisotropic growth of crystals with the oriented attachment mechanism to produce the high-yield ring- and tribulus-shaped nanocrystals.

1.4 *Applications of nanoparticles*

The applications of nanoparticles in the following section are discussed based on CdTe nanoparticles.

1.4.1 *Biological applications*

1.4.1.1 *Imaging and labelling of cells*

Previous work have shown that solution based fluorescent nanoparticles prepared in the aqueous phase or QDs could be utilised as fluorescence tools for the biological imaging of cells [66,67]. When compared with flourescent dyes such as rhodamine,

ethidium, flourescein and methyl coumarin the QDs have a narrow, tunable, symmetric emission spectrum and are much brighter and stable against photobleaching. Zhang *et al.* [68] have reported biological labelling of living mouse L929 cells with mercaptocarboxylic acid-capped CdTe nanoparticles. The CdTe nanoparticles were conjugated with interferon or avidin and injected to a living mouse where they were able to bind to the receptor of the L929 cells as shown by the photoluminescence images in Figure 1.6.

The highly luminescent 3-mercaptopropionic acid (MPA)-capped CdTe QDs prepared in the aqueous phase has been used for live cell imaging [69]. Since the CdTe QDs were prepared in aqueous phase using MPA as a stabilizer, their surface can be easily coupled to the amine group on biomolecules. The QDs were conjugated to *Ulex europaeus* 1 (UEA-1) using 1-ethyl-3-(3-dimethylaminopropyl) carbodiimide) (EDC) as a coupling agent. When the QDs probes with UEA-1 were incubated with the human umbilical vein endothelial cells (HUVECs), they were able to specifically bind the corresponding cell receptor. The laser confocal scanning microscopy showed good cell images when live cells were analysed.

The CdTe QDs capped with thioglycolic acid (TGA) have been used as live cell imaging tools to investigate their uptake and cellular localisation in (Human acute monocytic leukemia cell line), THP-1 cells [70]. After numerous extended incubation periods these QDs were able to display strong luminescence and photostability. The QDs were found to pass across the cell membrane, illuminating the cytoplasm and decorating the nucleus. The mercaptosuccinic acid-capped CdTe nanoparticles have been conjugated with human transferrin (TRF) using EDC as a coupling agent [71].

These TRF-QDs conjugates were delivered into Human embryonic kidney, HEK 293, cells via the transferrin receptor-mediated endocytosis pathway. The CdTe QDs were found accumulating mainly in the cytoplasm. The effectiveness of TRF was proven when a control experiment was also carried in which only unconjugated QDs were incubated in the cells. When comparing the two experiments, cell labelling was only achieved with the TRF-conjugated CdTe QDs while the unconjugated QDs gave very weak fluorescence signals.

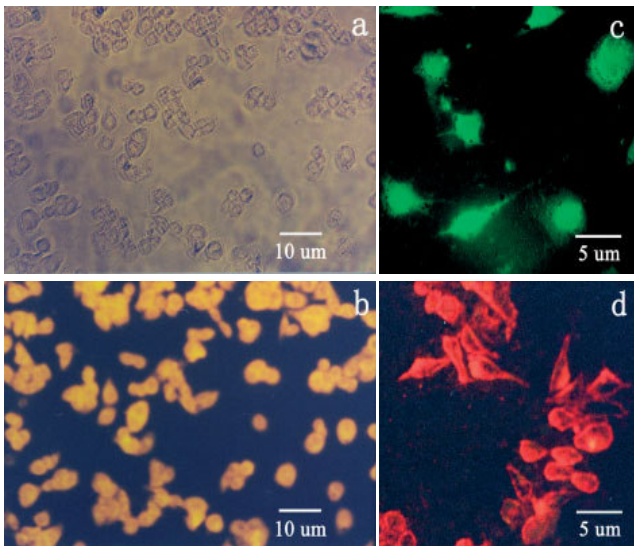

Figure 1.6 Labelled mouse L929 cells with 3-mercaptopropionic acid stabilized CdTe nanocrystals. (a,b) overview of living cells labeled with yellow emitting nanocrystals; a) the image of cells in the light field, (b) the corresponding photoluminescence image, (c) Higher magnification PL image of the cells labelled with green emitting nanocrystals and (d) red emitting nanocrystals [68].

1.4.1.2 *FRET and CRET Biosensors*

The detection of molecular binding events in response to interactions with a particular target molecule or to change in the solution environment is necessary when materials are used for biological applications. This can be achieved by using fluorescence

resonance energy transfer (FRET) which is a technique for searching any changes in the distance between the molecule donating and accepting fluorescence. The process of emission involves the excitation of an electron when a molecule absorps a photon and then the return to a lower energy state accompanied by the emission of a photon. In FRET the energy of an electron produced after emission of a photon from the donating molecule is transferred to the accepting molecule which results in the quenching of fluorescence from the donor. Analyte binding produces conformational changes that separate the two molecules which may be a disadvantage of FRET. This is a distance-dependence process which does not occur when the fluorescence donor and acceptor move away from each other. QDs have been used in the studies based on FRET such as QD-protein-conjugate configuration and QD-protein sensing assemblies [72-74]. The use of QDs in FRET as both donors and acceptors is due to their unique optical and structural properties. The 3-mercaptopropionic acid-capped CdTe nanoparticles donors with gold (Au) nanoparticles acceptors have been used in FRET for DNA detection [75]. The 5'-NH_2-DNA was linked with CdTe nanoparticles through EDC as a linker while the 3'-SH-DNA was self-assembled onto the surface Au nanoparticles. FRET occurred after hybridization of complementary double stranded DNA (dsDNA) bound to the CdTe NPs and AuNPs (CdTe-ds-DNA-Au) because the donor and acceptors were in close proximity to each other. The decrease in the fluorescence of CdTe-DNA-Au conjugate as compared to CdTe-DNA indicates that the FRET occurred between CdTe QDs and Au nanoparticles.

Another technique similar to FRET is called chemiluminescent resonance energy transfer (CRET) which occurs by the oxidation of a luminescence substrate without an excitation source. It involves non-radiative (dipole-dipole) transfer of energy from a

chemiluminescent donor to a suitable acceptor molecule. Chemiluminescence is the emission of light with limited luminescence as the result of a chemical reaction. CRET have been investigated between luminol and mercaptopropyl-capped CdTe QDs bioconjugates [76]. The QDs were conjugated to HRP (horseradish peroxidase) proteins using EDC as a coupling agent. As shown in Figure1.7a, the chemiluminescent donor is not directly linked with the QDs and HRP is used as a catalyst. CdTe QDs were also linked with bovine serum albumin (BSA) and HRP was conjugated with the BSA antibody (anti-BSA). CRET can occur by binding the anti-BSA-HRP to the BSA-QDs (Figure 1.7b).

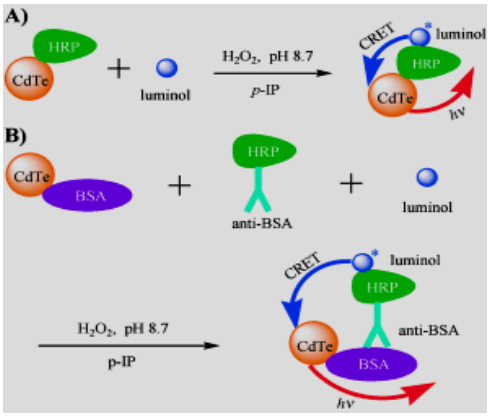

Figure 1.7 Schematic illustration of CRET based on luminol donors and HRP-labeled CdTe QD acceptors, B) Schematic illustration of CRET for luminol donors and QD accepters based on the immuno-reaction of QD-BSA and anti-BSA-HRP [76].

Thiol-capped CdTe nanoparticles have been applied to study the effect of metal ions on chemiluminescence (CL) of the CdTe/H_2O_2 system [77]. The effect of experimental factors such as pH, particle sizes, and reagent concentration on CL intensity of the CdTe/H_2O_2 was investigated. The experimental results showed that Ba^{2+}, Ca^{2+}, Fe^{2+}, Pb^{2+} and Cu^{2+} enhanced the CL intensity and Cr^{3+}, Ni^{2+}, Zn^{2+} and Ag^{+} inhibited the CL intensity.

1.4.2 *Electronic device applications*

1.4.2.1 *Light emitting diodes*

The bright and tunable luminescence properties of CdSe and CdTe nanoparticles make them very attractive as the emitters in light-emitting diodes (LEDs). When compared to CdSe very few reports describe the use of CdTe as the emitter in light-emitting devices. Gaponik *et al*. [78] reported a light-emitting device based on a CdTe nanocrystal/polyaniline (PAni) composite film as well as closely packed CdTe nanocrystal films sandwiched between magnesium (Mg) and indium tin oxide (ITO) as shown in Figure 1.8.

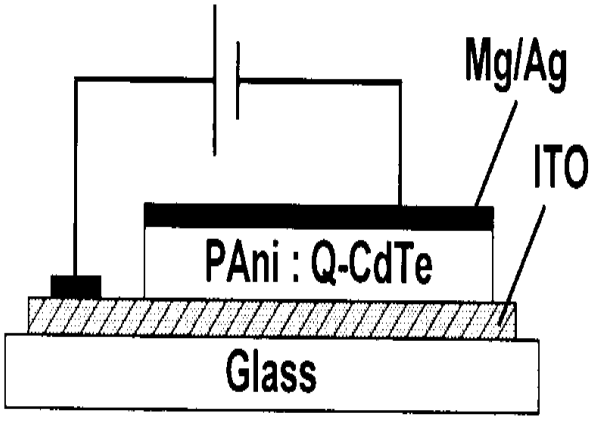

Figure 1.8 A schematic cross-sectional diagram of a light-emitting device based on a CdTe nanoparticle/polyaniline composite film.

The LEDs emission spectrum was tuned from green to red by simply varying the size of the nanocrystals. The quantum efficiency was increased when polyaniline film was used as the light emitting layer compared with the polymer-free device with closely packed CdTe nanoparticles. A LED based on CdTe nanoparticles/polypyrrole (PPy) composite between SnO_2 and Al electrodes have been reported [79]. The charge transport through the nanocrystals/polymer boundaries was more efficient in this LED

because of the closer contact between the individual nanocrystals and the PPy matrix compared to the CdTe NCs/PAni composite. In order to improve the efficiencies of LEDs caused by mismatch of energy levels and charge unbalance, various layers have been used to make the LED with relatively stable emission characteristics. Thiol-capped CdTe nanoparticles have been used to make LEDs consisting of an emissive CdTe nanoparticle multilayer sandwiched between ITO and a thermal evaporated aluminium electrode [80]. The improved structural homogeneity of the nanoparticles multilayer allowed for stable and repeatable current- and electroluminescence-voltage characteristics. The dodecylamine (DDA)-capped CdTe/CdSe nanoparticles in a hybrid polymer structure were used to construct LEDs as shown in Figure 1.9 [81]. The luminescence efficiency of this LED was found to be 0.35 cd A^{-1} similar in the range found for devices based on highly luminescence CdSe nanoparticles.

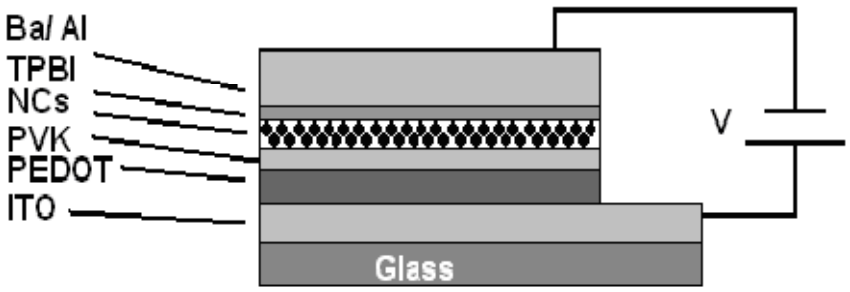

Figure 1.9 Schematic structure of the light-emitting device.

1.4.2.2 *Solar cells*

A solar cell is a device that converts light from the sun into electric current. Several nanoparticles such as CdS, CdSe and CdTe have been used in fabricating the hybrid absorber layer for organic solar cells [82-84]. The high absorption coefficient and high carrier mobility makes CdTe a promising material. These inorganic nanoparticles

are mixed with the polymer forming a hybrid material which has the potential of bridging the efficiency gap that exists between organic and inorganic semiconductor materials. Organic polymers such as MEH-PPV [Poly(2-methoxy, 5-(2-ethyl-hexy-loxy)-p-phenyl vinylene)], P3HT [poly(3-hexylthiophene)], and MDMO-PPV [poly[2-methoxy-5-(3′,7′-dimethyloctyloxy)-1,4-phenylene vinylene] have been reported as hole transporting materials for making hybrid solar cells [82,85,86]. Some studies on the hybrid solar cells have shown that nanoparticles capped using ligands like TOPO results in low cell efficiency [87,88]. The findings revealed the lack of charge transfer between the polymer and nanoparticles which is attributed to the surfactant associated with the nanoparticles. The first realization of the solar cell based on the material formed by combining CdTe nanoparticles and MEH-PPV have been reported by Kumar and Nann [82]. The high surface energy of the CdTe nanoparticles caused the inhomogenity of the solution that was formed. They also saw the necessity of a chemical method to remove the surfactant from the surface of the CdTe nanoparticles. Shiga *et al*. [84] have reported the fabrication of the solar cell containing the pyridine-capped CdTe nanocrystals and MEH-PPV (Figure 1.10).

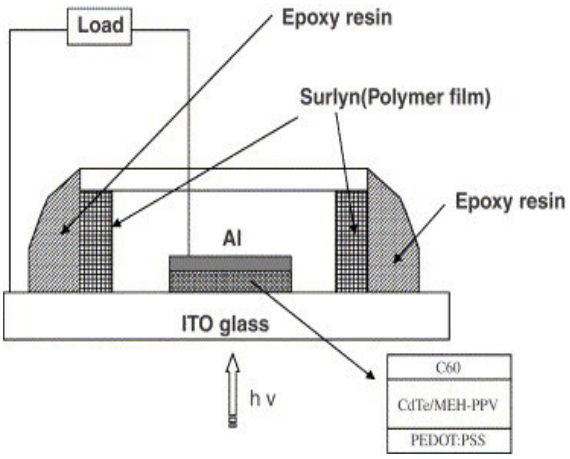

Figure 1.10 A schematic illustration of solar cell device structure

Verma *et al*. [89] have fabricated the solar cell containing surfactant free CdTe nanoparticles mixed with MEH-PPV to achieve a power conversion efficiency of ~0.06%. The two materials were mixed in different weight ratios and the solution was heated to achieve homogeneity. The photoluminescence spectra results were quenched which show the degree of dispersity of the nanoparticles in the MEH-PPV matrix and that the required dissociation of excitons was taking place.

1.4.3 *Other applications*

1.4.3.1 *Fingerprint detection*

Fingermarks detection plays a significant role in individual identification. The latent fingermarks are the most commonly found fingermarks at crime scences. The first fingerprints detection reported by Menzel *et al*. [90] using CdS/dendrimer nanocomposites has made a significant interest to the usage of fluorescence semiconductor nanomaterials as labelling agents in fingerprint developments. The CdSe QDs synthesized in aqueous solution using TGA as the stabilizer can produce significant less background development and better contrast for the detection of latent fingerprints on adhesives [91]. The multicolour TGA-capped CdTe QDs have been used to develop fingerprints on objects with different background colors by varying the color to get the best fingerprint image that is favourable to distinguish finger-prints from different color objects [92]. Figure 1.11 shows the fingerprint images show-assisted by multicolour CdTe QDs at different refluxing times on the blue objects which were deposited on the adhesive-side of a piece of tape and developed by two colors of green and yellow. The fingerprint details immersed in the CdTe QDs solution clearly developed as compared with that of the non-immersed counterpart, in

which the yellow color image of fingerprint is brighter and clearer indicating a smooth and defined finger-print image with more details.

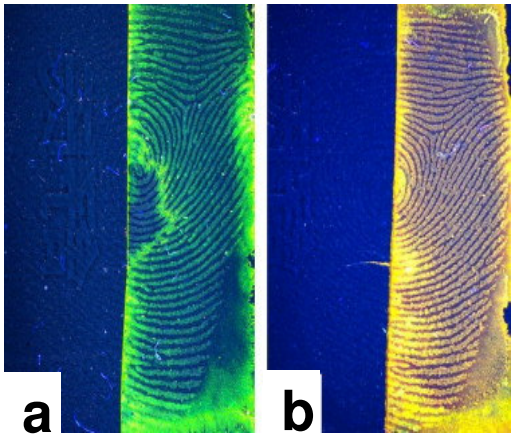

Figure 1.11 Fingerprint images show-assisted by multicolour CdTe QDs (a) 0 and (b) 2 h.

The CdTe QDs stabilized by a thiol ligand can be selectively anchored in the ridges of the fingerprint via a chemical reaction and electrostatic adsorption between fingerprint residues such as protein, grease and amino-acid etc. and the carboxyl group of the TGA ligand on the surface of CdTe QDs (Figure 1.12). Therefore, the fingerprint details on the surface of smooth objects can be clearly developed with a CdTe QDs solution under the irradiation of UV light.

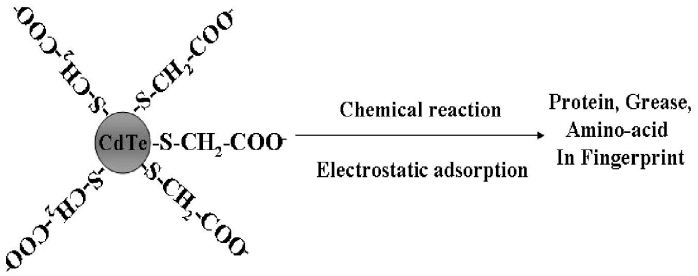

Figure 1.12 Scheme of the combination of fingerprint residues with CdTe QDs stabilized by TGA.

1.4.3.2 *Detection of organic componds*

Recently CdTe nanoparticles were labelled with anti-fluoranthene antibodies (anti-FL-ab) which resulted in an increased fluorescence intensity and good stability [93]. The CdTe-anti-FL-ab was used for fluorescent immunoassay to detect flouranthene in water samples. The results revealed that fluoranthene could be determined in the concentration range of 10^{-1} to 10^{3} µg/L and the sensitivity (IC50) was 12.4 µg L^{-1} and detection limit (IC20) was 13.1 ngL^{-1}. The method was shown to be accurate and reliable for the detection of polycyclic aromatic organic pollutants in the environment.

1.5 *Problem Identification*

Nanostructured cadmium telluride has received great attention for both fundamental research and potential applications due to high fluorescence quantum yields, short radiative lifetimes, low thresholds for optical gain and linearly polarized emission. The size-dependent properties make it especially suitable as building blocks for light-emitting diodes [80], photovoltaics [84], and biological and chemical sensor applications [69,76]. The key issue in most research based semiconductor nanoparticles is the ability to synthesize high quality nanoparticles with well-defined properties. That is, high crystallinity, achievement of desirable particle sizes over the largest possible range, desired surface passivation and high luminescence.

There have been many routes to CdTe nanoparticles which will be reviewed in detail in Chapter 2 and 3. However many of these routes require high temperatures, use of toxic, unstable starting materials. Some require the use of an additional stabilizing agent which increases the cost. Other approaches that have also been used for the synthesis of cadmium telluride nanoparticles include electrodeposition [94], vapour

deposition [95] and the aerosol flow system [96]. Although most of these developed methods do not require difficult laboratory condition, there are still some limitations to their utilities such as dissatisfying photoluminescence quantum yield in many cases, relatively broad particle size distribution, low solubility of the precursors in the dispersing solvent and longer reaction times for processing the precursor material to be used. In addtition to that comparing the product yield to the total cost of production (taking into consideration the cost of the equipment and starting materials), these techniques seem to be cost-effective and may not be desirable for large scale production.

The synthesis of nanomaterials via solution route appears to be the most simple, cheap and convenient approach to prepare the cadmium telluride nanoparticles in a controlled environment. Most of the solution methods involve arrested precipitation or titration in aqueous solution. However the quality of the particles is compromised as crystalline materials are not obtained at low temperatures. Also the control of the shape is difficult as the reactions are under kinetic control.

Therefore there is still a need to develop a suitable route for the synthesis of high quality CdTe nanoparticles with good optical properties and control over growth and morphology. The aim of this work is to develop a novel route to high quality CdTe nanoparticles which have properties that can be used in applications.

1.6 *Objectives of the study*

- To synthesize and characterize organically soluble CdTe nanoparticles using a hybrid solution based high temperature thermolysis method.

- To study the influence of the reaction parameters such as Cd:Te precursor ratio, reaction time, capping group, reaction temperature, reduction time for Te and cadmium source on the final morphology and optical properties of the particles.
- To synthesize water soluble CdTe nanoparticles.
- To study the influence of the capping group, reaction time, pH and cadmium source on the morphology and optical properties of the CdTe nanoparticles.

1.7 *References*

[1] T. Trindade, P. O'Brien, N. Pickett, *Chem. Mater*., **13** (2001) 3843-3858.

[2] A. Eychmuller, *J. Phys. Chem. B*., **104** (2000) 6514-6528.

[3] C. B. Murray, C. R. Kagan, M. G. Bawendi, *Annu. Rev. Mater. Sci*., **30** (2000) 545-610.

[4] A. Henglein, *Chem. Rev*., **89** (1989) 1861-1873.

[5] L. E. Brus, *J. Chem. Phys*., **79** (1983) 5566-5571.

[6] Z. A Peng, X. Peng, *J. Am. Chem. Soc*., **124** (2002) 3343-3353.

[7] M. A. Malik, P. O'Brien, N. Revaprasadu, *S. Afr. J. Sci*., **96** (2000) 55-60.

[8] J. Turkevich, *Gold Bull*., **18** (1985) 86-91.

[9] J. Gao and B. Xu, *Nano Today*., **4** (2009) 37-51.

[10] S. Yong, P. Muralidharan, S. H. Jo, D. K. Kim, Mater. Lett., **64** (2010) 1551-1554.

[11] X. Peng, *Nano. Res*. **2** (2009) 425-447.

[12] L. E. Brus, *J. Chem. Phys*., **80** (1984) 4403-4409.

[13] http://en.wikipedia.org/wiki/Photoluminescence, 02-02-2011

[14] X.Chen, Y. Lou and C. Burda, *Int. J. Nanotechnol*., **1** (2004) 105-118.

[15] G. Ledoux, O. Guillois, F. Huisken, B. Kohn, D. Porterat, C. Reynaud, *A. A*., **377** (2001) 707-720.

[16] T. Yamaki, T. Yamada, K. Asai, K. Ishigure, H. Shibata, *Thin. Solid. Film*., **327-329** (1998) 581-585.

[17] A. P. Alivisatos, *Science*., **271** (1996) 933-937.

[18] K. Fabisiak, W. Bala, K. Paprocki, M. Szreiber, C. Uniszkiewicz, *Opt. Mater*. **31** (2009) 1873-1876.

[19] N. Revaprasadu, S. N. Mlondo, *Pure. Appl. Chem*. **78** (2006) 1691-1702.

[20] T. Jonson, V. K. La Mer. *J. Am. Chem. Soc*., **69** (1947) 1184-1192.

[21] R. Rossetti, J. L Ellison, J. M. Gibson, L. E. Brus, *J. Chem. Phys*., **80** (1984) 4464-4469.

[22] R. Rossetti, R. Hull, J. M. Gibson, L. E. Brus, *J. Chem. Phys*., **82** (1985) 552-559.

[23] H. Weller, *Angew. Chem. Int. Ed. Engl*., **32** (1993) 41-53.

[24] S. Baral, A. Fojtik, H. Weller, *J. Am. Chem. Soc*., **108** (1986) 375-378.

[25] A. Eychmuller, L. Katsikas, H. Weller, *Langmuir*., **6** (1990)1605-1608.

[26] A. Fojtik, H. Weller, U. Koch, *Ber. Bunsen-Ges. Phys. Chem*., **88** (1984) 969-977.

[27] H. Weller, *Adv. Mater*., **5** (1993) 88-95.

[28] M. L. Hassan, A. F. Ali, *J. Cryst. Growth*., **310** (2008) 5252-5258.

[29] S. O. Oluwafemi, N. Revaprasadu and A. Ramirez, *J. Chem. Growth*., **310** (2008) 3230-3234.

[30] S. O. Oluwafemi, *Colloids and Surface B: Biointerfaces*., **73** (2009) 382-386.

[31] V. S. R. Rajasekhar Pullabhotla, N. Revaprasadu, *Mater. Lett*., **63** (2009) 2097-2099.

[32] V. Singh, P. Chauhan, *J. Phys. Chem. Solids*., **70** (2009) 1074-1079.

[33] Z. B. Shang, Y. Wang, W. J. Jin, *Talanta*., **78** (2009) 364-369.

[34] H. Miyaji, D. S. Kim, B. Y. Chang, E. Park, S. M. Park, K. H. Ahn, *Chem. Commun*., **27** (2008) 753-755.

[35] I. H. J. Arellano, J. Mangadlao, I. B. Ramiro, K. F. Suazo, *Mater. Lett*., **64** (2010) 785-788.

[36] C. B. Murray, D. J. Norris, M. G. Bawendi, *J. Am. Chem. Soc*., **115** (1993) 8706-8715.

[37] J. E. Bowen-Katari, V. L. Colvin, A. P. Alivisatos, *J. Phys. Chem.*, **98** (1994) 4109-4117.

[38] T. Trindade, P. O'Brien, *Adv. Mater*., **8** (1996) 161-163.

[39] T. Trindade, P. O'Brien. *Chem. Mater*., **9** (1997) 523-530.

[40] M. A. Malik, P. O'Brien, N. Revaprasadu, *Phosphorus, Sulphur, and Silicon*., **180** (2005) 689-712.

[41] B. Geng, X. Liu, Q. Du, J. Ma, X. Liu, *Mater. Res. Bull.*, **43** (2008) 1093-1098.

[42] T. Mthethwa, V. S. R. Rajasekhar Pullabhotla, P. S. Mdluli, J. Wesley-Smith, N. Revaprasadu, *Polyhedron*., **28** (2009) 2977-2982.

[43] Z. A. Peng, X. Peng, *J. Am. Chem. Soc*., **123**, (2001) 183-184.

[44] D. V. Talapin, A. L. Rogach, A. Kornowski, M. Haase and H. Weller, *Nano. Lett*., **1** (2001) 207-211.

[45] D. V. Talapin, A. L. Rogach, E. V. Shevchenko, A. Kornowksi, M. Haase, and H. Weller, *J. Am. Chem. Soc*., **124** (2002) 5782-5790.

[46] L. Qu, Z. A. Peng and X. Peng, *Nano. Lett*., **1** (2001) 333-337.

[47] O. S. Oluwafemi, N. Revaprasadu, *New. J. Chem*., **10** (2008) 1432-1437.

[48] N. N. Maseko, N. Revaprasadu, V. S. R. Rajasekhar Pullabhotla, R. Karthik, P. O'Brien, *Mater. Lett.*, **64** (2010)1037-1040.

[49] D. Deng, Y. Qin, X. Yang, J. Yu, and Y. Pan, *J. Cryst. Growth*., **296** (2006) 141-149.

[50] http://en.wikipedia.org/wiki/Ostwald_ripening. 16-07-2010.

[51] L. Ratke, P. W. Voorhees, *Springer*. (2002) 117-118.

[52] X. Peng, J. Wickham, A. P. Alivisatos, *J. Am. Chem. Soc*., **120** (1998) 5343-5344.

[53] S. O. Oluwafemi, N. Revaprasadu, *Physica B*., **404** (2009) 1204-1208.

[54] R. S. Yadav, P. Mishra, R. Mishra, M. Kumar, A. C. Pandey, *Ultrasonics Sonochemistry*., **17** (2010) 116-122.

[55] L. Lu, A. Kobayashi, Y. Kikkawa, K. Tawa, Y. Ozaki, *J. Phys. Chem. B*., **110** (2006) 23234-23241.

[56] C. Pacholski, A. Kornowski, H. Weller, *Angew. Chem. Int. Ed*., **41** (2002) 1188-1191.

[57] D. Zhang, L. Sun, J. Yin, C. Yan, R. Wang, *J. Phys. Chem. B*., **109** (2005) 8786-8790.

[58] J. Zhang, K. Sun, A. Kumbhar, J. Fang, *J. Phys. Chem. C*., **112** (2008) 5454-5458.

[59] Q. Wang, D. Pan, S. Jiang, X. Ji, L. An, B. Jiang, *J. Cryst. Growth*., **286** (2006) 83-90.

[60] R. L. Penn, J. F. Banfield, *Geochin. Cosmochim. Acta*., **63** (1999) 1549-1557.

[61] J. D. Donnay, D. Harker, *Am. Mineral*., **22** (1937) 446-467.

[62] Y. Deng, C-W. Nan, L. Guo, *Chem. Phys. Lett*., **383** (2004) 572-576.

[63] J. Yu, J. Joo, H. M. Park, S. –I. Baik, Y. W. Kim, S. C. Kim, T Hyeon, *J. Am. Chem. Soc*., **127** (2005) 5662-5670.

[64] K.-S. Cho, D. V. Talapin, W. Gaschler, C. B. Murray, *J. Am. Chem. Soc*., **127** (2005) 7140-7147.

[65] W. Cai, Z. Li and J. Sui, *Nanotechnology*., **19** (2008) 465606-465611.

[66] P. Hu, D. Jia, Y. Cao, Y. Huang, L. Liu, J. Luo, *Nanoscale. Res. Lett*., **4** (2009) 437-443.

[67] W.C. Chan, S. Nie, *Science*, **281** (1998) 2016-2018.

[68] M. Jr. Bruchez, M. Morone, P. Gin, S. Weiss, A. P. Alivisatos., *Science*, **25** (1998) 2013-2016.

[69] H. Zhang, L. Wang, H. Xiong, L. Hu, B. Yang, W. Li, *Adv. Mater*. **15** (2003) 1712-1715.

[70] J. F. Weng, X. T. Song, L. Li, H. F. Qian, K. Y. Chen, X. M. Xu, C. X. Cao, J. C. Ren, *Chinese. Chemical. Letters*., **17** (2006) 675-678.

[71] E. Ying, D. Li, S. Guo, S. Dong, J. Wang, *PLoS One* **3** (2008), p. e2222.

[72] Y. Qi-Yan, Z. Hui-Sheng, W. Qiong-E, Z. Jin-Yan, Z. Chun, *Chin. J. Anal. Chem*., **38** (2010) 385-388.

[73] I. L. Medintz, J. H. Konnet, A. R. Clapp, I. Stanish, M. E. Twigg, H. Mattoussi, J. M. Mauro, J. R. Deschamps, *Proc. Natl. Acad. Sci*. **101** (2004) 9612-9617.

[74] I. L. Medintz, A. R. Clapp, H. Mattoussi, E. R. Goldman, B. Fisher, J. M. Mauro, *Nat. Mater.* **2** (2003) 630-638.

[75] E. R. Goldman, I. L. Medintz, J. L. Whitley, A. Hayhurst, A. R. Clapp, H. T. Uyeda, J. R. Deschamps, M. E. Lassman, H. Mattoussi*, J. Am. Chem. Soc*. **127** (2005) 6744-6751.

[76] D. Zhao, Z. Jimei, D. Quanxi, G. Ning, X. Shichao, S. Bo, B. Yuehua, *Chin. J. Chem. Eng*., **15** (2007) 791-794.

[77] X. Huang, L. Li, H. Qian, C. Dong, J. Ren, *Angew. Chem. Int. Ed*. **45** (2006) 5140-5143.

[78] X. Li, J. Li, J. Tang, J. Kang, Y. Zhang, *J. Lumin*. **128** (2008) 1229-1234.

[79] N. P. Gaponik, D. V. Talapin, A. L. Rogach, *Phys. Chem. Phys*., **1** (1999) 1787-1789.

[80] N. P. Gaponik, D. V. Talapin, A. L. Rogach, A. Eychmuller, *J. Mater. Chem*. **10** (2000) 2163-2166.

[81] C. Bertoni, D. Gallardo, S. Dunn, N. Gaponik, A. Eychmuller, *Appl. Phys. Lett* **90** (2007) 034107-034109.

[82] S. Kumar, T. Nann, *J. Mater. Res*. **19** (2004) 1990-1994.

[83] P. T. K. Chin, J. W. Stouwdam, S. S. Bavel, R. A. J. Janssen, *Nanotech* **19** (2008) 205602-205609.

[84] T. Shiga, K. Takechi, T. Motohiro, *Sol. Energy Mater. Sol. Cells* **90** (2006) 1849-1858.

[85] Y. Kang, D. Kim, *Sol. Energy Mater. Sol. Cells* **90** (2006) 166-174.

[86] M. A. Ibrahim, H. K. Roth, U. Zhokhavets, Gobsch, S. Sensfuss, *Sol. Energy Mater. Sol. Cells* **85** (2005) 13-20.

[87] Y. Zhou, L. Yunchao, H. Zhong, J. Hou, Y. Ding, C. Yang, Y. Li, *Nanotech* **17** (2006) 4041-4047.

[88] A. A. R. Watt, P. Meredith, J. D. Riches, S. Atkinson, H. R. Dunlop, *Curr. Appl. Phys*. **4** (2004) 320-322.

[89] D. Verma, A. R. Rao, V. Dutta, *Sol. Energy Mater. Sol. Cells* **93** (2009) 1482-1487.

[90] E. R. Menzel, M. Takatsu, R. H. Murdock, K. Bouldin, K. H. Cheng, *J. Forensic Sci*. **45** (2000) 770-773.

[91] Y. F. Wang, R. Q. Yang, Y. J. Wang, Z. X. Shi, J. J. Liu, *Forensic Sci. Int.* **185** (2009) 96-99.

[92] S. J. Byren, S. A. Corr, T. Y. Rakovich, Y. K. Gun'ko, Y. P. Rakovich, J. F. Donegan, S. Mitchell, Y. Volkov, *J. Mater. Chem*., **16** (2006) 2896-2901.

[93] J. Liu, Z. Shi, Y. Yu, R. Yang, S. Zuo, *J. Coll. Int. Sci*. **324** (2010) 278-282.

[94] D. K. Ivanou, E. A. Streltsov, A. K. Fedotov, A. V. Mazanik, D. Fink, A. Petrov, *Thin Solid Films*., **490** (2005) 154-160.

[95] N. N. Kolesnikov, V. V. Kveder, R. B. James, D. N. Borisenko, M. P. Kulakov, *Nuclear Instruments and Methods in Physics Research, A*., **527** (2004) 73-75.

[96] D. Kim, H. D. Jang, E. J. Kim, K. Koo, *Ultramicroscopy.*, **108** (2008) 1278-1282.

CHAPTER TWO

SYNTHESIS OF ORGANICALLY SOLUBLE CADMIUM TELLURIDE NANOPARTICLES

`

2.0 *Introduction*

Semiconductor nanoparticles such as cadmium selenide (CdSe) and cadmium telluride (CdTe) have been extensively studied due to their novel properties which are determined by their size, shape and surface modification. The high photoluminescence (PL) quantum efficiencies of CdTe makes it an interesting material for use in applications such as light emitting devices [1], photovoltaic and photoelectrochemical devices [2,3] and biological labels [4]. Aqueous and organometallic routes have been the principal synthetic routes to functionalized CdTe, although there have also been reports of CdTe nanoparticles grown by physical methods such as electrodeposition [5] and vapour deposition methods [6]. The landmark paper by Murray describes the synthesis of tri-*n*-octylphosphine oxide (TOPO) capped CdSe and CdTe nanoparticles using a metal alkyl and a chalcogenide source as precursors [7]. This route and adaptations thereof has been extensively used to synthesize CdTe nanoparticles for the study of their fundamental properties. The method allows for the kinetic control, where parameters such as reaction temperature and precursor concentration can control the final morphology and size of the particles.

Alivisatos and co-workers reported CdTe nanoparticles from the thermal reaction of dimethyl cadmium ($CdMe_2$) and tri-*n*-octylphosphine telluride (TOPTe) in a hot surfactant mixture of TOPO and hexylphosphonic acid (HPA) [8]. Talapin *et al.* [9] reported the synthesis of highly luminescent CdTe nanoparticles by reacting dimethylcadmium with tellurium sources in a mixture of dodecylamine (DDA) and tri-*n*-octylphosphine (TOP). The drawback of these hot injection methods is the use of extremely pyrophoric, toxic, expensive and unstable starting materials such as dimethyl cadmium at high temperatures. Peng and Peng [10] reported the synthesis of

CdTe nanoparticles using CdO or Cd-fatty acid as precursors by replacing $Cd(CH_3)_2$. This so called 'green route' proved to be reproducible involving mild and simple reaction conditions, and could have potential for scale up and industrial applications. However, this process involves the presence of additional stabilizer such as hexylphosphonic acid (HPA) or tetradecylphosphonic acid (TDPA) which increases cost of production and the initial temperature of the reaction is still very high. Adaptations of this route whereby CdTe nanoparticles with varying shapes such as spheres, rods and tetrapods have been reported [11,12]. Dagtepe *et al*. [13] also observed the formation of small magic-sized CdTe quantum dots (QDs) in the presence of hexadecylamine (HDA) and TOPO as the coordinating solvent mixture at 240 ^{o}C using CdO as the cadmium-precursor. The growth kinetics of the CdTe QDs indicates coalescent or quantized growth of smaller QDs into larger QDs. Highly luminescent CdTe nanocrystals have been synthesized using $Li_2[Cd_4(SPh)_{10}]$ as the cluster compound and elemental tellurium with dodecylamine as a capping agent at 147 ^{o}C [14]. This reaction represents a safe and reproducible route for the formation of rod-shaped and branched particles.

An alternative to the organometallic route is the synthesis of water soluble thiol stabilized CdTe nanoparticles [15-17]. This route is generally simple, cheaper and yield particles that have higher quantum yields than the organically soluble particles. Recently one dimensional CdTe nanoparticles have been synthesized by an ambient pressure aqueous solution synthesis by employing inorganic precursors and L-cysteine as the stabilizing agent [18].

Recently our group have reported a hybrid method employing both solution chemistry and thermolysis at high temperatures for the synthesis of CdSe nanocrystals [19-21]. As an expansion of the range of high quality nano-sized semiconductors we have synthesized via this hybrid method [19-22], we have studied the effect of varying reaction parameters on the size and shape of the nanoparticles. This chapter describes the synthesis of high quality HDA and TOPO-capped CdTe nanocrystals using this method. A systematic study of the effect of reaction time, reduction time, Cd to Te precursor ratio, temperature and cadmium source on the size, optical properties and the morphology of the as-synthesized nanoparticles was also investigated.

2.1 *Experimental*

Tellurium powder, sodium borohydride ($NaBH_4$), deionized water, cadmium chloride, cadmium acetate, cadmium carbonate, cadmium nitrate, methanol, toluene, hexadecylamine (HDA), tri-*n*-octylphosphine oxide (TOPO) and tri-*n*-octylphosphine (TOP) were purchased from Aldrich. All chemicals were of analytical grade and used directly as purchased, without further purification.

2.1.1 *Synthesis of HDA-capped CdTe nanoparticles*

In a typical room temperature reaction, tellurium powder (0.041 g, 0.32 mmol) was mixed with deionised water (20.0 mL) in a three-necked flask. Sodium borohydride (0.031 g, 0.79 mmol) was carefully added to this mixture and the flask was immediately purged with nitrogen gas to create an inert atmosphere. After 2 h, the Cd source, $CdCl_2$ (0.059 g, 0.32 mmol) was dissolved in deionized water (20.0 mL) and added to the light grey tellurium ion solution. The solution was stirred for 30 min followed by the addition of excess methanol. The resultant solution was then

centrifuged. The CdTe produced was dispersed in tri-*n*-octylphosphine, TOP (6.0 mL) and stirred continuously to form a TOP-CdTe solution, which was then injected into hot hexadecylamine, HDA (6.0 g) at 160 ^{o}C. A sudden decrease in temperature was observed. The temperature was kept constant at 160 ^{o}C for 30 min with aliquots being removed at 5, 15, and 30 min. An immediate addition of methanol resulted in the reversible flocculation of the nanoparticles. The flocculate was separated from the supernatant by centrifugation. The resultant particles were dissolved in toluene to give a solution of CdTe nanoparticles for characterization.

The above reaction procedure was repeated with variation in the reaction parameters as described in 2.1.2-2.1.4

2.1.2 ***Effect of reduction time***

The Te powder reduction time was varied for a period of 4 and 6 hrs.

2.1.3 ***Effect of Cd:Te ratio***

To study the effect of Cd:Te ratio on the reaction, the Te powder precursor ratio was varied (0.08, 0.16, 0.24, 0.32 and 0.40 mmol).

2.1.4 ***Effect of cadmium source***

The reaction was further studied by replacing $CdCl_2$ with 0.32 mmol of $Cd(CH_3COO)_2$ (0.0853 g), $Cd(NO_3)_2$ (0.075 g), $CdCO_3$ (0.052 g). Reaction temperatures of 190, 230 or 270 ^{o}C were used.

2.1.5 *Synthesis of TOPO-capped CdTe nanoparticles*

The procedure is similar to the one described in section 2.1.1. Tellurium powder (0.041 g, 0.32 mmol) was mixed with deionized water (20.0 mL) in a three-necked flask. Sodium borohydride (0.031 g, 0.79 mmol) was carefully added to this mixture and the flask was immediately purged with nitrogen gas to create an inert atmosphere. After 2 h, the Cd source, $CdCl_2$ (0.059 g, 0.32 mmol) was dissolved in deionized water (20.0 mL) and added to the light grey tellurium ion solution. The solution was stirred for 30 min followed by the addition of excess methanol. The resultant solution was then centrifuged. The CdTe produced was dispersed in tri-*n*-octylphosphine, TOP (6.0 mL) and stirred continuously to form a TOP-CdTe solution, which was then injected into hot tri-*n*-octylphosphine oxide, TOPO (15.0 g) at 230 ^{o}C. A sudden decrease in temperature was observed. The temperature was kept constant at 230 ^{o}C with the reaction removed at 30 min. Methanol was immediately added to the solution to separate the liquid from the CdTe nanoparticles. After the process of centrifugation, the liquid layer was decanted and the particles were dissolved in toluene for characterization.

2.1.6 *Effect of reduction time*

The above reaction in section 2.1.6 was carried by varying the reduction times of Te powder for a period of 4 and 6 hrs.

2.2 *Characterization*

The as-synthesized particles were characterized by UV-Visible spectroscopy (UV), photoluminescence spectroscopy (PL), powder X-ray diffraction (XRD), transmission

electron microscopy (TEM), high resolution transmission electron microscopy (HRTEM) techniques.

2.2.1 *Optical characterization*

A Cary 50 conc. UV-Vis spectrometer was used to carry out optical measurements in the 200-800 nm wavelength range at room temperature. Diluted samples were placed in quartz cuvettes (1 cm path length). Toluene was used as a solvent.

Room-temperature PL spectra were recorded on a Perkin Elmer LS 55 luminescence spectrometer with Xenon lamp over 200-800 nm range. The samples were placed in quartz cuvettes (1 cm path length). Toluene was also used as a solvent.

2.2.2 *Powder X-Ray diffraction*

The crystallinity of the dried colloids was studied by using powder XRD. Powder diffraction patterns were recorded in the high angle 2θ range of 5-80^{o} using a Bruker AXS D8 Advance X-Ray diffractometer, equipped with nickel filtered Co Kα radiation (λ = 1.5418 Å) at 40 kV, 40 mA and at room temperature. The scan speed and step sizes were 0.05^{o} min^{-1} and 0.00657, respectively.

2.2.3 *TEM and HRTEM*

Samples were prepared by placing a drop of dilute solution of nanoparticles on Formvar-coated grids (150 mesh) for TEM and holey carbon grids for HRTEM. The samples were allowed to dry completely at room temperature and viewed using a JEOL 1010 TEM and JEOL 2100 HRTEM. Viewing was done at an accelerating voltage of 100 kV (TEM) and 200 kV (HRTEM), and images captured digitally

using a Megaview III camera; stored and measured using Soft Imaging Systems iTEM software.

2.3 Results and discussion

The method used in this study is an adaptation of the procedure reported by Oluwafemi and Revaprasadu [19] for CdSe nanoparticles. In this procedure, HDA-capped CdTe nanoparticles have been synthesized by the addition of an aqueous cadmium chloride solution to a freshly prepared oxygen-free NaHTe followed by injection into hot HDA. The reaction is shown in Scheme 2.1 below:

$$4\ NaBH_4 + 2\ Te + 7\ H_2O \xrightarrow[N_2,\ RT]{2\ h} 2\ NaHTe + Na_2B_4O_7 + 14\ H_2$$

$$NaHTe + CdCl_2 \xrightarrow[RT]{N_2} CdTe + NaCl + HCl$$

$$CdTe + TOP \xrightarrow[HDA]{160\ ^{\circ}C} HDA\ capped\ CdTe$$

Scheme 2.1 Equation for the formation of organically soluble CdTe nanoparticles (RT = room temperature).

2.3.1 *Effect of reaction time*

The synthesis of nanocrystals involves stages of nucleation and growth that may either take place separately or partially overlap in time. This is realized when the hot injection technique is applied, whereby the precursors are rapidly injected into a hot coordinating solvent resulting in very fast nucleation followed by subsequent growth of the nuclei at low temperatures. During the growth stage, a large number of colloidal particles compete for a finite amount of monomers, and the total number of particles decreases slowly due to dissolution of the small ones. The strong size

dependence of the optical properties of semiconductor nanocrystals allows one to monitor the mean particle size and the size distributions through the temporal evolution of UV-Visible and PL spectra [23].

2.3.1.1 *Effect of reaction time on HDA-capped CdTe nanoparticles: Optical properties*

The UV-Vis absorption spectrum (Figure 2.1a) of the HDA-capped CdTe nanoparticles prepared after 5 min. thermolysis exhibited a band gap at 691 nm (1.50 eV), a blue shift in relation to bulk CdTe (826 nm). The distinct excitonic shoulder characteristic of monodispersed CdTe nanoparticles is visible at *ca.* 620 nm. The corresponding photoluminescence spectrum shows defect free narrow band-edge emission, with the emission maximum at 668 nm (Figure 2.1b). Figure 2.2 shows the combined absorption spectra of the 5, 15 and 30 min. sample of the HDA-capped CdTe nanoparticles. There is a shift in the band gap to lower energies (15 min, 736 nm; 30 min, 775 nm) as the reaction time increases, indicating increase in average particle sizes from 5 to 30 min. It is evident from the pronounced excitonic feature of the 5 min sample that the smallest particles with a 'focused' size distribution are obtained early in the reaction [23]. This is in contrast with previous reports by Talapin *et al.* [24] who reported that prolonged (up to 20 h) heating improved the crystallinity and size distribution of dodecylamine (DDA) capped CdTe nanoparticles. In this work as the reaction time increases the sharpness of the transitions in the absorption spectra decreases or broadens, indicating an increase in the size distribution of the particles. The broadening of the absorption spectra with increase in reaction time could also be due to the presence of anisotropic particles.

The corresponding PL spectra of the particles obtained at the various reaction times (5, 15 and 30 min) show narrow emission peaks indicative of band-edge emission (Figure 2.3). There is a red shift as the reaction time increases indicative of particle growth. The full width at half-maximum (FWHM) of the emission peaks is 38 nm (5 min); 44 nm (15 min.) and 51 nm (30 min.). The lower value of the FWHM for the 5 min. sample confirms the narrow size distribution. There is also no evidence of recombination of electrons and holes from defect sites as observed previously for dodecylamine (DDA) capped CdTe nanoparticles. HDA as a capping group improves the photoluminescence quantum efficiency of the particles by effectively passivating the surface defects behaving as a non-radiative relaxation centre [25,26]. This is due to its high electron donating ability and high capping density as a result of its small stereochemical interference [27].

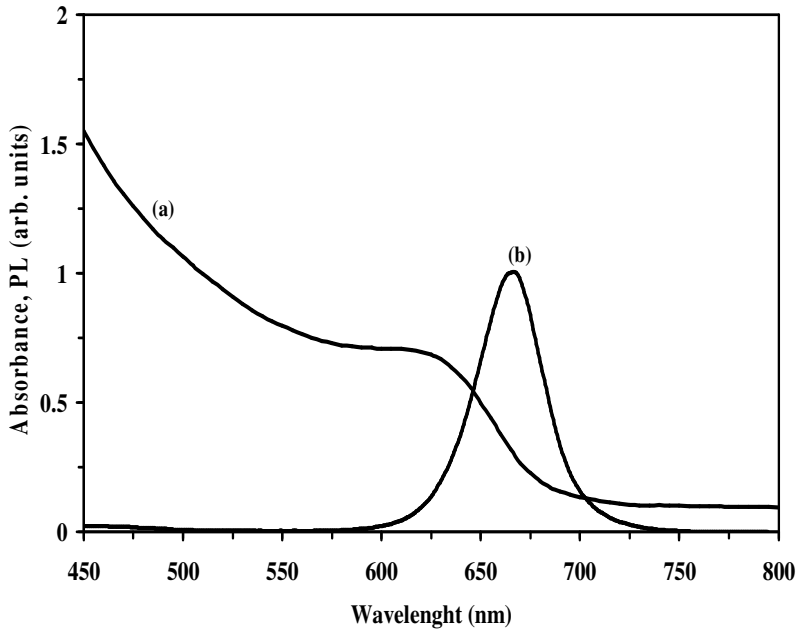

Figure 2.1 HDA-capped CdTe nanoparticles (5 min sample) (a) UV-Vis absorption and (b) Photoluminescence (PL) spectra.

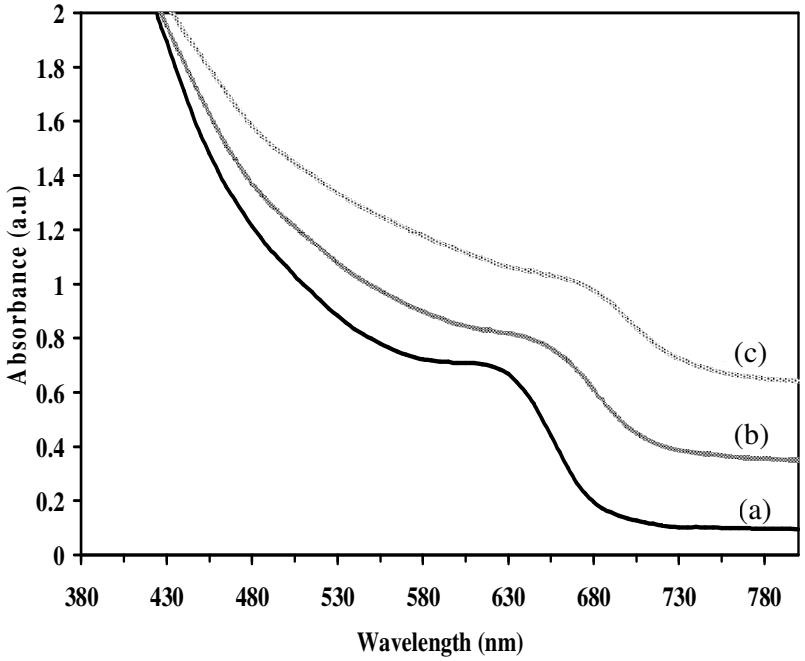

Figure 2.2 Absorption spectra of HDA-capped CdTe NPs at varying reaction times (a) 5, (b) 15 and (c) 30 min.

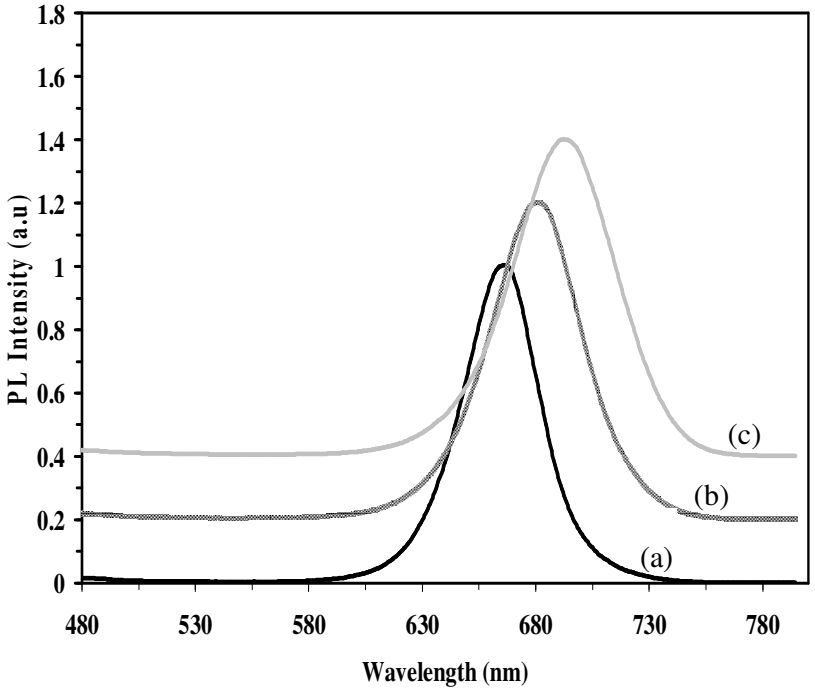

Figure 2.3 Photoluminescence spectra of HDA-capped CdTe NPs at varying reaction times (a) 5, (b) 15 and (c) 30 min. (λ_{exc} = 400 nm).

2.3.1.2 ***Effect of reaction time on HDA-capped CdTe particles: Structural properties***

The TEM and HRTEM study of the particles provides more information on the growth and shape of the particles with increase in reaction time. The TEM image of the 5 min. sample shows monodispersed, spherical particles with an average size of 5.51 ± 11 % (Figure 2.4a). The relatively narrow size distribution from the TEM measurements is consistent with the sharp band edge observed in the absorption spectrum. There is some aggregation of particles within the capping group matrix. The high resolution TEM image shows a well defined single particle with a diameter of 5.3 nm (Figure 2.4b). Distinct lattice fringes are observed; with the lattice spacing of 3.67 Å confirming the (111) plane of cubic CdTe. The HRTEM image of the 15 min. sample shows an array of elongated CdTe particles (Figure 2.4c). The anisotropic nature of the particles made it difficult to estimate particle sizes. The 30 min. sample is made up of spherical and elongated particles with the spherical particles having an average size of 7.53 ± 16 % (Figure 2.4d). From the electron microscopy studies it is evident that particle size, size distribution and shape change as the reaction proceeds during the first 30 min.

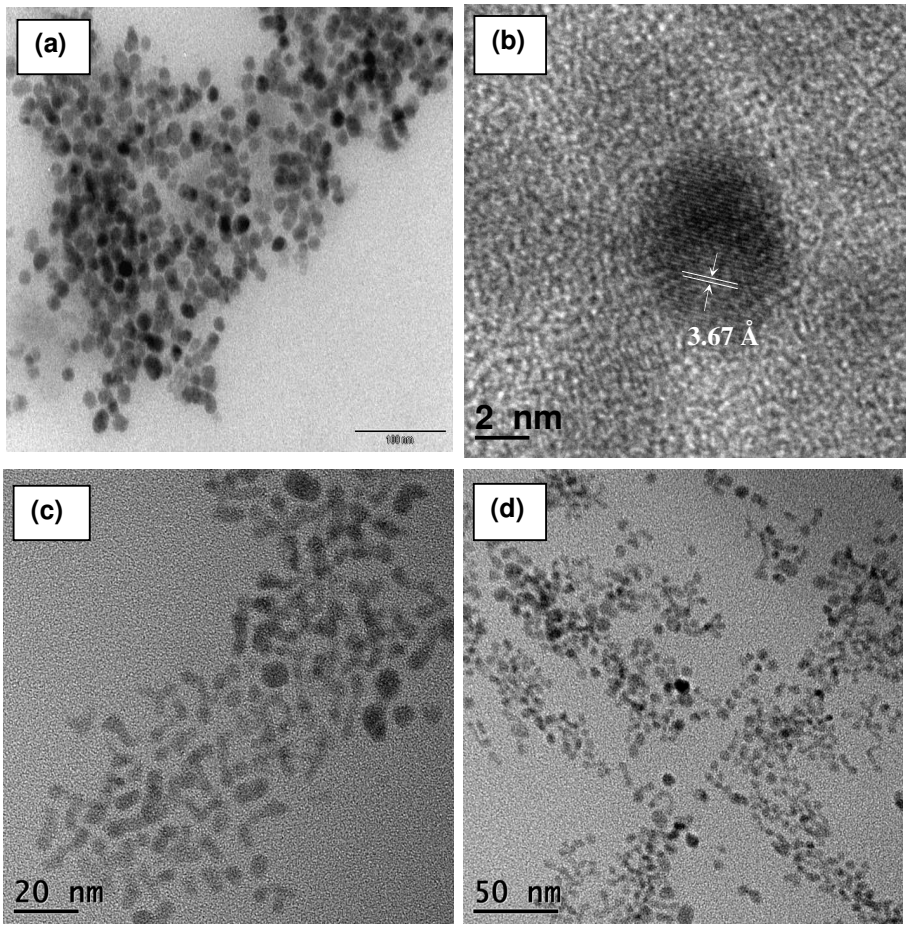

Figure 2.4 HDA-capped CdTe nanoparticles (a) TEM image of 5 min. sample and (b) corresponding HRTEM image showing a single spherical particle (c) 15 min. sample and (d) 30 min. sample.

The wide-angle powder X-ray diffraction peaks of the as-prepared CdTe nanoparticles appear broadened due to the reduced size of the particles. Three distinct diffraction peaks at 2θ values of 23.5°, 39.5° and 46.3° are observed corresponding to the (111), (220) and (311) reflections of the cubic zinc blend phase of bulk CdTe as shown in Figure 2.5. The high intensity of (111) peak indicates that the elongated particles have a large number of (111) planes, thus making that peak the dominant reflection in the first diffraction feature.

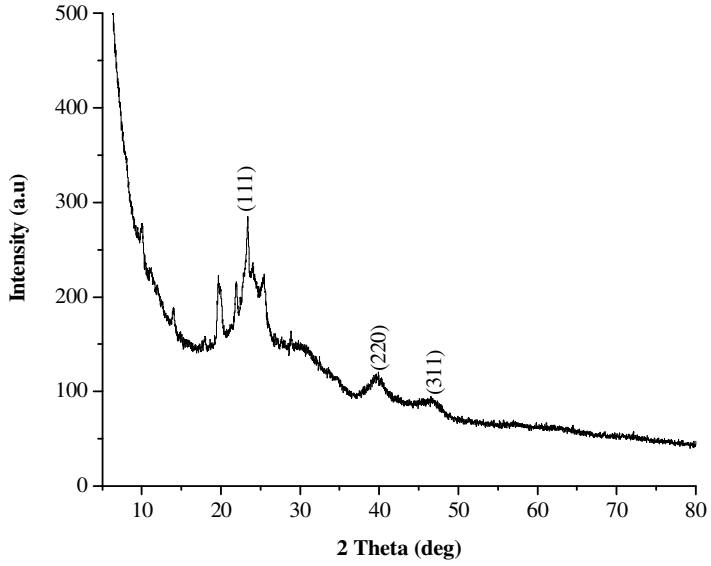

Figure 2.5 Powder X-ray diffraction pattern of HDA-capped CdTe nanoparticles of 30 min. sample.

2.3.1.3 ***Effect of reaction time on HDA-capped CdTe nanoparticles: Particle growth***

The sharp absorption transition and strong, narrow band edge emission of the particles obtained after just 5 min. reaction time shows that particles of high quality, defect free particles with a narrow size distribution can be obtained without prolonged heating as reported previously [23]. Focusing of the size distribution in the first 5 min. of the reaction occurs because small nanocrystals present in the solution are slightly larger than the critical size and grow faster than the larger ones [23]. Monodispersity is achieved through short nucleation period whereby kinetic control and focusing of the size occur. During the growth or Ostwald ripening stage a large number of colloidal particles compete for a finite amount of monomer and, the total amount of particles decreases slowly due to the dissolution of the small ones. The larger particles will continue to grow resulting in a defocusing of the size distribution. The capping group has significant influence on the size distribution of the particles, however in this work

the presence of monodispersed particles at 5 min. is likely due to a combination of factors that include the capping group, concentration of CdTe/TOP and reaction temperature. The rate of reduction of tellurium in the first step of the reaction procedure determines the concentration of tellurium ions and finally the concentration of the as formed CdTe after the addition of the cadmium salt. Due to the ionic nature of the as-formed CdTe, injection of the CdTe/TOP into the HDA at 160 °C results in the immediate decomposition of the monomers. The decomposition and nucleation stages are instantaneous, facilitating fast growth or focusing of particle size. The Ostwald ripening stage follows immediately, resulting in an increase in size distribution. We have observed a similar trend for HDA capped CdSe nanoparticles prepared by the same route [20].

The surfactant or capping group plays an important role in the final shape of the particle. In our work the appearance of particles of CdTe with an anisotropic morphology after 15 min. is due to the competition between the binding mechanism of the capping agent and the growth of nanocrystal by the Ostwald ripening process. Shape control is mainly through the preferential growth of a particular crystallographic surface during kinetically controlled growth. By using surfactants that bind differently to the crystallographic faces, one can control the shape of the nanocrystals [28]. At high temperatures (200 - 400 °C) the surfactant molecules are dynamically adsorbed to the surface of the growing crystal. A good surfactant molecule must be mobile enough to provide access for the addition of the monomer units, while stable enough to prevent aggregation of the nanocrystals. The surface molecule must be stable at the high temperature required for the growth. The choice of surfactants varies; a molecule that binds too strongly to the surface of the crystal is

not suitable, as it would hinder crystal growth. On the other hand, a weakly coordinating molecule would yield large particles, or aggregates. HDA gets absorbed selectively (with its amine) on the surface of the CdTe favouring the formation of anisotropic morphology and appreciable solubility [14]. There have been many previous reports of anisotropic (mainly rods) shaped CdTe particles capped by HDA [14,21,22,29,30].

2.3.2 *Effect of Te powder reduction time*

Any reaction in which the oxidation numbers of the atoms are changed is an oxidation-reduction reaction. Oxidation involves an increase in oxidation number, while reduction involves a decrease in oxidation number. In our reaction, tellurium is reduced from the 0 to -2 oxidation state, thus the first step of the reaction in Scheme 2.1 is referred to as a reduction reaction. The reduction reaction time was varied to 4 and 6 h. All the tellurium powder dissolved in water within 2 h, give rise to a light pink solution. The pink colour remained unchanged as the reduction time is increased. Before the addition of $CdCl_2$ at 4 and 6 h reduction times, the solution became pink for the entire reaction. The effect of these reduction times on the optical and structural properties of the HDA and TOPO-capped CdTe nanoparticles was studied.

2.3.2.1 *Effect of the reduction time on HDA-capped CdTe nanoparticles: Optical properties*

Figures 2.6 and 2.7 show the temporal evolution of the absorption and photoluminescence spectra of HDA-capped CdTe nanoparticles synthesized at 4 and 6 h reduction time. The absorption spectra (Figure 2.6) at 4 and 6 h reduction time reveals two excitonic peaks towards the blue part of the absorption spectrum and a

weak absorption peak towards the red (marked by arrows). The absorption peaks towards the blue originate from a subset of very small CdTe particles. Chin *et al.* [14] have reported this type of absorption pattern for CdTe synthesized from a cluster compound. In this work the first excitonic peak is broader and of low intensity than the second excitonic peak in the blue part of the absorption spectra for both 4 and 6 hrs reduction time. There is a shift in the absorption maxima to lower energies from 440 nm (first peak), 485 nm (second peak) to 442 nm (first peak), 485 nm (second peak) as the reduction time increased from 4 to 6 h, respectively.

The presence of two obvious emission peaks in all our photoluminescence spectra (Figure 2.7) is in agreement with the two excitonic peaks towards the blue. On the basis of previous reports this can be assigned to smaller magic-sized nanoclusters as well [13]. The first emission peak is narrow and of higher intensity than the second emission peak. The emission maximum is at 493 nm (first peak); 595 nm (second peak) and 493 nm (first peak); 590 nm (second peak) at the reduction times of 4 and 6 h respectively. This is in agreement with the prediction from the pink colour of the solution, before the addition of $CdCl_2$ in which no change in colour was observed, signifying no change or very slight increase in particle size as reduction time increases. The broad emission peaks seen in the PL spectra at 6 h reduction time (Figure 2.6) can be attributed to the presence of nanoparticles with different particle sizes and/or poor passivation within the growth time [31].

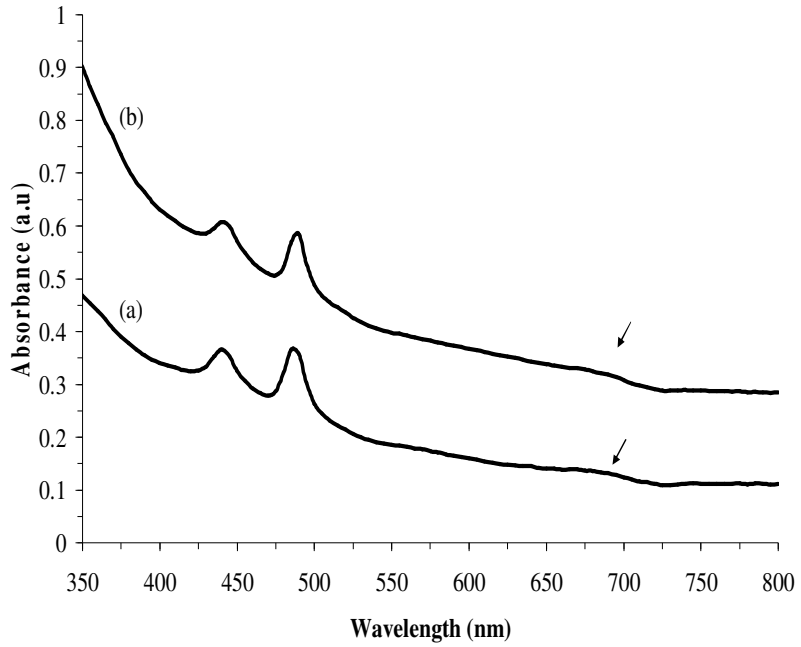

Figure 2.6 Absorption spectra of HDA-capped CdTe NPs at reduction times of (a) 4 and (b) 6 h.

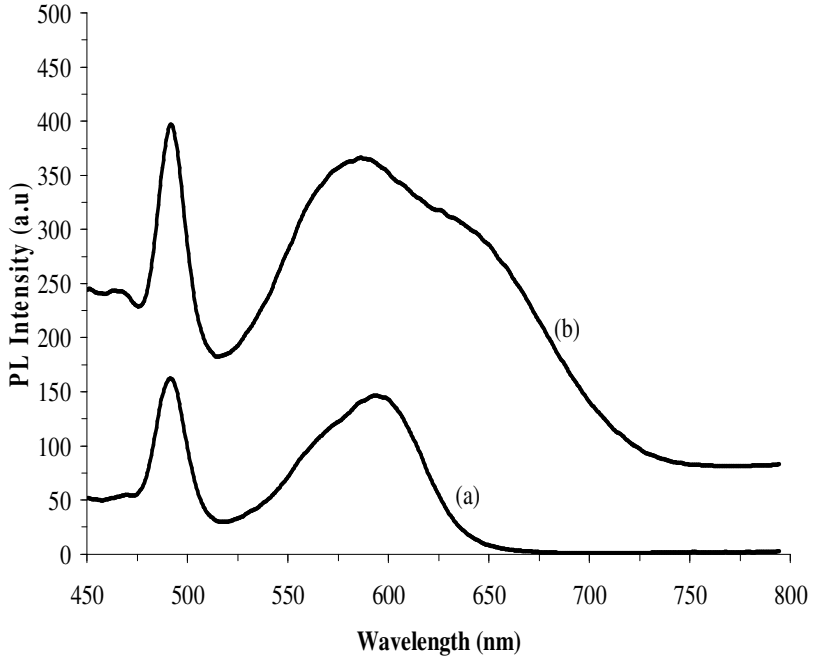

Figure 2.7 Photoluminesce spectra of HDA-capped CdTe NPs at reduction times of (a) 4 and (b) 6 h (Excitation wavelength is 400 nm).

2.3.2.2 *Effect of the reduction time on TOPO-capped CdTe nanoparticles: Optical properties*

To further investigate the effect of reduction time on the CdTe nanocrystals, the surface of the particles was passivated with TOPO a bulky capping group. The temporal evolution of the absorption and photoluminescence spectra of TOPO-capped CdTe nanocrystals synthesized at 2, 4 and 6 h reduction times are shown in Figure 2.8 and 2.9. All the UV-Vis absorption spectra for the TOPO-capped CdTe nanoparticles obtained with different reduction times showed well-resolved absorption peaks for the first electronic transition (Figure 2.8). The absorption band-edges are 502 nm (2 h), 537 nm (4 h) and 553 nm (6 h). This indicates that the particle size increases as the reduction time is increased.

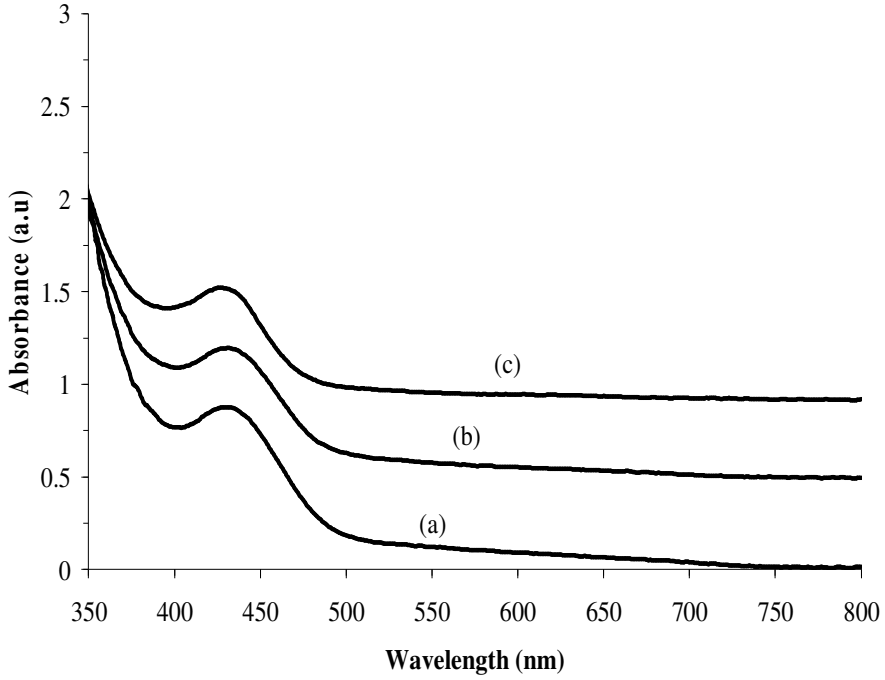

Figure 2.8 Absorption spectra of TOPO-capped CdTe NPs at reduction times of (a) 2 (b) 4 and (c) 6 h.

The emission maxima vary with the samples at different reduction time and are red-shifted from their respective absorption band-edges as shown in Figure 2.9. The emission maxima are 600 nm (2 h), 589 nm (4 h) and 598 nm (6 h) for the 2, 4 and 6 h samples, respectively. There is no clear trend in the position of the emission maxima with increase in reduction times. The FWHM is at 88 nm, 96 nm and 114 nm at 2, 4 and 6 h, respectively, indicating a broad size distribution. As expected, the CdTe nanocrystals synthesized in TOPO revealed broad photoluminescence spectra. This is due to a bulky nature of TOPO which provides increazed steric hindrance creating a smaller capping density [32,33].

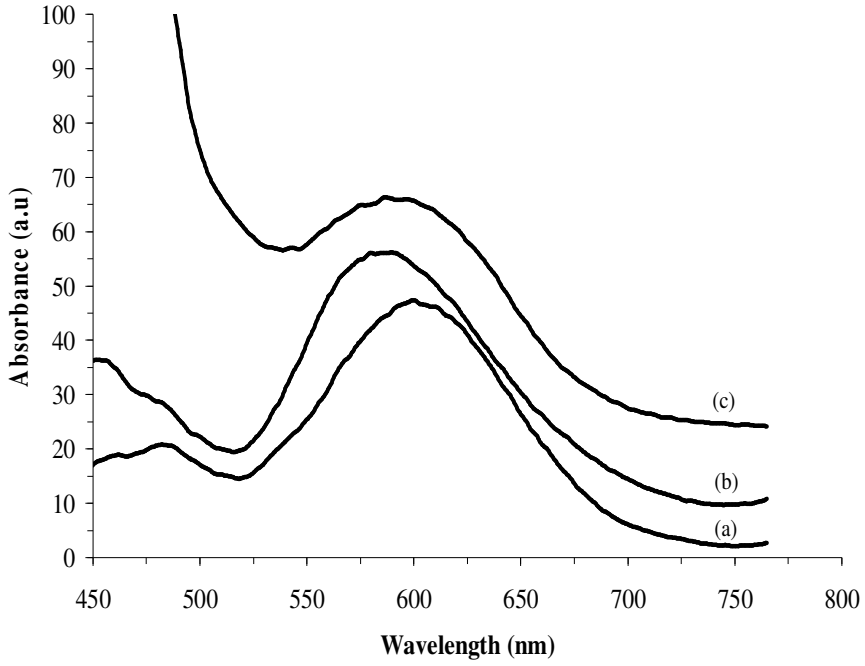

Figure 2.9 Photoluminescence spectra of TOPO-capped CdTe NPs at reduction times of (a) 2 (b) 4 and (c) 6 h.

2.3.2.3 *Effect of Te reduction time on TOPO-capped CdTe nanoparticles: Structural properties*

Figure 2.10 shows the TEM micrographs of CdTe samples prepared in TOPO after 2, 4 and 6 h reduction. The particles of all the samples (2, 4 and 6 h) have close to spherical, anisotropic morphologies, with a degree of aggregation also observed. The average particle sizes of close to spherical particles from 2 and 4 h sample of TOPO capped CdTe particles as calculated from the TEM image are 13.03 ± 2.90 nm and 8.26 ± 1.83 nm, respectively. The higher degree of aggregation of the close to spherical particles observed from the 6 h sample made it difficult to calculate the particles size.

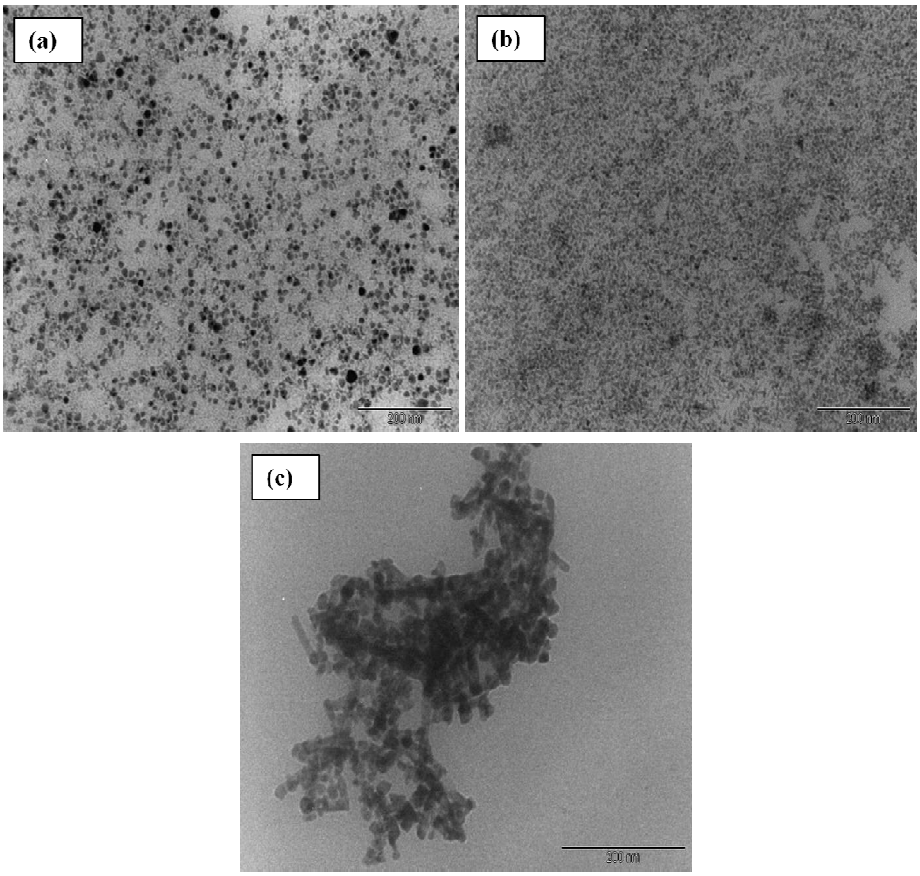

Figure 2.10 TEM images of TOPO-capped CdTe nanocrystals at reduction times of (a) 2 (b) 4 and (c) 6 h.

Figure 2.11 present the X-ray diffraction pattern of TOPO-capped CdTe nanoparticles synthesized after 2 h reduction. The broad nature of the XRD peaks was attributed to the nanocrystalline nature of the CdTe particles. The XRD pattern of the TOPO-capped CdTe nanocrystals shows four distinct diffraction peaks at 2 theta values of 24.2, 39.7, 43.4 and 46.8^{o}, respectively, corresponding to the (002), (110), (103) and (200) crystalline planes of hexagonal CdTe.

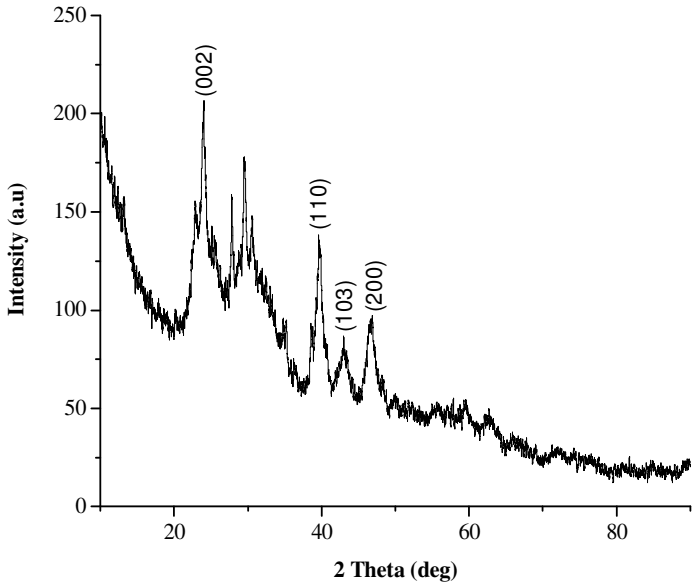

Figure 2.11 Powder X-ray diffraction pattern of TOPO-capped CdTe nanoparticles synthesised from $CdCl_2$ at 160 ^{o}C after 2 h reduction.

2.3.3 *Effect of Cd:Te ratio*

The influence of the precursor Cd to Te ratio on the properties of organically soluble CdTe nanoparticles has still not been investigated in detail. From the literature, the precursor Cd:Te ratio is usually set at 1:2 to 1:5 in the growth of water soluble CdTe nanoparticles [35-38]. We studied the effect of the Cd:Te precursor ratio on the optical features of the obtained CdTe nanocrystals with the other experimental

parameters fixed. The five equal concentration of $CdCl_2$ precursor solution, were added to different concentrations of NaHTe solution to obtain CdTe particles with Cd:Te precursor ratios of 1:0.25, 1:0.5, 1:0.75, 1:1 and 1:2.5 respectively. In the reactions tellurium was reduced for 2 h before the addition of $CdCl_2$, in five reaction vessels containing TOP-CdTe and HDA heated to 160 ^oC for CdTe growth.

2.3.3.1 *Effect of Cd:Te ratio on HDA-capped CdTe nanoparticles: Optical properties*

The results presented in Figure 2.12 and 2.13, indicate that the Cd to Te precursor ratio has an influence on the size and size distribution of HDA-capped CdTe nanocrystals under the adopted synthetic conditions; however no clear trend is observed. The absorption spectra (Figure 2.12) shows a shift in the band gap to 670 nm (1:0.25), 760 nm (1:0.5), 764 nm (1:0.75), 770 nm (1:1) and 854 nm (1:1.25) as Cd:Te ratio decreases. With the decrease of Cd:Te ratio from 1:0.25 to 1:0.5 and 1:1 to 1:1.25 the absorption maxima decrease from 595 to 584 nm and 635 to 612 nm, respectively. While, when the Cd:Te ratio was decreased from 1:0.5 to 1:0.75 and 1:0.75 to 1:1 the absorption maxima increased from 584 to 620 nm and 620 to 630 nm, respectively. The presence of extra lower wavelength peaks for 1:0.5, 1:0.75 and 1:1.25 ratio indicates the presence of small CdTe nanoparticles that disappears as growth time increases in favour of the formation of larger nanoparticles [13].

The photoluminescence spectra of the particles obtained at Cd:Te ratio of 1:0.25 to 1:1.25 shows narrow emission peaks indicative of band-edge emission (Figure 2.13). The FWHM of the emissions are 45, 42, 48, 36 and 42 nm at 1:0.25, 1:0.5, 1:0.75, 1:1 and 1:1.25, respectively. The lowest value of the FWHM (36 nm) indicates the

narrowest size distribution for the 1:1 ratio. There is no evidence of recombination of electrons and holes from defect sites. The emission maxima are 623 nm (1:0.25), 606 nm (1:0.5), 627 nm (1:0.75), 668 nm (1:1) and 630 nm (1:1.25). The additional lower wavelength emission peaks observed for 1:0.5, 1:0.75 and 1:1.25 are in agreement with the corresponding absorption spectra results.

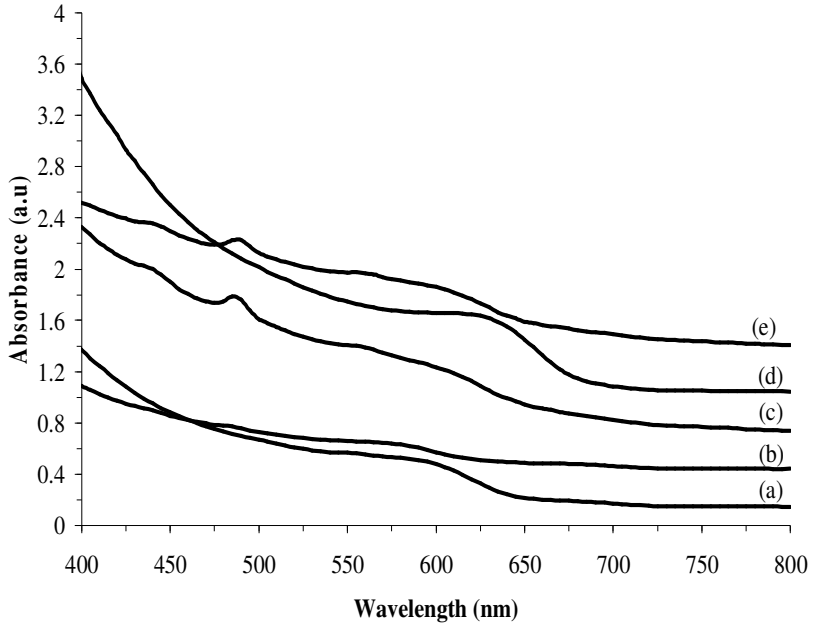

Figure 2.12 Absorption spectra of HDA-capped CdTe NPs obtained after 30 min. reaction time at different Cd:Te ratio (a) 1:0.25, (b) 1:0.5, (c) 1:0.75, (d) 1:1 and (e) 1:1.25.

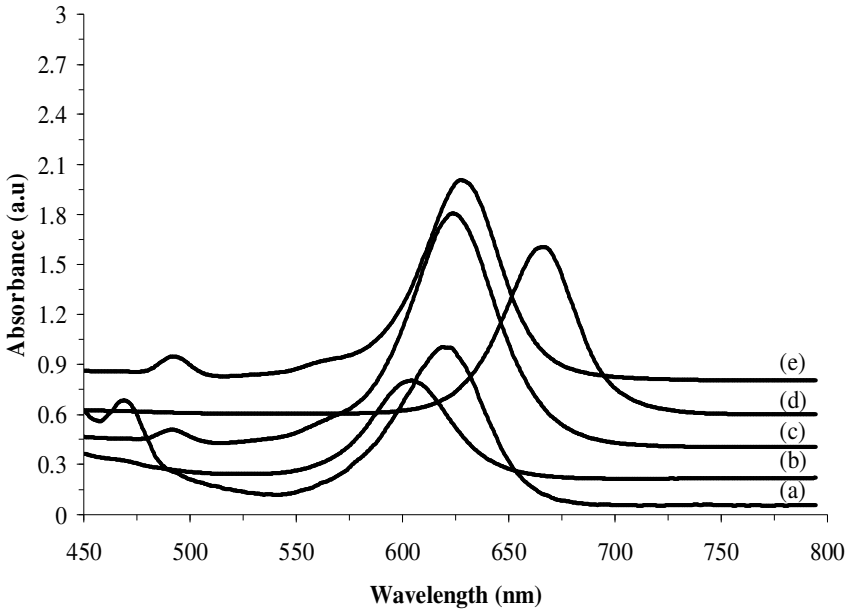

Figure 2.13 Photoluminescence spectra of HDA-capped CdTe NPs obtained at different Cd:Te ratio (a) 1:0.25, (b) 1:0.5, (c) 1:0.75, (d) 1:1 and (e) 1:1.25.

2.3.4 *Effect of cadmium source*

Ideally a system should form a relatively small amount of nuclei in a short period of time, and these formed nuclei will not consume the remaining monomers in a noticeable manner as they grow quickly to a desired elongated shape [10,27,41,42]. Therefore, less reactive precursors would be desirable. In principle, the alternative cadmium precursors which are more stable than the conventional dimethyl cadmium should be more suited for the growth of anisotropic nanostructures. In the previous work our group has chosen cadmium and lead salts as the metal sources for the synthesis of CdSe and PbTe nanoparticles [21,22]. These metal precursors were environmentally friendly, less reactive and relatively inexpensive. In the case of CdSe, the TOPO-capped CdSe nanoparticles synthesized using $CdCl_2$ and $CdSO_4$ were spherical in shape. However, when $CdCO_3$ is used as the cadmium source rod shaped particles are obtained for both the TOPO and HDA-capped CdSe

nanoparticles. A similar trend was observed for PbTe synthesized by the same method [22]. The HDA-capped PbTe particles were synthesized with $PbCl_2$, $Pb(NO_3)_2$ and $PbCO_3$ at temperatures of 190, 230 and 270 ^oC. The chloride and nitrate salts only produced spherical particles whereas the carbonate source gave distinct well aligned rods at reaction temperatures of 230 and 270 ^oC. The explanation given for this finding was that the suspension of the lead carbonate formed a shell of PbTe on its surface. This idea was confirmed by the FT-IR measurement on the intermediate. On injection, decomposition of the carbonate with subsequent kinetically controlled decomposition occurs leading to the formation of anisotropic PbTe particles. With the soluble salts, it seems likely that the particles are formed in an aqueous suspension and are subsequently annealed in the HDA or TOPO. The resultant fully formed metal chalcogenide particles are decomposed and grow into thermodynamically stable spherical particles.

In view of the above findings it was decided in this study to vary the cadmium source. The cadmium salts, $Cd(CH_3COO)_2$, $Cd(NO_3)_2$ and $CdCO_3$ were used as sources of cadmium. The reactions were carried out at elevated temperatures of 160, 230 and 270 ^oC similar to the temperatures used for PbTe synthesis.

2.3.4.1 *Effect of cadmium source on HDA capped CdTe nanoparticles: Structural and Optical properties*

Figure 2.14 shows the TEM and HRTEM images of HDA-capped CdTe nanoparticles synthesized from cadmium acetate at 190, 230 and 270 °C. The TEM image of the particles synthesized at 190 °C shows well defined particles with a uniform size and shape (Figure 2.14a). The shape of the particles is predominantly oblate with some

particles appearing elongated as confirmed by the corresponding HRTEM image. The particles are very crystalline with distinct lattice fringes observed. The lattice spacing of 3.79 Å corresponds to the (111) plane of cubic CdTe.

An increase in the reaction temperature to 230 °C resulted in particles with a slightly irregular shape with some degree of ordered aggregation. The particles tend to form chains (shown by arrows in Figure 2.14b) with attachment at the ends of the quasi spherical particles. The mechanism of growth involving the epitaxial fusion of particles through aggregation whereby the lattice planes are aligned relative to each other is known as oriented attachment [41-46]. The process is driven by the reduction in surface area that occurs during the aggregation process. The HRTEM image shows a particle which is imperfectly aligned, dislocations and stacking faults (shown by arrows) in the lattice planes are visible.

The use of cadmium acetate at the highest growth temperature, 270 °C produced larger irregular shaped CdTe particles (Figure 2.14c). The HRTEM image of a single particle shows distinct lattice fringes and no stacking faults. Further evidence for oriented attachment growth mechanism is observed for the CdTe particles synthesized from cadmium nitrate at 230 ºC. The TEM image (Figure 2.15a) show well defined nanorods with average lengths of (17.8 ± 5 nm) and breadths of (6.7 ± 1.3 nm). The HRTEM image (Figure 2.15b) shows a single nanorod with a length of 19.8 nm and width of 5.2 nm. There are discontinuities in the lattice fringes which are due to dislocations and stacking faults, an indication that the rods are not perfect single crystals.

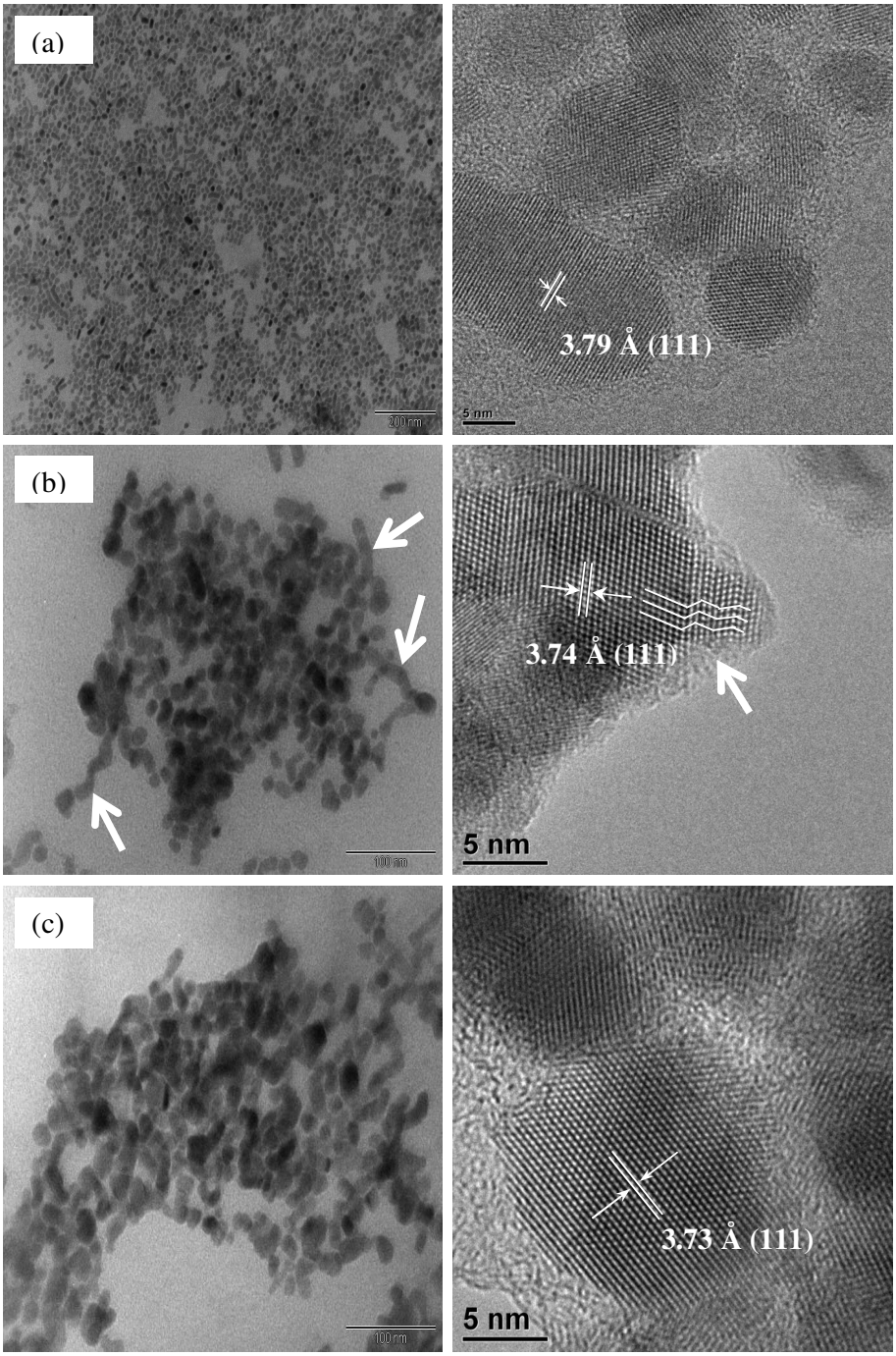

Figure 2.14 HDA-capped CdTe nanocrystals synthesized using $Cd(CH_3COO)_2$ after 2 h reaction time (TEM, left hand side and HRTEM, right hand side) at reaction temperatures of (a) 190 (b) 230 and (c) 270 ^oC.

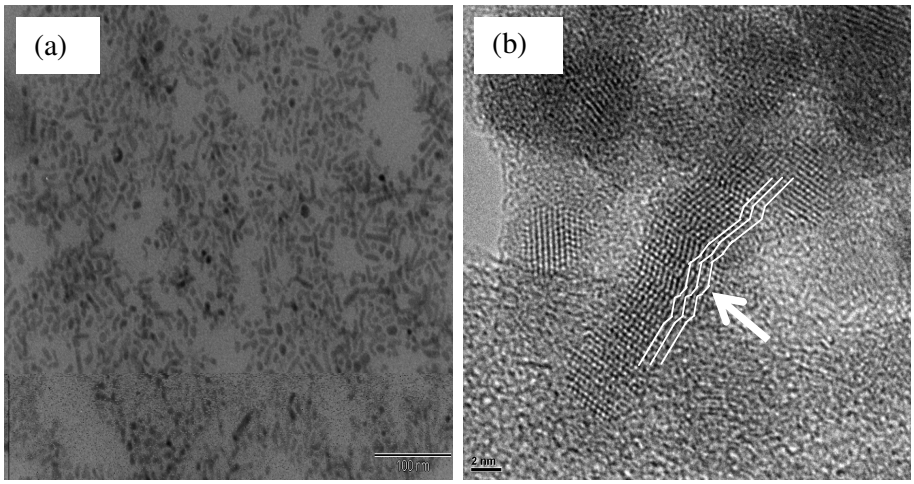

Figure 2.15 HDA-capped CdTe nanocrystals synthesized from $Cd(NO_3)_2$ at 230 °C after 2 h reaction time (a) TEM and (b) corresponding HRTEM images.

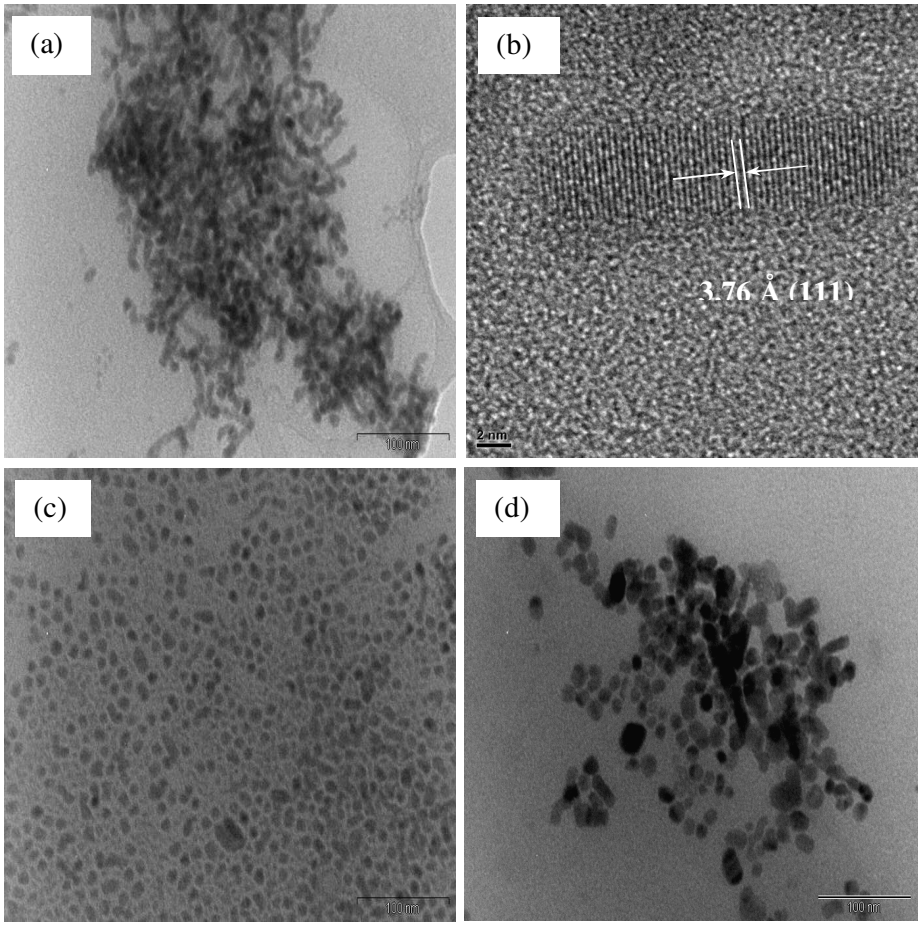

Figure 2.16 HDA-capped CdTe nanocrystals synthesized from $CdCO_3$ after 2 h reaction time synthesized at (a) 230 ^oC and (b) corresponding HRTEM; (c) TEM for 190 and (d) 270 ^oC.

The use of cadmium carbonate at a temperature of 230 ºC produced rod shaped particles (Figure 2.16a). The HRTEM image shows a well defined rod shaped particle (Figure 2.16b). The lattice planes show no discontinuities or stacking faults with the lattice spacing of 3.76 Å indexed to the (111) plane of cubic CdTe. When the growth temperature is lowered (190 °C), close to spherical particles (Figure 2.16c) are observed and at the highest temperature (270 °C) larger irregular shaped particles are present (Figure 2.16d). The powder X-ray diffraction patterns for the CdTe nanoparticles synthesized from the acetate, nitrate and carbonate sources are indexed to the cubic phase. The broadened (111), (220) and (311) planes of cubic CdTe observed in Figure 2.5 are also present in the diffraction patterns of the CdTe particles from the other three cadmium sources as shown in Figure 2.17

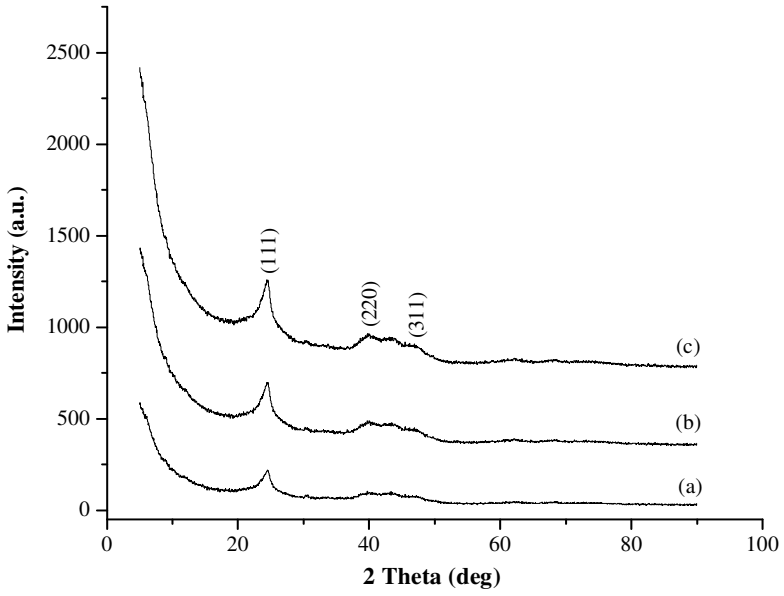

Figure 2.17 Powder X-ray diffraction patterns of HDA-capped CdTe nanoparticles synthesized from (a) $Cd(CH_3COO)_2$, (b) $Cd(NO_3)_2$ and (c) $CdCO_3$ sources at 230 °C after 2 h reaction.

The absorption spectra of the CdTe nanoparticles synthesized at 230 ºC from cadmium acetate, nitrate and carbonate are shown in Figure 2.18. The optical spectra of the CdTe particles show a distinct excitonic peak at 478 nm for both the acetate and nitrate samples, with additional peaks observed at 440 and 443 nm for the acetate and nitrate, respectively. Chin *et al.* have reported this type of absorption pattern for CdTe synthesized from a cluster compound [14]. They attributed the absorption peaks to small CdTe clusters. The band gaps are blue shifted from the bulk material with the acetate sample at 647 nm and the nitrate at 650 nm. The photoluminescence spectra show narrow emission with the emission maxima at 671 nm (acetate, Figure 2.19a) and 667 nm (nitrate, Figure 2.19b). The CdTe particles synthesized from cadmium carbonate shows a broad absorption curve with the absence of any excitonic features. The lack of excitonic features and a distinct absorption peak is due to the occurrence of rod shaped particles which do not always have a constant width and appear bent. The emission from the particles was very weak.

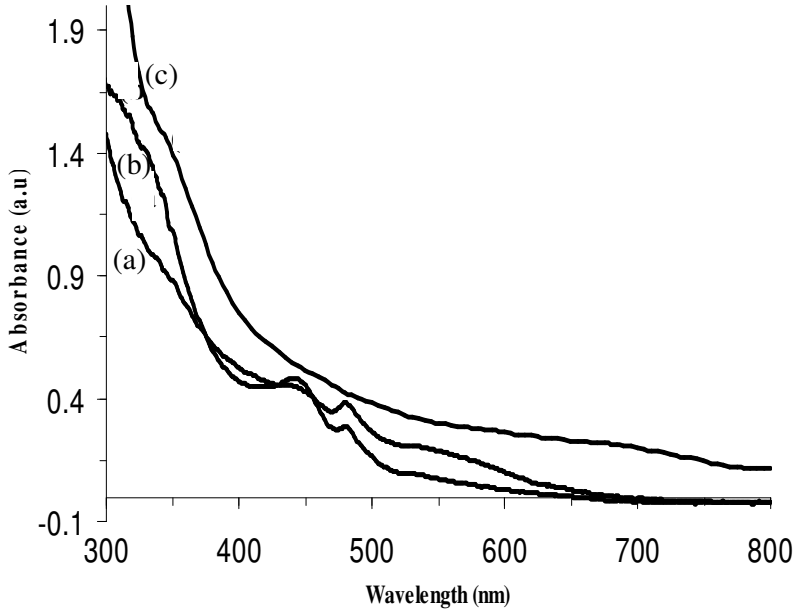

Figure 2.18 Absorption spectra of HDA-capped CdTe nanocrystals synthesized at 230 ^{o}C from (a) $Cd(CH_3COO)_2$, (b) $Cd(NO_3)_2$ and (c) $CdCO_3$.

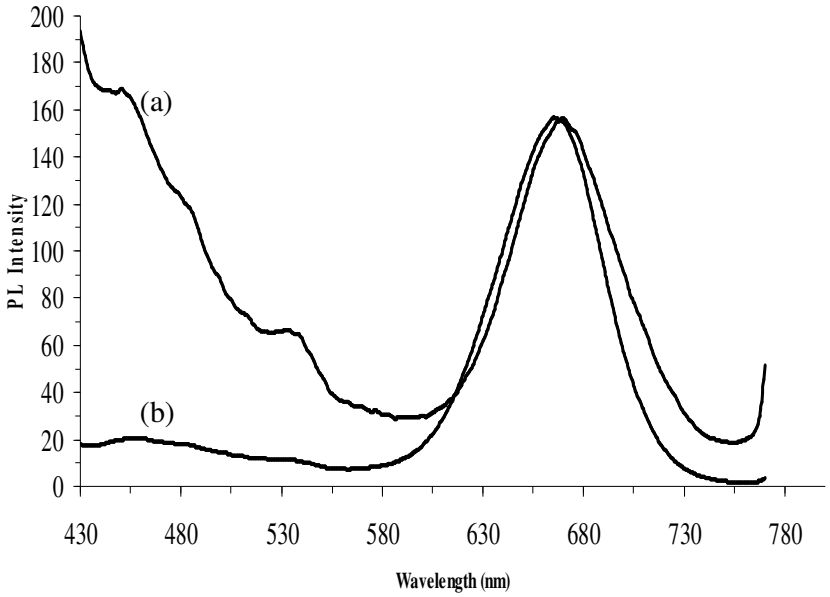

Figure 2.19 Photoluminescence spectra of HDA-capped CdTe nanocrystals synthesized at 230 ^{o}C (a) $Cd(CH_3COO)_2$ and (b) $Cd(NO_3)_2$.

We have observed from our previous work on PbTe and CdSe nanoparticles that the cadmium or lead source plays an important role in determining the final morphology of the particles [21,22]. When cadmium chloride or nitrate was used as a source of cadmium distinct spherical particles were observed; however, when the carbonate was used rod shaped particles were formed [21]. This shape evolution was attributed to the suspension of the lead or cadmium carbonate forming a shell of PbTe or CdSe on its surface as confirmed by FT-IR measurements on the intermediate [22].

2.3.4.2 *Effect of cadmium source on HDA-capped CdTe particles: Mechanism of growth*

Classically the growth of crystals has been explained by the Ostwald ripening process [20,46,47]. Small crystalline nuclei are formed in a supersaturated solution followed by crystal growth. During the growth or Ostwald ripening stage a large number of

colloidal particles compete for a finite amount of monomer and, the total amount of particles decreases slowly due to the dissolution of the small ones. The larger particles will continue to grow resulting in a defocusing of the size distribution. An emerging view of crystal growth is a process called 'oriented attachment' whereby larger particles are formed from smaller primary nanoparticles through attachment along a similar crystallographic direction as shown in Figure 2.20. The reduction in the overall surface free energy is the driving force for this spontaneous attachment process. This growth mechanism has been reported for several systems such as TiO_2 [42], CdTe [44], CdSe [48], ZnO [43] and PbSe nanorods [45].

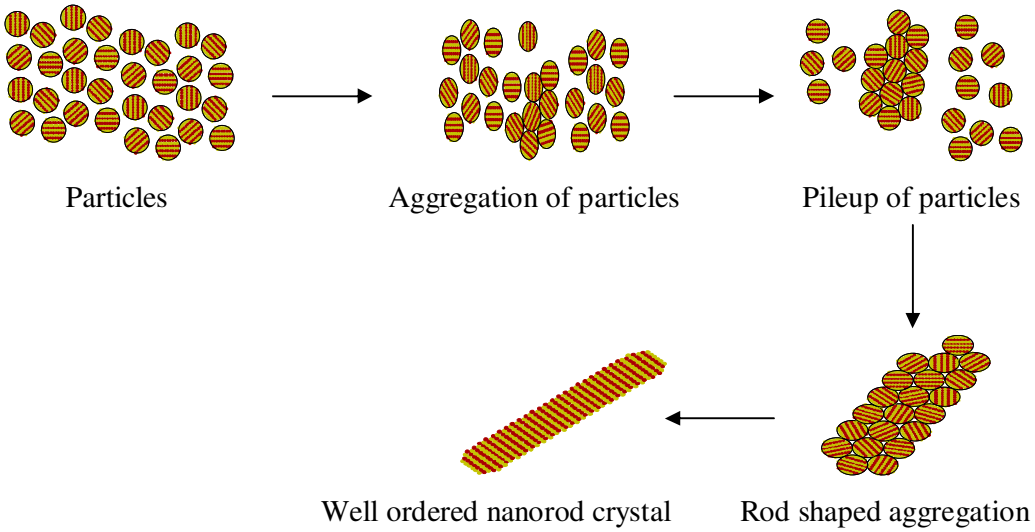

Figure 2.20 Basic scheme for mechanism of oriented attachment growth [18].

In this work we propose that the particles grow by two different mechanisms as determined by the cadmium source. The rods obtained by the acetate and nitrate sources show discontinuities or disruptions in the lattice planes, an indication that growth occurs via an oriented attachment process. The nanorods obtained from the carbonate source show no discontinuities in the lattice planes thereby indicating a

perfect crystal, where kinetically induced anisotropic growth occurs. The surface energy of the crystallographic faces of the initially formed seeds has a dominant effect on the anisotropic growth pattern of the nanoparticles. The surfactant, in this case hexadecylamine, can be selectively adsorbed onto the surface thereby modulating the surface energy. In this instance the suspension of the undissolved cadmium carbonate also selectively adheres to the surface of the CdTe nanoparticles thereby accentuating the difference in the growth rate between the crystallographic phases. Growth also occurs via Ostwald ripening resulting in the formation of nanorods.

2.4 ***Conclusions***

HDA and TOPO-capped CdTe nanoparticles have been synthesized via a facile non-organometallic route. A systematic study of the effect of reaction time, reduction time, Cd to Te precursor ratio, cadmium source and temperature on the optical and structural properties of the as-synthesized organically soluble CdTe nanoparticles was investigated. The increase in size and size distribution as the reaction proceeds in the first half an hour is due to dynamic reaction condition as the ionic precursor is thermolysed at high temperature. XRD studies show the formation of pure cubic crystal phase of CdTe. The absorption maxima are slightly shifted to lower energies (higher wavelengths) as the reduction time of Te increased from 2 to 6 h, indicating a slight increase in particle size for both the HDA and TOPO-capped CdTe. Decreasing the Cd:Te precursor ratio from 1:0.25 to 1:0.5 and 1:1 to 1:1.25 leads to a shift of absorption and emission maxima to lower wavelengths, while, decreasing Cd:Te from 1:0.5 to 1:0.75 and 1:0.75 to 1:1 leads to a shift of absorption and emission maxima to higher wavelengths when HDA was used as a capping agent. When the cadmium source is varied (cadmium acetate, nitrate and carbonate), changes in the morphology

of the HDA-capped CdTe particles were observed. The appearance of close to spherical or rod-shaped particles is due to the mechanism of growth associated with the variation of cadmium source and reaction temperature. The HRTEM images of the particles synthesized from the acetate and nitrate sources reveal discontinuities and faults in the lattice fringes indicating that growth occurs via an oriented attachment mechanism. The defect free rods obtained from the carbonate source also suggest that growth occurs via the traditional Ostwald ripening process.

2.5 *References*

[1] N. P. Gaponik, D. V. Talapin, A. L. Rogach, A. Eychmuller, *J. Mater. Chem.*, **10** (2000) 2163-2166.

[2] W. U. Huynh, J. J. Dittmer, A. P. Alivisatos, *Science*., **295** (2002) 2425-2427.

[3] Y. Wang, Z. Y. Tang, S. S. Tan, N. A. Kotov, *Nano Lett*., **5** (2005) 243-248.

[4] J. Lee, A. O. Govorov, N. A. Kotov, *Nano Lett*., **4** (2004) 2323-2330.

[5] D. K. Ivanou, E. A. Streltsov, A. K. Fedotov, A. V. Mazanik, D. Fink, A. Petrov, *Thin Solid Films*., **490** (2005) 154-160.

[6] N. N. Kolesnikov, V. V. Kveder, R. B. James, D. N. Borisenko, M. P. Kulakov, *Nuclear Instruments and Methods in Physics Research, A*., **527** (2004) 73-75.

[7] C. B. Murray, D. J. Norris, M. G. Bawendi, *J. Am. Chem. Soc.*, **115** (1993) 8706-8715.

[8] X. Peng, A. P. Alivisatos, *Nature*., **404** (2000) 59-61.

[9] D.V. Talapin, S. Haubold, A.L Rogach, A. Kornowski, M. Haase, H. Weller, *J. Phys. Chem. B*., **105** (2001) 2260-2263.

[10] Z. A. Peng and X. G. Peng, *J. Am. Chem. Soc*., **123** (2001) 183-184.

[11] S.D Bunge, K.M Krueger, T.J Boyle, M.A. Rodriguez, T.J. Headley, V.L Colvin, J. *Mater. Chem*., **13** (2003) 1705-1709.

[12] F. Shieh, A.E. Saunders, B.A. Korgel, *J. Phys. Chem. B*., **109** (2005) 8538-8542.

[13] P. Dagtepe, V. Chikan, J. Jasinski, V. L. Leppert, *J. Phys. Chem. C*., **111**, (2007) 14977-14983.

[14] P.T. K. Chin, J. W. Stouwdam, S.S van Bavel, R.A. J. Janssen, *Nanotechnol.*, **19** (2008) 205602-205610.

[15] T. Rajh, O.I. Micic, A.J. Nozik, *J. Phys. Chem*., **97** (1993) 11999-12005.

[16] L. Zou, Z. Gu, N. Zhang, Y. Zhang, Z. Fang, W. Zhu, X. Zhong, *J. Mater. Chem*., **18**, (2008) 2807-2815.

[17] M. Green, H. Harwood, C. Barrowman, P. Rahman, A. Eggeman, F. Festry, P. Dobson, T. Ng, *J. Mater. Chem*., **17** (2007) 1989-1994.

[18] T. Wang, Z. Jin, Y. Shi, W. Li, J. Yang, *Cryst. Growth and Design*., **9** (2009) 5077-5082.

[19] S. O. Oluwafemi, N. Revaprasadu, *New. J. Chem*., **10** (2008) 1432-1437.

[20] S. O. Oluwafemi, N. Revaprasadu, *Physica B*., **404** (2009) 1204-1208.

[21] N. N. Maseko, N. Revaprasadu, V. S. R. Rajasekhar Pullabhotla, R. Karthik, P. O'Brien, *Mater. Lett*., **64** (2010) 1037-1040.

[22] Ziqubu, N.; Ramasamy, K.; Revaprasadu, N.; Rajasekhar Pullabhotla V. S. R.; O'Brien, P. *Chem. Mater*., **22** (2010) 3817-3819.

[23] X. Peng, J. Wickham, A. P. Alivisatos, *J. Am. Chem. Soc*., **120** (1998) 5343-5344.

[24] D.V Talapin, S. Haubold, A.L Rogach, A. Kornowski, M. Haase, H. Weller, J. *Phys. Chem. B*., **105** (2001) 2260-2263.

[25] L. Qu, X. Peng, *J. Am .Chem. Soc*., **124** (2002) 2049-2055.

[26] D. V. Talapin, A. L. Rogach, A. Kornowski, M. Haase, H. Weller, *Nano. Lett*.,

1 (2001) 207-211.

[27] K. Nose, H. Fujita, T. Omata, S. O. Y. Matsuo, H. Nakamura, H. Maeda, *J. Lumin*., **126** (2007) 21-26.

[28] Y. Li, X. Li, C. Yang, Y. Li, *J. Chem. Mater*., **13** (2003) 2641-2648.

[29] S.N. Mlondo, N. Revaprasadu, P. Christian, P. O'Brien, *Polyhedron*., **28** (2009) 2097-2102.

[30] N. Moloto, N. Revaprasadu, P. L. Musetha, M. J. Moloto, *J. Nanosci. Nanotechnol*., **9** (2009) 4760-4766.

[31] K. Yu, S. Singh, N. Patrito, V. Chu, *Langmuir*., **20** (2004) 11161-11168.

[32] J. E. Bowen-Katari, V. L. Colvin, A. P. Alivisatos, *J. Phys. Chem.*, **98** (1994) 4109-4117.

[33] K. Satoh, Y. Takahashi, T. Suzuki, K. Sawasa, *Dalton Trans*., **259** (1989) 2185-2195.

[34] S. Kumar, T. Nann, *Chem. Comm*., **19** (2003) 2478-2479.

[35] H. Zhang, Z. Zhou, B. Yang, M. Y. Gao, *J. Phys. Chem. B*., **107** (2003) 8-13.

[36] J. Guo, W. Yang, C. Wang, *J. Phys. Chem. B*., **109** (2005) 17467-17473.

[37] L. Li, H. Qian, J. Ren, *Chem. Commun*., (2005) 528-530.

[38] Y. He, L. M. Sai, H. T. Lu, M. Hu, W. Y. Lai, Q. L. Fan, L. H. Wang, W. Huang, *Chem. Mater*., **19** (2007) 359-365.

[39] L. Manna, E. C. Scher, A. P. Alivisatos, *J. Am. Chem. Soc*., **122** (2000) 12700-12706.

[40] Z. A. Peng, X. G. Peng. *J. Am. Chem. Soc*., **123** (2001) 1389-1395.

[41] J. F. Banfield, S. A. Welch, H. Zhang, T. T. Ebert, R. L. Penn, *Science*., **289** (2000) 751-754.

[42] R. L. Penn, J. F. Banfield, *Geochim Cosmochim. Acta*., **63** (1999) 1549-1557.

[43] C. Pacholski, A. Kornowski, H. Weller, *Angew. Chem. Int. Ed*., **41**(7) (2002) 1188-1191.

[44] Z. Tang, N.A. Kotov, M. Giersog, *Science*., **297** (2002) 237-240.

[45] K-S. Cho, D.V. Talapin, W. Gaschler, C.B. Murray, *J. Am. Chem. Soc*., **127** (2005) 7140-7147.

[46] X. Peng, *Nano Res*., **2** (2009) 425-447.

[47] Q. Zhang, S. J. Liu, S.H. Yu, *J. Mater. Chem*., **19** (2009) 191-207.

[48] N. Pradhan, H. Xu, X. G. Peng, *Nano. Lett.*, **6** (2006) 720-724.

CHAPTER THREE

SYNTHESIS OF WATER SOLUBLE CADMIUM TELLURIDE NANOPARTICLES

3.0 *Introduction*

Colloidal quantum dots (QDs) are of interest in biological and biomedical fields because of their unique properties, which include their tunable emission wavelength, broad absorption and sharp emission spectra, high quantum yields (QY), resistance to the chemical degradation and photobleaching, and versatility in surface modification [1-3]. Some water-soluble QDs conjugated with biomolecules have been successfully used in fluorescent resonance energy transfer (FRET), *in vivo* and *in vitro* imaging, immunoassay, DNA hybridization and potential photodynamic therapy [4-10]. Water-soluble semiconductor nanoparticles can be obtained by two principal methods. The first is to replace the organically soluble surface-capping molecules on the particles with water-soluble thiols or a silica shell [11-14]. However, after the substitution of the surface-capping molecules by hydrophilic molecules, the nanoparticle photoluminescence decreases markedly [11,15,16]. The second method is to directly synthesize the semiconductor nanoparticles in an aqueous solution using water-soluble stabilizers such as thiols [16-18]. This method is cheaper, simpler, less toxic and yields particles that exhibit higher quantum yields.

CdTe is one of the most important II-VI semiconductor materials due to its very high PL quantum efficiencies. CdTe nanocrystals illuminate within the visible spectral range from 500 to 730 nm depending on the particle size. The utilization of highly luminescent thiol-capped CdTe nanocrystals in light-emitting devices (LEDs) [19], photonic [20] and core-shell structures [21], and as biological labels [22] has been reported. Some reports have shown the attraction of this material for light to energy conversion [23]. After the first aqueous synthesis of mercaptoethanol and thioglycerol-capped CdTe nanocrystals [24], tremendous progress has been made in

the preparation and the design of the surface properties of thiol-capped CdTe nanocrystals. In the past decade, there have been major efforts towards improving the spectral properties of CdTe nanocrystals (NCs) prepared directly in the aqueous phase. For example, Weller and co-workers have explored the effects of various thiol ligands (including mercapto acid, mercapto alcohol, and mercapto amine) on the preparation of CdTe QDs in the aqueous phase [17]. Gao *et al.* have also investigated the influence of pH and photo-illumination on the luminescence of water-dispersible CdTe QDs [25-27].

Several groups have systematically explored the influence of various synthetic variables (including pH value, precursor concentration, ligand:Cd ratio, and Te:Cd ratio) on the growth of CdTe nanoparticles [28-30]. Zou *et al.* [31] reported a facile aqueous phase route to prepare high-quality CdTe NCs with mercaptopropionic acid as the capping agent. The CdTe nanoparticles prepared with this method have emission efficiency up to 50 % within 1 h reflux time under the optimized experimental conditions. The influence of various experimental variables, including Te:Cd ratio, ligand:Cd ratio, pH values as well as the precursor concentration, on the growth rate and luminescent properties of the obtained CdTe nanoparticles was also investigated. Abd El-Sadek *et al.* [32] synthesized water-soluble CdTe nanoparticles in aqueous solution with the assistance of mercaptoacetic acid (MAA) by a wet chemical route method. More recently, Li *et al.* [33] reported a convenient way for the synthesis and purification of L-cysteine stabilized CdTe QDs. The prepared QDs possessed good fluorescent properties such as wide UV absorption, symmetrical emission peaks with FWHM of 20-50 nm and high fluorescence intensity.

The Revaprasadu group have reported a facile one-pot synthetic route for the synthesis of highly water-soluble CdSe and Au-CdSe hybrid nanoparticles passivated with cysteine without the use of any additional stabilizer [34,35]. The cysteine amino acid was chosen to cap the CdSe and Au-CdSe hybrid nanoparticles as it passivates the surface states of nanoclusters more effectively than other thiols thereby enhancing their emission properties [36,37]. These bio-conjugated nanoparticles could be of use as tags for proteins, or DNA, recognition of specific antibodies or antigens through luminescence emission measurements and for the potential development of bionsensors. The work was extended to the synthesis of ascorbic acid-capped ZnSe nanoparticles at room temperature [38]. By varying the pH of the solution, the optical properties and morphology of the material were tuned. The use of ascorbic acid, which can act as conjugating agent, allows for attachment of nanoparticles to biomolecules such as cyclodextrins, collagen for medical applications. This chapter describes the synthesis of CdTe nanocrystals capped by two water-soluble ligands, cysteine and triethanolamine in an aqueous medium. The effect of various experimental variables, including the capping ligand, pH, reaction time and cadmium source on the particle growth, optical properties and morphology were systematically investigated.

3.1 *Experimental*

Tellurium powder, sodium borohydride ($NaBH_4$), deionized water, cadmium chloride, cadmium acetate, cadmium carbonate, cadmium nitrate, methanol, acetone, L-cysteine ethyl ester hydrochloride, and triethanolamine (TEA) were purchased from Aldrich. All chemicals were of analytical grade and used directly as purchased without further purification.

3.1.1 *Synthesis of cysteine-capped CdTe nanoparticles*

In a typical room temperature reaction, tellurium powder (0.041 g, 0.32 mmol) was mixed with deionized water (10.0 mL) in a three-necked flask. The 10.0 mL aqueous solution of sodium borohydride (0.031 g, 0.79 mmol) was carefully added to this mixture and the flask was immediately purged with nitrogen gas to create an inert atmosphere. After 2 h, 20.0 mL aqueous solution of $CdCl_2$ (0.059 g; 0.32 mmol) was added to the light grey tellurium ion solution, followed by the addition of L-cysteine ethyl ester hydrochloride solution (20.00 ml) with a molar ratio of 1:20 (Cd^{2+}: cysteine ester). The pH of the solution was raised to 7, after which the solution was then heated at 90 ^{o}C for 24 h. An aliquot was withdrawn after 3 h. An immediate addition of methanol resulted in the reversible flocculation of the nanoparticles. The flocculate was separated from the supernatant by centrifugation. The resultant particles were dissolved in acetone to give a solution of nanocrystallites for characterization.

The reaction procedure described in 3.1.1 was modified with the following changes in the experiments described in 3.1.2-3.1.4

3.1.2 *Effect of pH*

The reactions were studied at pH 4, 7 and 11.

3.1.3 *Effect of reaction time*

To study the effect of reaction time, the aliquots were withdrawn at different reflux times, 5 min, 15 min, 30 min, 1 h, 3 h, 5 h and 24 h.

3.1.4 *Effect of cadmium source*

The reactions were further studied by using different cadmium sources: $Cd(CH_3COO)_2$ (0.0853g), $Cd(NO_3)_2$ (0.075g) and $CdCO_3$ (0.052g).

3.1.5 *Synthesis of TEA-capped CdTe nanoparticles*

The procedure was similar to that described in section 3.1.1. Tellurium powder (0.041 g, 0.32 mmol) was mixed with deionized water (10.0 mL) in a three-necked flask. 10.0 mL of an aqueous solution of sodium borohydride (0.031 g, 0.79 mmol) was carefully added to this mixture and the flask was immediately purged with nitrogen gas to create an inert atmosphere. After 2 h, 20.0 mL aqueous solution of $CdCl_2$ (0.059 g; 0.32 mmol) was added to the light grey tellurium ion solution, followed by the addition of 20.0 mL triethanolamine (TEA) solution with a molar ratio of 1:20 (Cd^{2+}: TEA). The pH of the solution was raised to 7 after which the solution was then heated at 90 ^{o}C for 24 h. An aliquot was withdrawn after 3 h. An immediate addition of methanol resulted in the reversible flocculation of the nanoparticles. The flocculate was separated from the supernatant by centrifugation. The resultant particles were dissolved in acetone to give a solution of nanocrystallites for characterization.

The reaction procedure described in 3.1.5 was modified with the following changes in the experiments described in 3.1.6 -3.1.8

3.1.6 *Effect of pH*

The reactions were studied at pH 4, 7 and 11.

3.1.7 *Effect of reaction time*

For the study of the effect of reaction time, the aliquots were withdrawn at different refluxing time, 5 min, 15 min, 30 min, 1 h, 3 h, 5 h and 24 h.

3.1.8 *Effect of cadmium source*

The reactions were further studied by using different cadmium sources: $Cd(CH_3COO)_2$ (0.0853g), $Cd(NO_3)_2$ (0.075g) and $CdCO_3$ (0.052g).

3.2 *Instrumentation*

The as-synthesized particles were characterized using similar techniques as described in Chapter Two. In addition Fourier Transform Infrared Spectroscopy (FT-IR) was also used to characterize the nanoparticles and capping agents.

3.2.1 *IR Spectroscopy*

For FT-IR measurements, pure solid samples were dried and ground to fine powder while liquid TEA was measured directly and the spectra were recorded using a Tensor 27, Bruker FT-IR Spectrometer.

3.3 *Results and discussion*

In this synthetic procedure, colloidal CdTe nanoparticles have been synthesized by the simultaneous addition of an aqueous solution of cadmium chloride and ligand, to a freshly prepared oxygen-free NaHTe solution. The reaction was then refluxed at 90 ^oC for 3 h. The capping ligands used were cysteine and triethanolamine (TEA). The reactions are shown in Scheme 3.1:

$$4\ NaBH_4 + 2\ Te + 7\ H_2O \xrightarrow[N_2,\ R.T]{2\ h} 2\ NaHTe + Na_2B_4O_7 + 14\ H_2$$

$$NaHTe + CdCl_2 \xrightarrow[90\ ^oC,\ 24\ h]{Ligand} \text{Ligand-capped CdTe} + NaCl + HCl$$

Scheme 3.1 Equation for the formation of ligand-capped CdTe nanoparticles at 90 ^oC (R.T = room temperature, Ligand = cysteine, TEA).

3.3.1 *Effect of capping agent*

Previous research has focused on pure thio-stabilized CdTe [28,39-41], but there are only few reports on the effect of other water soluble ligands on these functionalized nanomaterials on luminescence performance and structure. We have selected two such ligands, i.e. cysteine and triethanolamine, as capping agents for water soluble CdTe quantum dots. The molecular structures of cysteine and triethanolamine are shown in Figure 3.1.

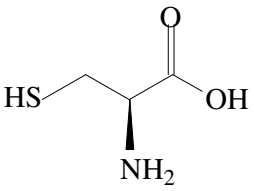

L-Cysteine

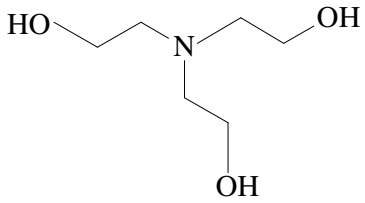

Triethanolamine

Figure 3.1 The molecular structures of cysteine and triethanolamine.

3.3.1.1 *Effect of the capping agent on CdTe nanoparticles: Optical properties*

To analyze the effect of the capping agent, TEA and cysteine were used as capping agents. Figure 3.2 shows the absorption spectra of TEA and cysteine capped CdTe nanoparticles prepared under similar conditions. The absorption peak at 264

(cysteine) and 255 nm (TEA) can be attributed to the Cd-ligand complex. Similar observations have been reported for water-soluble cysteine-capped CdS and CdSe nanoparticles [34,37]. The cysteine-capped CdTe nanoparticles display an absorption peak (439 nm) further with a band edge at 523 nm. The TEA-capped particles also display several low intensity absorption peaks at low energies which are characteristic of CdTe nanoparticles. The increase in number of absortion peaks in TEA-capped CdTe probably reveals the polydispersity of the material. The size of sulphur in cysteine is also larger than nitrogen of TEA therefore increasing the capping efficiency of cysteine [42,43].

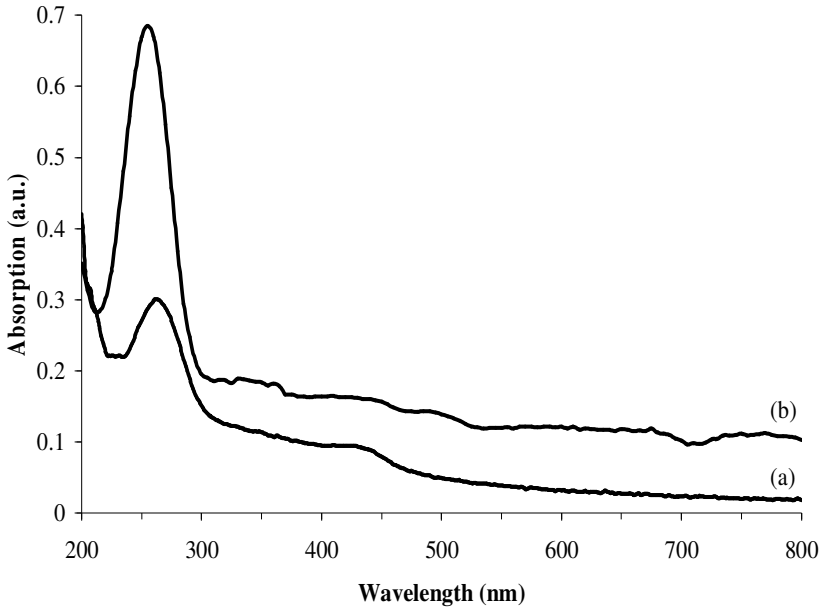

Figure 3.2 UV-Vis absorption spectra of CdTe nanoparticles from $CdCl_2$ at pH 7 with different capping agents; (a) cysteine and (b) TEA.

Figure 3.3 shows the room temperature PL spectra of CdTe nanoparticles excited at 275 nm for the two surfactants (TEA and cysteine). The emission maxima are observed at 416 nm (cysteine) and 413 nm (TEA) with a FWHM of 92 and 97 nm,

respectively. There is very little difference in PL maxima position for both samples. The difference in the intensity of the absorption and photoluminescence spectra of the two samples may be attributed to the difference in concentration of CdTe nanoparticles in the solutions [44].

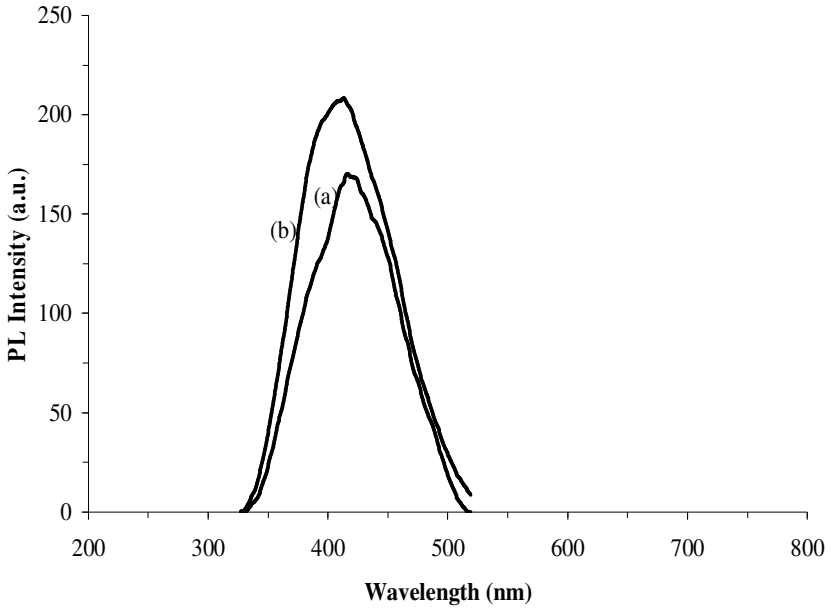

Figure 3.3 Photoluminescence spectra of CdTe nanoparticles from $CdCl_2$ at pH 7 with different capping agents; (a) cysteine and (b) TEA.

3.3.1.2 *Effect of capping agent on CdTe particles: Structural properties*

Figure 3.4 shows TEM images of CdTe particles capped with cysteine and TEA with similar magnifications. Figure 3.4a shows that the cysteine-capped CdTe particles are close to spherical in nature, with an average size of 3.07 ± 0.66 nm. The TEA-capped particles (as shown) in Figure 3.4b are also close to spherical with an average particle size of 3.26 ± 0.41 nm. In both TEM images the particles appear well defined and are generously dispersed.

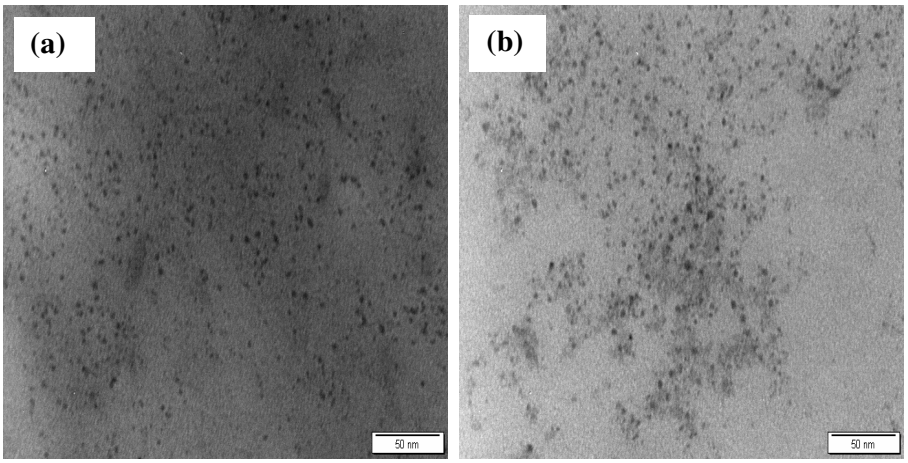

Figure 3.4 TEM images of CdTe nanoparticles from $CdCl_2$ at pH 7 synthesized with different capping agents (a) cysteine and (b) TEA.

3.3.2 *Effect of pH*

In the aqueous synthesis of quantum dots, pH is an important factor that influences the photoluminescence quantum yield of aqueous QDs [39,40]. In the investigation of the pH effect on the CdTe nanoparticles, we fixed the Cd:Te:ligand ratio at 1:1:20 and varied the pH from 4.0, to 7.0 and 11.0.

3.3.2.1 *Effect of pH on cysteine-capped CdTe nanoparticles: Optical properties*

The normalized absorption spectra of the cysteine-capped CdTe nanoparticles synthesized using three different pH values (4, 7 and 11) after 3 h of reflux are shown in Figure 3.5. The presence of an absorption maxima in the UV region of the spectrum located at 265 nm (pH 4), 267 nm (pH 7) and 268 nm (pH 11), is attributed to Cd^{2+}- cysteine complex. The sample obtained at pH 11 shows a distinct additional absorption peak at 455 nm with a band edge at 516 nm attributed to the cysteine-capped CdTe particles. The value for the absorption edge is significantly blue shifted from the bulk CdTe value which is 826 nm indicating strong quantum confinements [45]. There is an absence of clearly resolved absorption shoulders for samples at pH 4

and pH 7. Optical spectroscopy studies on cadmium thiol complexes has revealed that the ionisation of thiol groups and subsequent complexation with the nanoparticle surface, dramatically decreases as the pH of the solution decreases from neutral to the acidic range and no complexation occurs at pH < 4 [46-48]. Chatterjee *et al*. [37] have shown that the rate of ionisation and complexation of the thiol group increases as the pH of the solution increases from acidic to basic. As the pH of the solution increases from acidic to basic, the ionisation of the thiol group is enhanced, the particle size becomes smaller and absorption shoulder becomes narrower, hence there is little influence from the unreacted thiol group. In this work, the appearance of the absorption shoulder on the sample prepared at pH 11 reveals that as pH increases, complexation increases resulting in the formation of the cysteine-capped CdTe nanoparticles.

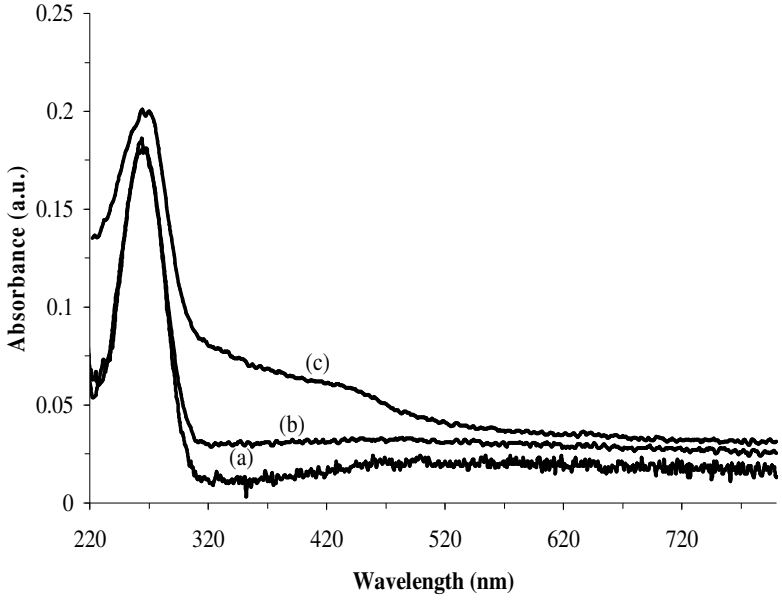

Figure 3.5 Absorption spectra of cysteine-capped CdTe nanoparticles from $CdCl_2$ at (a) pH 4 (b) pH 7 and (c) pH 11.

The cysteine-stabilized CdTe nanoparticles also show pH-dependent photoluminescence (Figure 3.6). Previous reports also indicate strong dependence of PL on the pH of solution [27,45]. The emission maxima of the particles at different pH are 416 nm (pH 4), 410 nm (pH 7) and 450 nm (pH 11). The emission wavelength did not reveal any clear trend with an increase in the pH values. The FWHM of the band-edge luminescence was 97 nm (pH 4), 96 nm (pH 7) to 108 nm (pH 11), which indicates a broad size distribution of the as-prepared CdTe nanoparticles. The abrupt shift in the emission maxima as the pH changes from acidic to basic implies that ionisation and complexation of the thiol groups, has an influence on the growth rate of the particles.

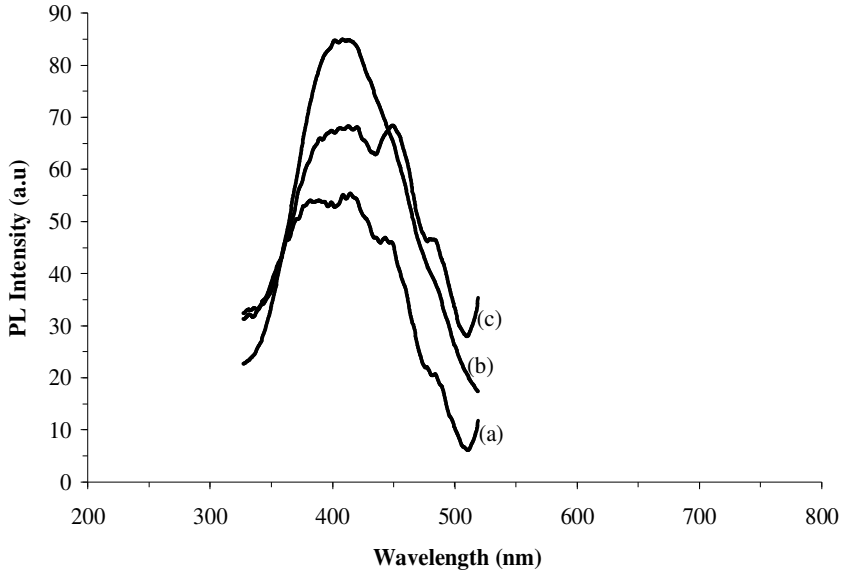

Figure 3.6 Photoluminescence spectra of cysteine-capped CdTe nanoparticles from $CdCl_2$ at (a) pH 4 (b) pH 7 and (c) pH 11.

3.3.2.2 *Effect of pH on cysteine-capped CdTe nanoparticles: Structural properties*

The TEM images of the cysteine-capped CdTe particles at different pH under 3 h of reflux are shown in Figure 3.7. The images confirm the extent of ionization and

complexation of the thiol groups on the surface of the nanoparticles. At pH 4 (Figure 3.7a), the TEM image of the material shows monodispersed, spherical particles of CdTe within the matrix of the capping agent. There is some degree of assembly within the matrix, however particle size estimation is difficult. A similar pattern is observed for the particles synthesized at pH 7 whereby particles are assembled within the matrix of the capping group (Figure 3.7b). This is probably due to the high ionization and low degree of complexation at this pH. The image confirms that the particles are small, spherical and appear monodispersed. At pH 11 the TEM image shows small, close to spherical particles that are joined together in a well ordered pattern (Figure 3.7c). The network pattern observed in all samples can be attributed to the Cd-thiolate end-to-end linkage as a result of complexation of the thiol groups on the surface of the nanoparticles. Such metal-thiolate end-to-end linkages have been reported for the interaction between metals and cysteine [49-51]. A typical representative HRTEM image of the cysteine-capped CdTe nanoparticles prepared at pH 7 is shown in Figure 3.7d. The existence of lattice planes in the HRTEM image confirms the crystallinity of the CdTe nanoparticles. The lattice fringe is observed with the lattice spacing of 3.60 Å confirming the (100) plane of hexagonal CdTe. The HRTEM image shows a particle which is imperfectly aligned with dislocations and stacking faults in the lattice visible.

The XRD pattern of the cysteine-capped CdTe nanoparticles, synthesized at pH 7 is shown in Figure 3.8. Seven distinct diffraction peaks at 2θ values of 25.4^{o}, 27.0^{o}, 28.6^{o}, 37.4^{o}, 44.3^{o}, 48.5^{o} and 52.5^{o}, are observed corresponding to the respective (100), (002), (101), (102), (110), (103) and (112) diffraction planes of hexagonal CdTe (JCPDS card no. 19-0193). The high intensity of (002) peak indicates that the

nanocrystals are elongated along the c-axis and the particles contain a large number of (002) planes, thus making that peak the dominant reflection in the first diffraction feature. This is in contrast to previous reports of CdTe nanoparticles via the aqueous method, where it yielded the cubic-zinc blende phase [32,52,53-56]. The hexagonal phase is usually obtained under the high-temperature organometallic route [57,58].

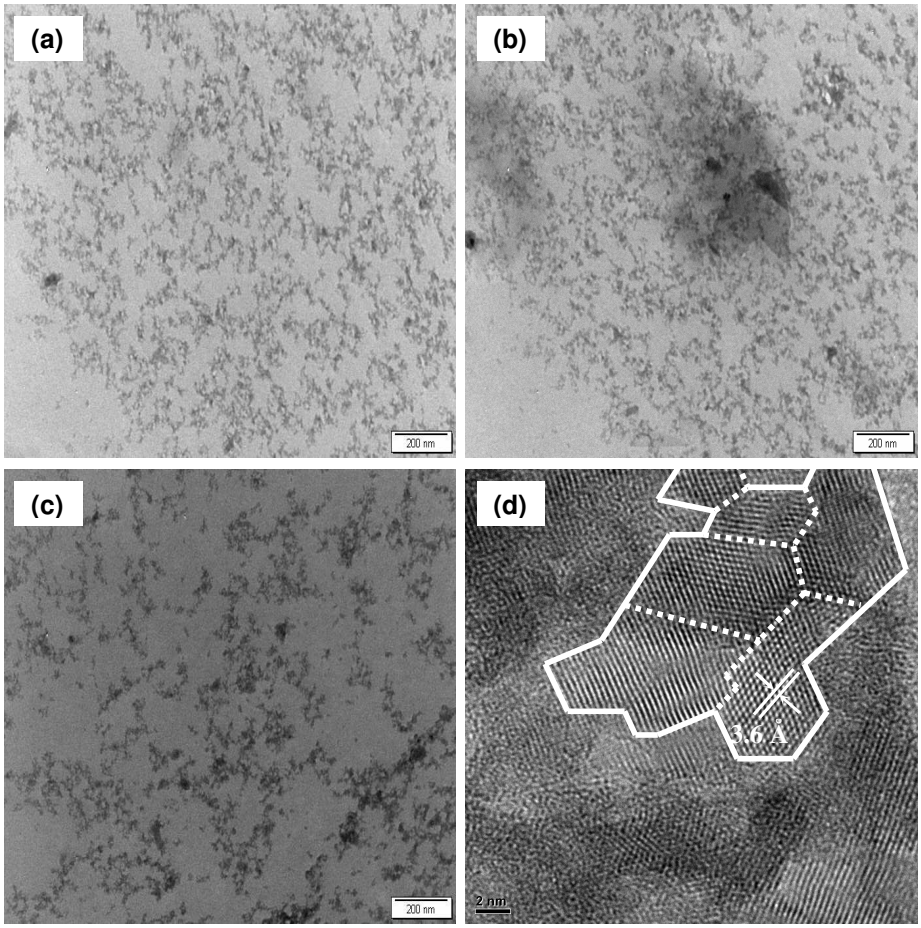

Figure 3.7 TEM images of cysteine-capped CdTe nanoparticles from $CdCl_2$ at (a) pH 4, (b) pH 7, (c) pH 11 and (d) corresponding HRTEM image of particles prepared at pH 7.

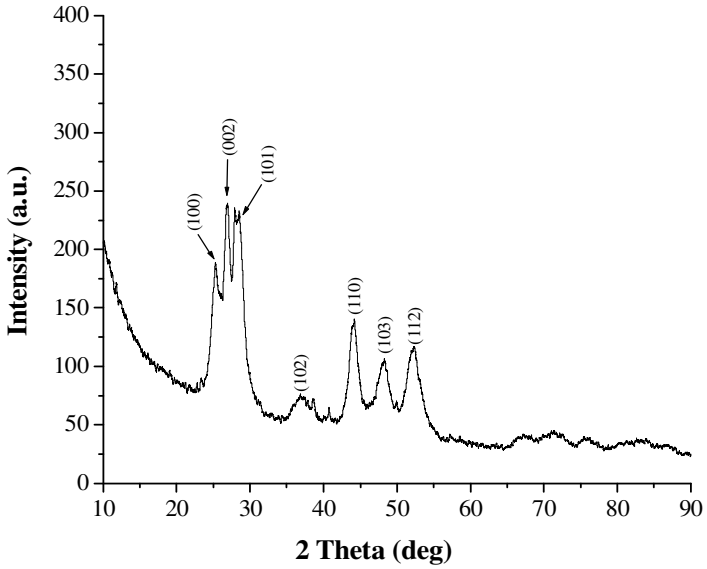

Figure 3.8 XRD pattern of cysteine-capped CdTe nanoparticles from $CdCl_2$ at pH 7.

The FT-IR of the L-cysteine ethyl ester hydrochloride and the cysteine-capped CdTe nanoparticles are shown in Figure 3.9 (a) and (b), respectively. Generally, amino acids exist as zwitterions (internal salts) and exhibit spectra characteristic of both the carboxylate and primary amine salt. They show a NH_3^+ stretch (very broad), N-H bend (asymmetric/symmetric) as characteristic vibrations [59]. The amino acid cysteine is water soluble and would readily bind to the surface of CdTe via the thiolate linkage. On comparison of the two spectra, the most significant observation is the bands at 2471 and 950 cm^{-1} corresponding to the S-H stretching and bending mode which are sharp and long for the free cysteine molecule, but are broad and small in the spectrum for cysteine-capped CdTe particles. This provides strong evidence for the surface binding of cysteine to CdTe particles via a Cd-S linkage. This may be attributed to the cleavage of most S-H bonds and the formation of a new S-Cd bond of the Cd-thiolate complex on the nanoparticle surface. It can also be observed that the bands at 1743 and 1223 cm^{-1} of cysteine which corresponds to the COO^- asymmetric

and symmetric stretch, a band at 1473 cm^{-1} corresponding to N-H asymmetric bend are shifted to slightly lower wave numbers, whereas the very broad band of NH_3^+ stretch observed in the 2735-3200 cm^{-1} is shifted slightly to higher wavenumber in the cysteine passivated CdTe nanoparticles. The shift in the COO^- and NH_3^+ stretching position is probably due to a change in the dipole moment when cysteine binds on the metal surface with a high electron density [51]. These observations confirm the capping of nanoparticles surface by cysteine i.e. the ester has been hydrolyzed during the reaction to produce the parent amino acid, which coordinates to the CdTe via the thiolate group [34].

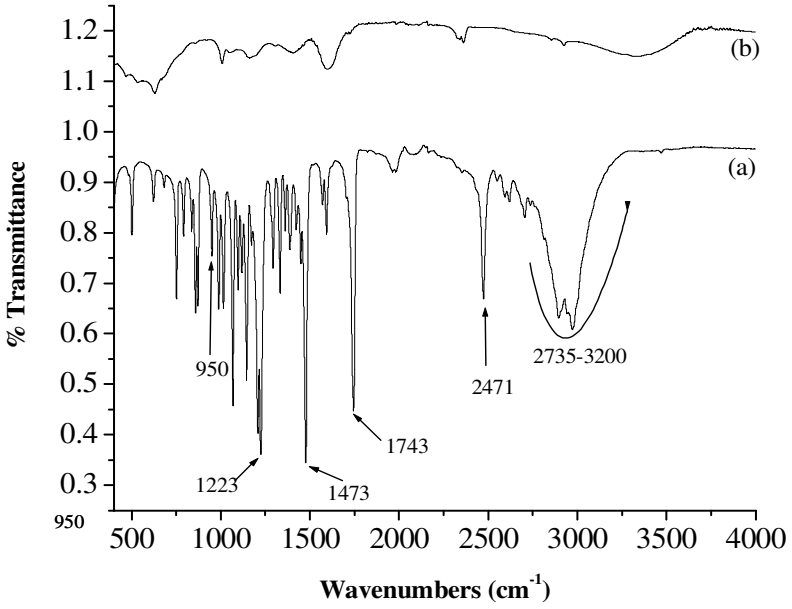

Figure 3.9 FT-IR spectra of (a) L-cysteine ethyl ester hydrochloride and (b) CdTe capped with cysteine from $CdCl_2$ at pH 7.

3.3.2.3 *Effect of pH on TEA-capped CdTe nanoparticles: Optical properties*

The temporal evolution of the absorption and PL spectra of an aqueous solution of TEA-capped CdTe prepared after 3 h reflux time under different pH is shown in Figures 3.10 and 3.11, respectively. The distinct absorption peak at 255 nm for the samples at all the pH values suggests the formation of the Cd^{2+}-TEA complex. There are some low intensity absorption peaks at higher wavelengths which can be attributed to the absorption by the TEA-capped CdTe nanoparticles. The PL spectra of the samples display emission maxima at 411 nm (pH 4), 406 nm (pH 7) and 408 nm (pH 11) with FWHM values of 89, 88, 90 nm, respectively. The high luminescence intensity, narrow emission line widths and sharp luminescence as pH increases, indicates the growth of crystallites with few electronic defects [60]. This signifies the efficiency of the capping group as the pH increases in electronically passivating the surface states or defects present in the band gap of the nanocrystals, which acts as trapping states for photogenerated charges [61-63].

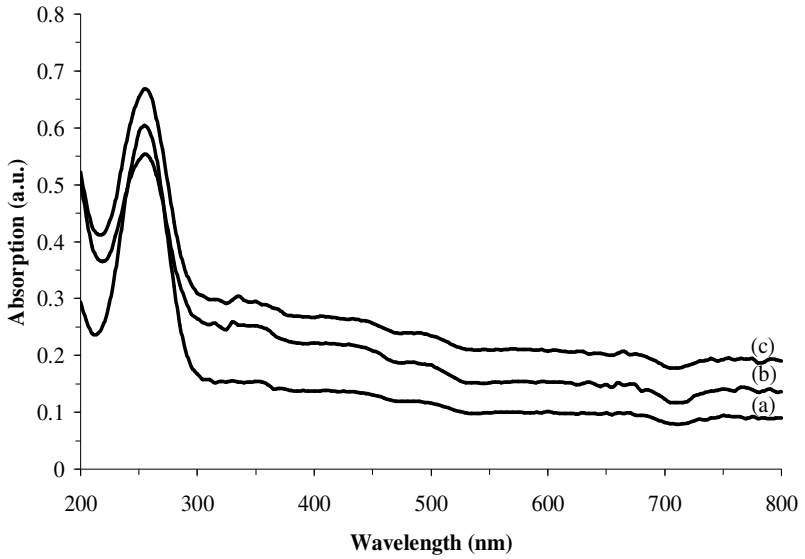

Figure 3.10 Absorption spectra of TEA-capped CdTe nanoparticles from $CdCl_2$ at (a) pH 4, (b) pH 7 and (c) pH 11.

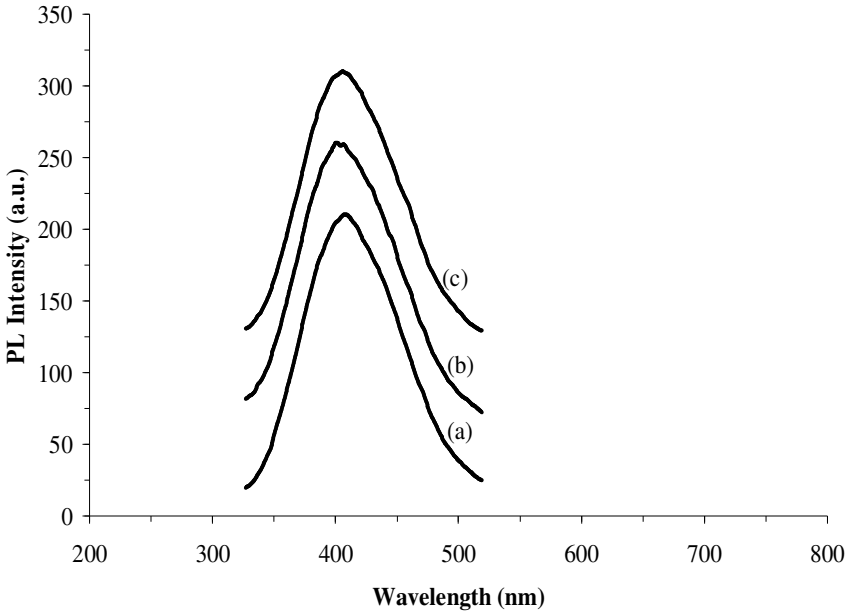

Figure 3.11 Photoluminescence spectra of TEA-capped CdTe nanoparticles from $CdCl_2$ at (a) pH 4, (b) pH 7 and (c) pH 11.

3.3.2.4 *Effect of pH on TEA-capped CdTe nanoparticles: Structural properties*

The typical representative TEM images of TEA-capped CdTe nanoparticles are shown in Figure 3.12. At pH 4 (Figure 3.12a), the TEM image shows close to spherical particles joined together forming a chain. The corresponding high resolution TEM image shows a well defined single particle with a size of 8.27 nm (Figure 3.12b). Distinct lattice fringes are observed with the lattice spacing of 3.3 Å confirming the (100) plane of hexagonal CdTe. At pH 7 (Figure 3.12c), the TEM image shows the presence of small, monodispersed, spherical particles with particle sizes of (3.70 ± 0.60 nm). The TEM image of the particles synthesized at pH 11 (Figure 3.12d) shows small spherical particles spaciously distributed with minimal aggregation. The average particle size is (4.05 ± 0.96 nm).

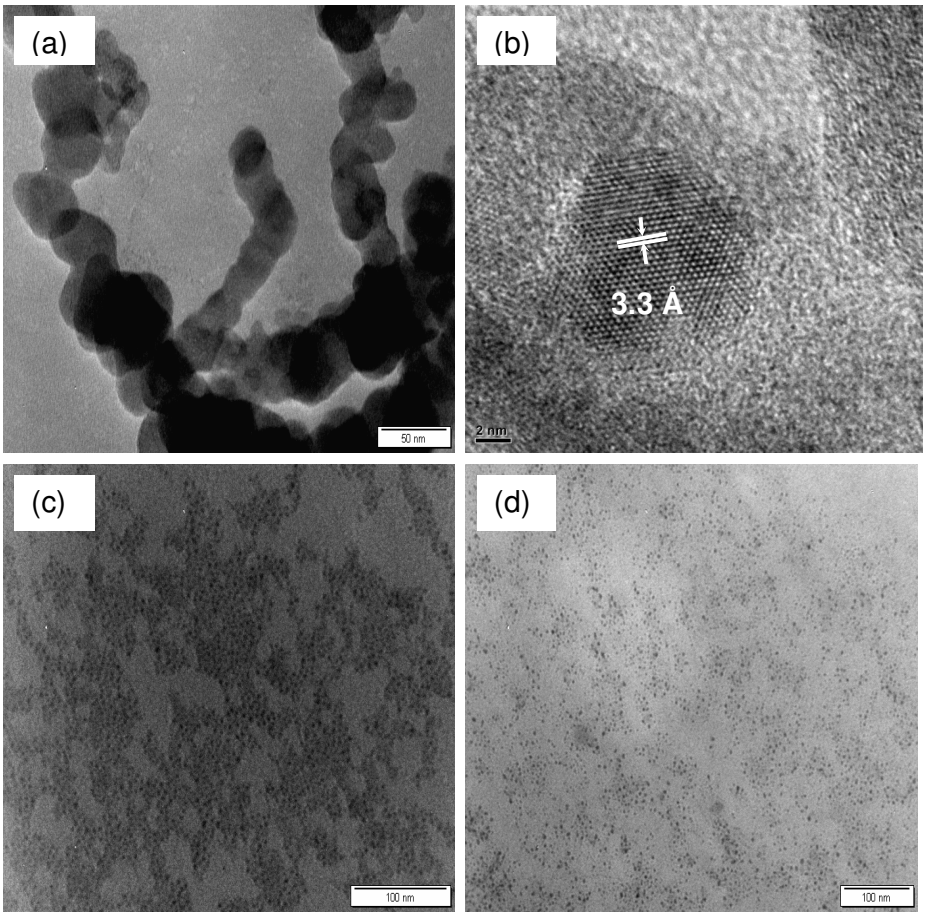

Figure 3.12 TEM images of TEA-capped CdTe nanoparticles from $CdCl_2$ at (a) pH 4, (b) corresponding HRTEM image; (c) pH 7 and (d) pH 11.

The XRD pattern (Figure 3.13) of the TEA-capped CdTe nanoparticles grown at pH 7 can be indexed to the cubic zinc-blende CdTe structure. The distinct diffraction peaks at 2θ values of 23.2°, 27.7°, 38.4°, 46.2°, 49.9°, 57.1°, 62.9° and 72.3° correspond to the respective (111), (200), (220), (311), (222), (400), (331) and (442) diffraction planes of CdTe (JCPDS card no. 15-0770). Other additional reflection peaks were observed which indicate the presence of impurities.

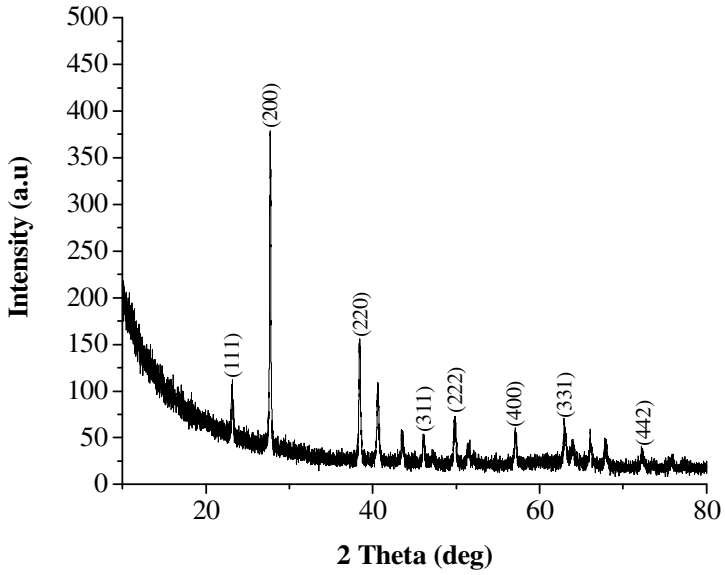

Figure 3.13 XRD pattern of TEA-capped CdTe nanoparticles from $CdCl_2$ at pH 7.

The formation of TEA-capped CdTe nanoparticles was further investigated by FT-IR. As shown in Figure 3.14, the strong band at 2995-3606 cm^{-1} (O-H group vibration) and those at 1026 and 1045 cm^{-1} (C-O group vibration) in Figure 3.14a are observed. The bands at 2988-3658 cm^{-1} (O-H group vibration), 1028 and 1070 cm^{-1} are shifted to high wave numbers from their corresponding band of the free TEA ligand (Figure 3.14b). It is inferred from the present results that the nitrogen atom of TEA coordinates with the Cd^{2+} ion on the CdTe QD surface, and the hydrophilic hydroxyl groups face outward and render CdTe QDs water-soluble [64].

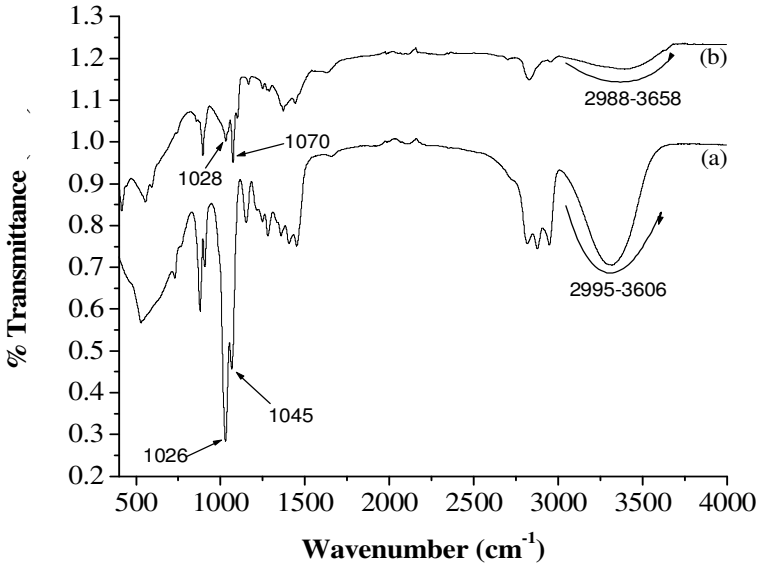

Figure 3.14 FT-IR spectra of (a) triethanolamine (TEA) and (b) TEA-capped CdTe nanoparticles from $CdCl_2$ at pH 7.

3.3.3 *Effect of reaction time*

As the reaction proceeds, the size and the corresponding PL emission of the CdTe nanoparticles are controlled by the duration of reflux, which can be observed in the absorption, PL spectra and TEM images. The following reactions were carried out using cadmium chloride ($CdCl_2$) as the cadmium source at pH 7 as the reaction time is varied from 5 min to 24 h.

3.3.3.1 *Effect of reaction time on cysteine-capped CdTe nanoparticles: Optical properties*

The absorption and photoluminescence spectra of the seven cysteine-capped CdTe dispersions with different reflux time were measured and are shown in Figure 3.15 and 3.16, respectively. The absorption maxima attributed to Cd^{2+}-cysteine complex are observed at 266 nm (5 min), 266 nm (15 min), 265 nm (30 min), 265 nm (1 h),

264 nm (3 h), 264 nm (5 h) and 266 nm (24 h). The following samples show strong absorption due to the CdTe nanoparticles at 428 nm (15 min), 432 nm (30 min), 444 nm (1 h), 455 nm (3 h), 467 nm (5 h) and 481 nm (24 h) with absorption band edges at 545, 558, 604, 606, 659 and 677 nm respectively.

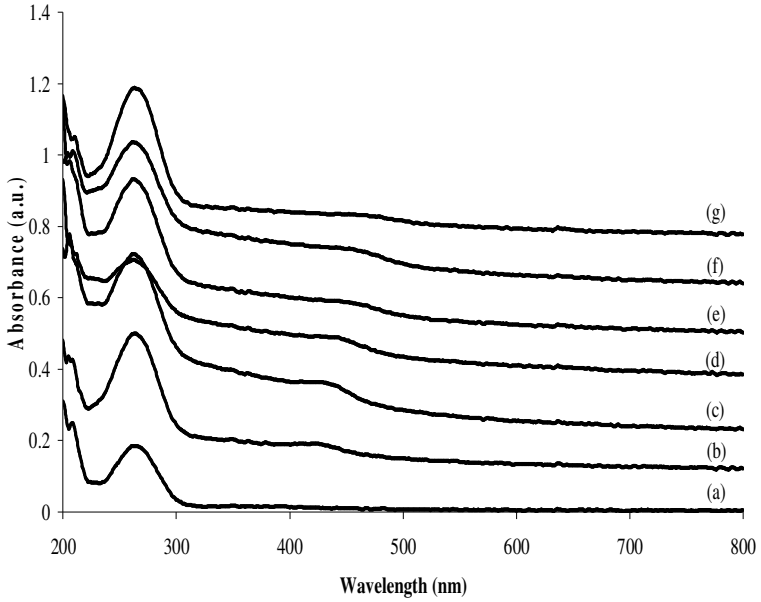

Figure 3.15 Absorption spectra of cysteine-capped CdTe nanoparticles from $CdCl_2$ at pH 7 with different reaction times: (a) 5, (b) 15, (c) 30, (d) 60, (e) 180, (f) 300, and (g) 1440 min.

The cysteine-capped CdTe nanoparticles also show reaction time dependent photoluminescence (Figure 3.16). The emission maxima for samples a-g (5 min-24 h) are 410, 417, 415, 413, 411, 409 and 413 nm, respectively. Clearly, the emission wavelength did not show any trend with the increase of the reaction time. The relatively broad emission spectra has also been reported previously for cysteine-capped nanoparticles [41,50]. The broad emission could be attributed to recombination from the surface defects.

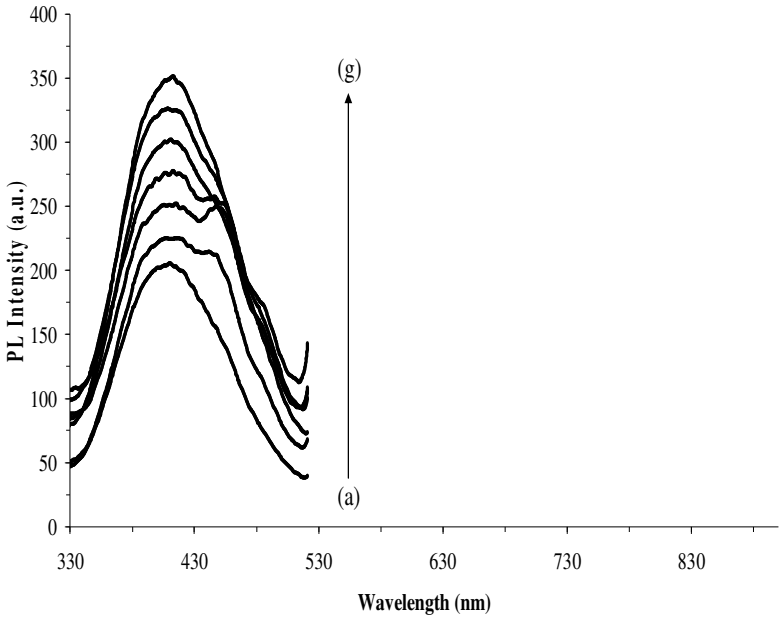

Figure 3.16 Photoluminescence spectra of cysteine-capped CdTe nanoparticles from $CdCl_2$ at pH 7 with different reaction time: (a) 5, (b) 15, (c) 30, (d) 60, (e) 180, (f) 300 and (g) 1440 min.

3.3.3.2 *Effect of reaction time on cysteine-capped CdTe particles: Structural properties*

The TEM images of cysteine-capped CdTe nanoparticles obtained by reflux for 30 min and 24 h are shown in Figure 3.17 (a) and (b), respectively. Figure 3.17(a) displays that the CdTe nanocrystals with 30 min reflux appear spherical. These spherical particles were found to have an average diameter of (3.68 ± 0.96) nm. The TEM image in Figure 3.17b of CdTe nanoparticles with 24 h reflux shows the sample containing spherical particles and some degree of aggregation. The average size of the particles is (9.37 ± 1.09) nm which is much higher than the 30 min sample size, an indication of growth.

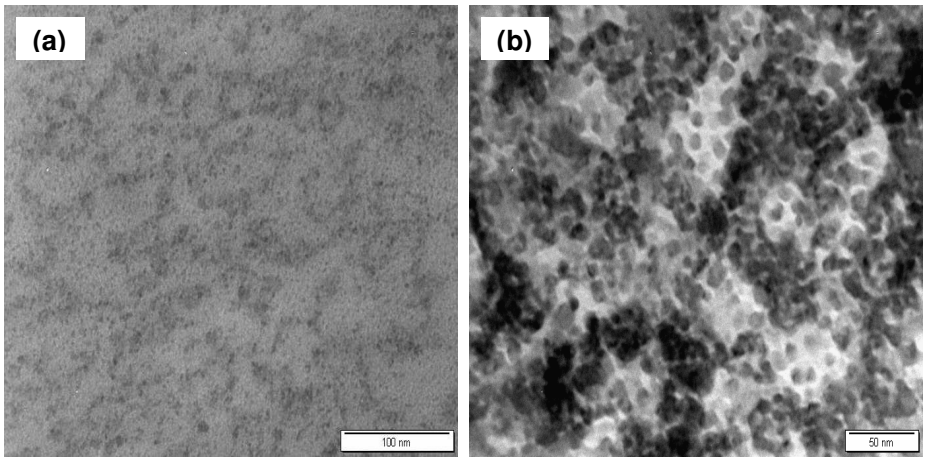

Figure 3.17 TEM images of cysteine-capped CdTe nanoparticles from $CdCl_2$ at pH 7 (a) 30 min and (b) 24 h.

Figure 3.18a and 3.18b are the typical HRTEM images of cysteine-capped CdTe nanocrystals obtained after 30 min and 24 h reflux time, respectively. The CdTe particles were found to be spherical and aggregated. The HRTEM images of the sample show clearly defined lattice fringes indicating the distinct crystalline nature of the CdTe particles. The lattice spacing of approximately 3.70 Å correspond with the (100) plane of the hexagonal phase of CdTe.

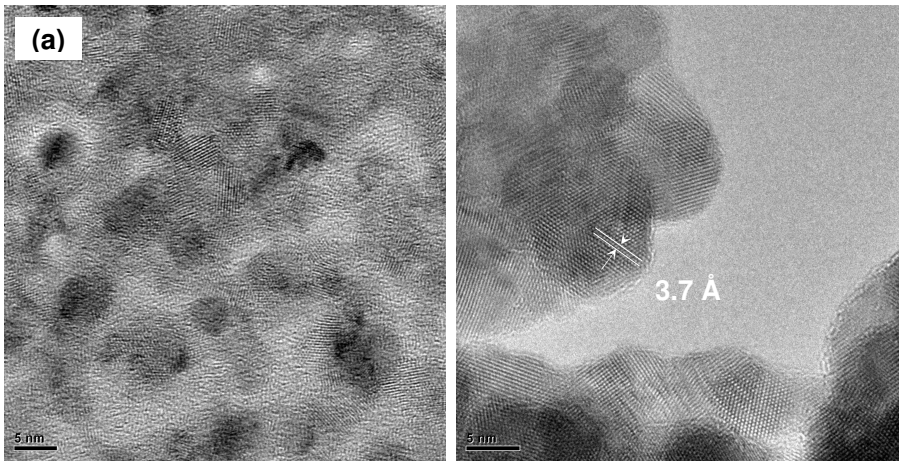

Figure 3.18 HRTEM images of cysteine-capped CdTe nanoparticles from $CdCl_2$ at pH 7 (a) 30 min and (b) 24 h.

3.3.3.3 *Effect of reaction time on TEA-capped CdTe nanoparticles: Optical properties*

The absorption spectra of the TEA-capped CdTe nanocrystals synthesized after 15 min, 5 h and 24 h reaction time are shown in Figure 3.19. Sharp absorption maxima of Cd-TEA complex are observed at 266, 267 and 267 nm for 15, 5 and 24 h samples, respectively. The several low intensity absorption peaks observed at higher wavelengths can be attributed to the absorption by the TEA-capped CdTe nanoparticles. The low intensity of these peaks makes the calculation of the band edge very difficult.

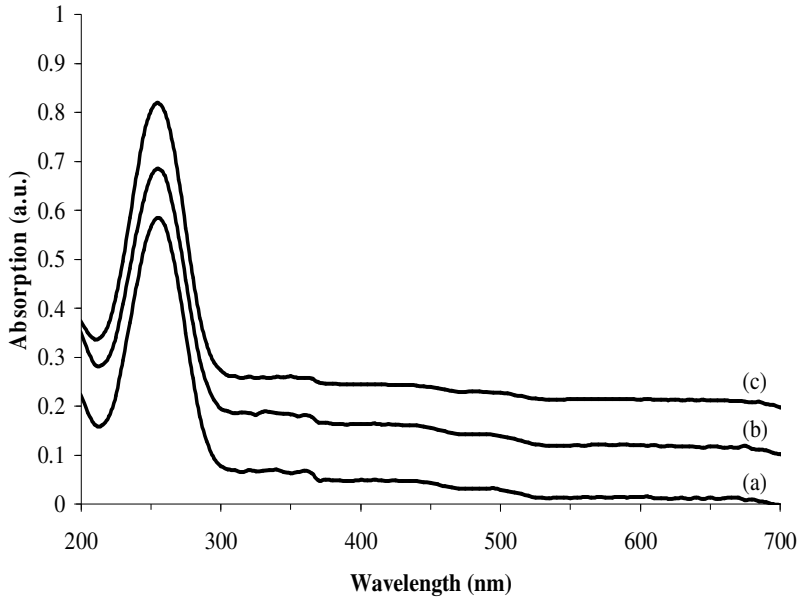

Figure 3.19 Absorption spectra of TEA-capped CdTe nanoparticles from $CdCl_2$ at pH 7 with different reaction time (a) 15 min (b) 5 h and (c) 24 h.

The PL spectra for the 15 min, 5 h and 24 h sample (excitation wavelength = 275 nm) are shown in Figure 3.20. The emission spectra of the samples show narrow band at 406, 401 and 408 nm for 15 min, 5 h and 24 h, respectively. The presence of the

emission bands close to the absorption maxima suggest that the emission can be attributed to band-edge luminescence [65]. Clearly, the emission wavelength is constant with the increase in reaction time, which is in agreement with the absorption results.

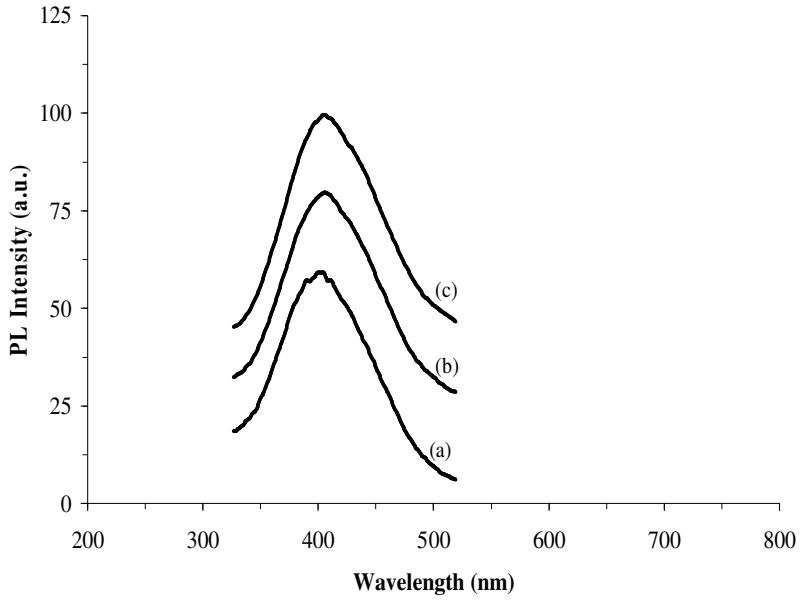

Figure 3.20 Photoluminescence spectra of TEA-capped CdTe nanoparticles from $CdCl_2$ at pH 7; with varying reflux times (a) 15 min, (b) 5 h and (c) 24 h.

3.3.3.4 *Effect of reaction time on TEA-capped CdTe nanoparticles: Structural properties*

Figure 3.21 shows the TEM and HRTEM images of TEA-capped CdTe nanoparticles with varying reflux times. The TEM image of TEA-capped CdTe particles after 15 min reflux is shown in Figure 3.21a, where the as-prepared CdTe nanocrystals appear as quasi-spherical particles with an average diameter of (3.18 ± 0.55) nm. There is no evidence for the presence of elongated particles. When the reflux time is increased to 5 h, the shape of the particles is maintained with an increase in particle size to 4.29 ± 0.65 (Figure 3.21b). When the reflux time was increased further to 24 h, the

nanocrystals appear as spherical and well dispersed within the matrix of the TEA capping agent and the particle size is increased further to (5.30 ± 0.93) nm (Figure 3.21c). The corresponding HRTEM image (Figure 3.21d) reveals the clearly observed lattice planes confirming the crystallinity of the CdTe nanoparticles. The lattice spacing of approximately 3.80 Å correspond with the (100) plane of the hexagonal phase of CdTe [66].

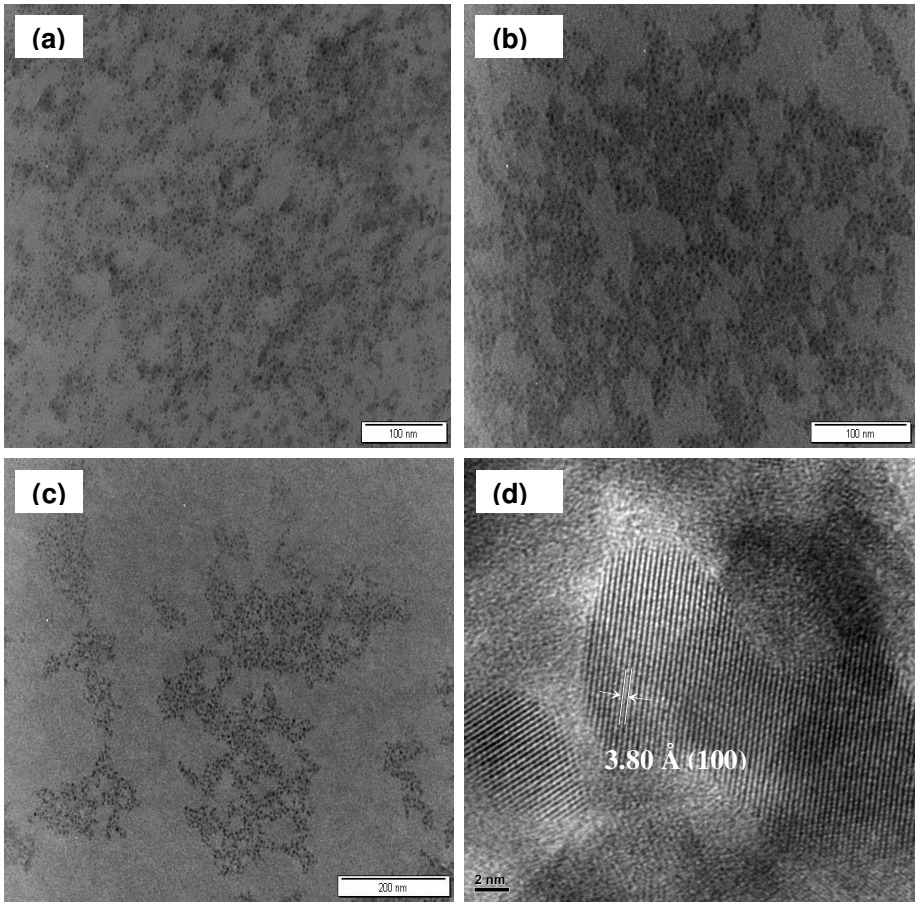

Figure 3.21 TEM images of TEA-capped CdTe nanoparticles from $CdCl_2$ at pH 7; (a) 15 min, (b) 5 h, (c) 24 h and (d) the corresponding HRTEM of 24 h sample.

3.3.4 *Effect of varying the Cd-source*

The four different cadmium sources, cadmium chloride ($CdCl_2$), cadmium acetate [$Cd(CH_3COO)_2$], cadmium nitrate [$Cd(NO_3)_2$] and cadmium carbonate ($CdCO_3$), were used to investigate the effect of metal source on the properties of the water soluble CdTe nanoparticles. All the reactions were carried out at pH 7 after 3 h reaction time.

3.3.4.1 *Effect of Cd-source on cysteine-capped CdTe nanoparticles: Optical properties*

The absorption spectra for the cysteine-capped CdTe nanoparticles from different cadmium sources are shown in Figure 3.22. The cysteine-capped CdTe nanoparticles exhibit a band edge at 552 nm ($Cd(CH_3COO)_2$) and 542 nm ($CdCO_3$) of a distinct excitonic peaks at 469 nm and 461 nm, respectively. The absorption maxima shown at 264 ($Cd(CH_3COO)_2$), 267 ($CdCl_2$), 265 ($CdCO_3$) and 267 nm ($CdCO_3$) are attributed to the Cd-cysteine complex. The absence of excitonic peak corresponding to the CdTe nanoparticles in the $CdCl_2$ and $Cd(NO_3)_2$ samples indicate polydisperity of the nanoparticles. The PL spectra (Figure 3.23) showed narrow emission curves with the maxima at 413 [$Cd(CH_3COO)_2$], 411 ($CdCl_2$), 416 ($CdCO_3$) and 417 nm [$Cd(NO_3)_2$] (Figure 3.22).

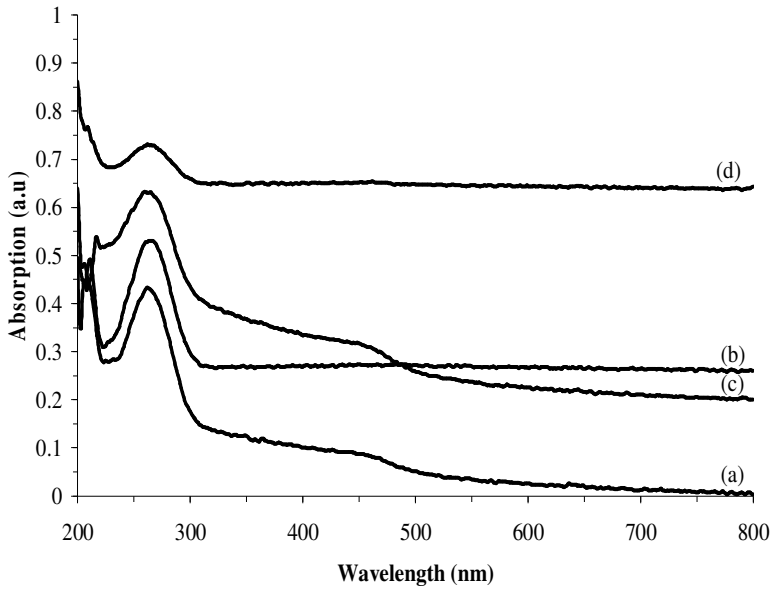

Figure 3.22 Absorption spectra of cysteine-capped CdTe nanoparticles at pH 7 from different cadmium precursors; (a) $Cd(CH_3COO)_2$, (b) $CdCl_2$, (c) $CdCO_3$ and (d) $Cd(NO_3)_2$.

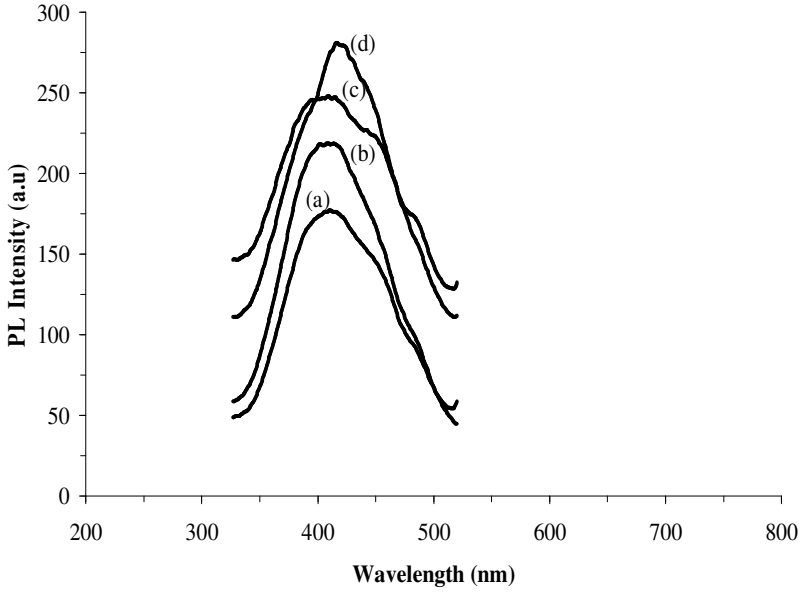

Figure 3.23 Photoluminescence spectra of cysteine-capped CdTe nanoparticles synthesized at pH 7 from different cadmium precursors; (a) $Cd(CH_3COO)_2$, (b) $CdCl_2$, (c) $CdCO_3$ and (d) $Cd(NO_3)_2$.

3.3.4.2 *Effect of Cd-source on cysteine-capped CdTe nanoparticles: Structural properties*

The TEM images of $CdCl_2$ (Figure 3.24b) and $Cd(NO_3)_2$ (Figure 3.24d) shows that the particles are spherical in shape. The average particle size of $CdCl_2$ and $Cd(NO_3)_2$, estimated from TEM images, are (2.83 ± 0.58) nm and (3.11 ± 0.66) nm, respectively. In the case of $Cd(CH_3COO)_2$ and $CdCO_3$, the TEM images of the material shows spherical particles within the matrix of the cysteine capping agent. Particle size estimation was difficult, due to apparent aggregation within the capping matrix.

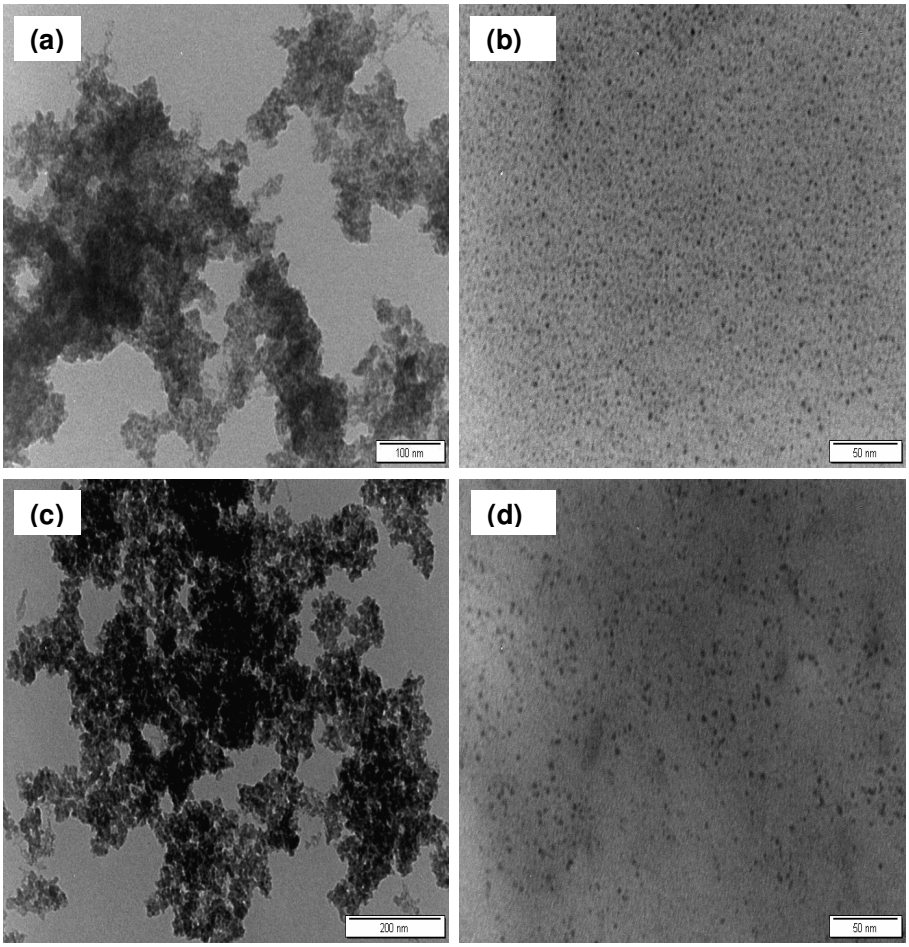

Figure 3.24 TEM images of cysteine-capped CdTe nanoparticles synthesized at pH 7 after 3 h from different cadmium precursors; (a) $Cd(CH_3COO)_2$, (b) $CdCl_2$, (c) $CdCO_3$ and (d) $Cd(NO_3)_2$

The HRTEM images of $CdCO_3$ (Figure 3.25a) and $Cd(NO_3)_2$ (Figure 3.25b) revealed the formation of crystalline CdTe. The lattice spacings are approximately 3.63 Å corresponds with the (100) plane of the hexagonal phase of CdTe (JCPDS card no. 19-0193).

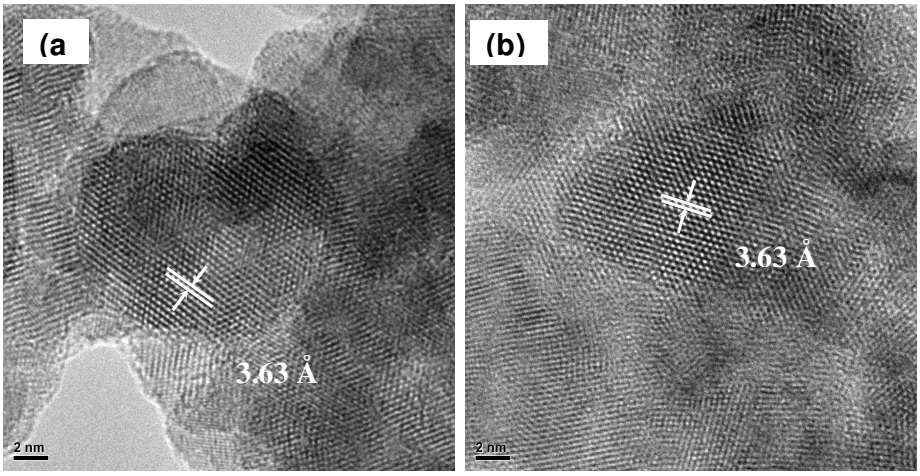

Figure 3.25 HRTEM images of cysteine-capped CdTe nanoparticles synthesized at pH 7 after 3 h from different cadmium precursors; (a) $CdCO_3$ and (d) $Cd(NO_3)_2$.

3.3.4.3 *Effect of Cd-source on TEA-capped CdTe particles: Optical properties*

The TEA-capped CdTe nanoparticles prepared displayed absorption maxima at 255 ($CdCl_2$), 267 ($CdCO_3$), 266 ($Cd(NO_3)_2$) and 265 nm ($Cd(CH_3COO)_2$) (Figure 3.26). The absorption maximum of the samples prepared using different cadmium sources are from Cd-TEA complex. There are no well defined absorption peaks due to the CdTe nanoparticles. The emission spectra (Figure 3.27) displayed peaks at 403 ($CdCl_2$), 410 ($CdCO_3$), 415 ($Cd(NO_3)_2$) and 417 nm ($Cd(CH_3COO)_2$). The spectra showed narrow emission peaks, implying that the particle size distribution is narrow.

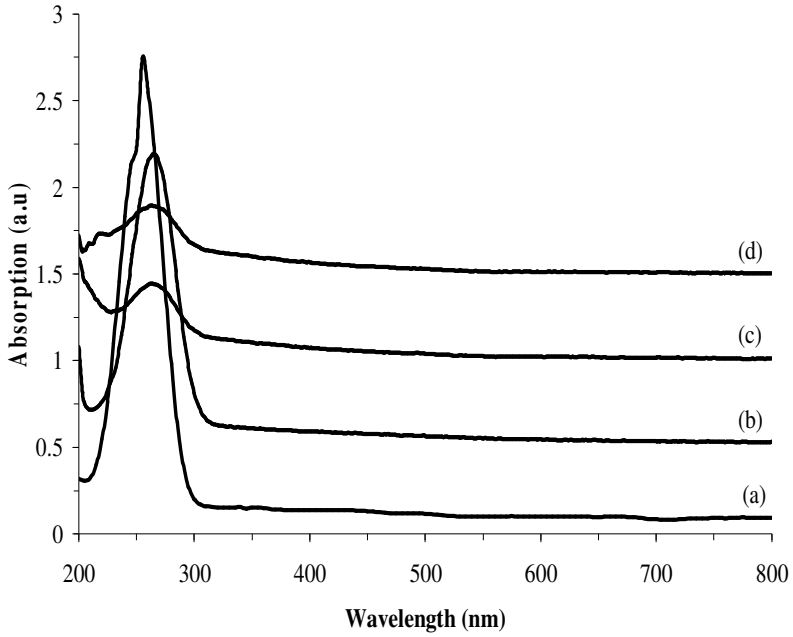

Figure 3.26 Absorption spectra of TEA-capped CdTe nanoparticles synthesized at pH 7 from different cadmium precursors; (a) $CdCl_2$, (b) $CdCO_3$, (c) $Cd(NO_3)_2$ and (d) $Cd(CH_3COO)_2$.

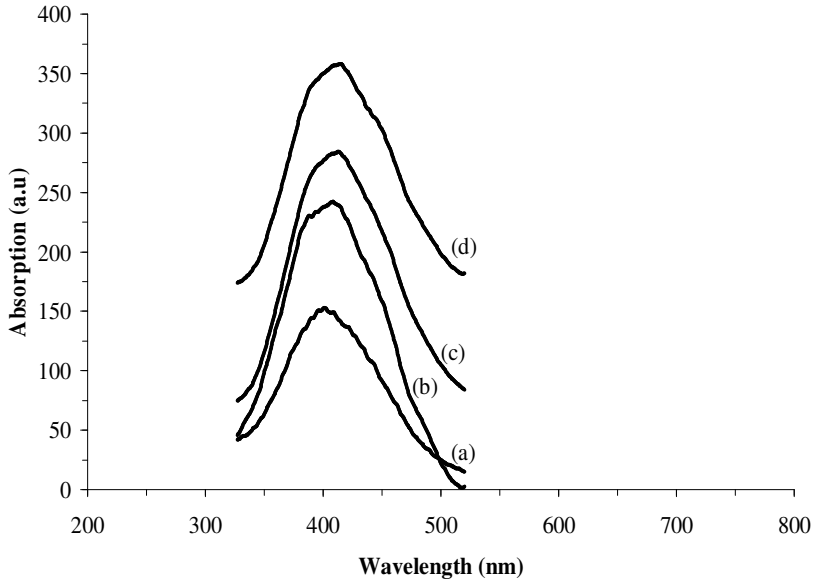

Figure 3.27 Photoluminescence spectra of TEA-capped CdTe nanoparticles synthesized at pH 7 from different cadmium precursors; (a) $CdCl_2$, (b) $CdCO_3$, (c) $Cd(NO_3)_2$ and (d) $Cd(CH_3COO)_2$.

3.3.4.4 *Effect of Cd-source on TEA-capped CdTe particles: Structural properites*

Figure 3.28 show the TEM images of TEA-capped CdTe nanoparticles synthesized from $CdCl_2$, $CdCO_3$, $Cd(NO_3)_2$ and $Cd(CH_3COO)_2$ as cadmium sources. The CdTe nanoparticles synthesized using $CdCl_2$, $Cd(NO_3)_2$ and $Cd(CH_3COO)_2$ were spherical with average particle sizes of (2.61 ± 0.58) nm, (3.26 ± 0.41) nm and (4.10 ± 0.81) nm respectively. However when $CdCO_3$ was used, spherical particles within the matrix of the capping agent were obtained.

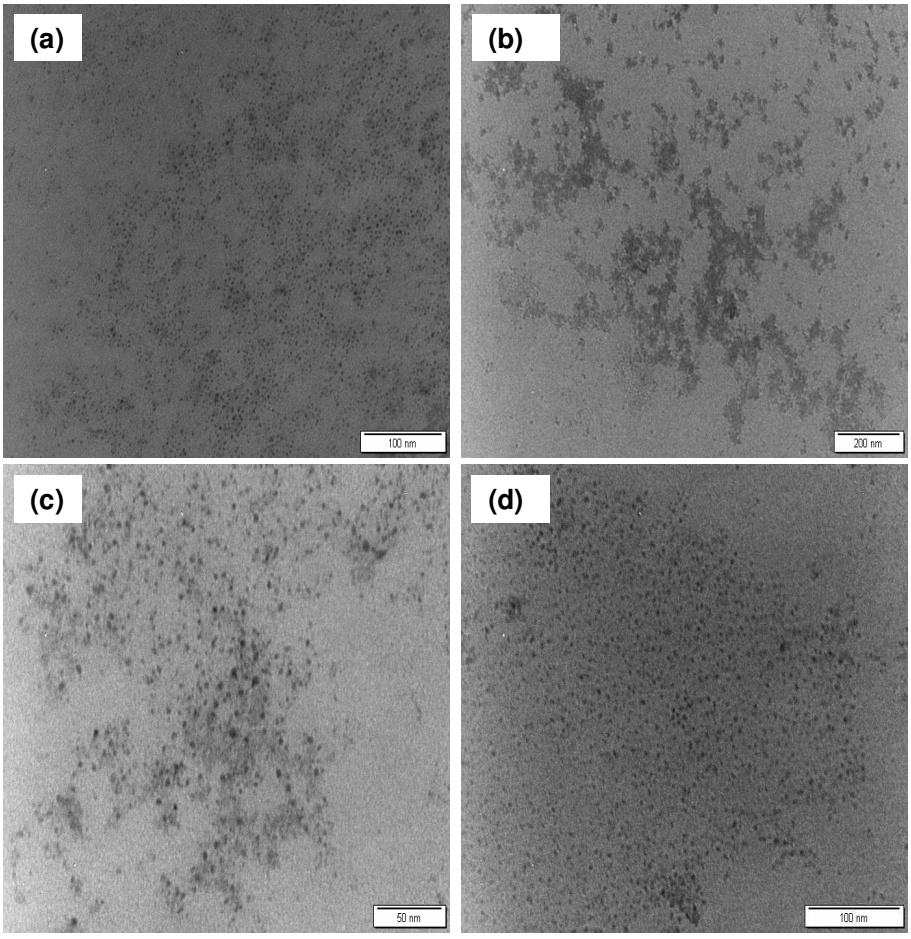

Figure 3.28 TEM images of TEA-capped CdTe nanoparticles synthesized at pH 7 from different cadmium precursors (a) $CdCl_2$, (b) $CdCO_3$, (c) $Cd(NO_3)_2$ and (d) $Cd(CH_3COO)_2$.

The HRTEM image of $Cd(NO_3)_2$ (Figure 3.29) shows the existence of well-resolved lattice planes showing that the TEA-capped CdTe nanoparticle possesses a highly crystalline structure. The interplanar distance is about 3.60 Å, which correspond to the (100) plane of hexagonal CdTe (JCPDS card no. 19-0193).

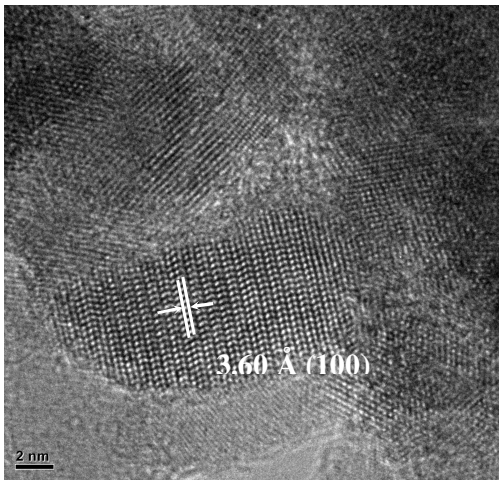

Figure 3.29 HRTEM image of TEA-capped CdTe nanoparticles synthesized at pH 7 from $Cd(NO_3)_2$.

3.4 *Conclusions*

Cysteine and triethanolamine-capped CdTe nanoparticles have been prepared via a facile solution-based method. A systematic study of the effect of reaction parameters such as capping agent, pH, reaction time and cadmium source on dispersibility, size, optical properties and morphology of the nanoparticles was investigated. The results of the effect of varying capping ligand showed that cysteine is more effective as a capping ligand as compared to TEA. The absorption spectra of TEA-capped CdTe nanoparticles have numerous absorption peaks at higher wavelength as compared to the cysteine-capped CdTe particles with only one peak at higher wavelength. Both capping agents revealed close to spherical particles in their TEM images. The FTIR

measurements were used to confirm the presence of the capping ligand on the surface of CdTe nanoparticles.

The absorption and emission spectra of cysteine and TEA-capped CdTe particles reveal that complexation increases as pH increases from acidic to basic resulting in the formation of the nanoparticles. The TEM images of both cysteine and TEA nanoparticles revealed spherical, monodispersed particles joined in a network pattern. The HRTEM and powder XRD results confirm that the particles are crystalline and in the nanosize regime with the predominance of the hexagonal and zinc blende phase for the cysteine and TEA-capped CdTe nanoparticles respectively. Varying the cadmium sources for both capping groups produced no observable changes to the morphology or optical properties of the particles.

3.5 *References*

[1] A. P. Alivisatos, W. W. Gu, C. Larabell, *Annu. Rev. Biomed. Eng*., **7** (2005) 55-76.

[2] X. Michalet, F. F. Pinaud, L. A. Bentolila, J. M. Tsay, S. Doose, J. J. Li, *Science*, **307** (2005) 538-544.

[3] I. L. Medintz, H. T. Uyeda, E. R. Goldman, H. Mattoussi, *Nat. Mater*., **4** (2005) 435-446.

[4] Y. Wang, Z. Tang, N. A. Kotov, *Mater. Today*, **8** (2005) 20-31.

[5] A. R. Clapp, I. L. Medintz, H. Mattoussi, *Chem. Phys. Chem.*, **7** (2006) 45-57.

[6] B. Ballou, B. C. Lagerholm, L. A. Ernst, M. P. Bruchez, A. S. Waggoner, *Bioconjug. Chem*., **15** (2004) 79-86.

[7] B. Sun, W. Xie, G. Yi, D. Chen, Y. Zhou, J. Cheng, *J. Immunol. Methods*, **249** (2001) 85-89.

[8] A. C. S. Samia, X. Chen, C. Burda, *J. Am. Chem. Soc*., **125** (2003) 15736-15737.

[9] S. Pathak, S. K. Choi, N. Arnheim, M. E. Thompson, *J. Am. Chem. Soc*., **123** (2001) 4103-4104.

[10] X. Wu, H. Liu, J. Liu, K. N. Haley, J. A. Treadway, J. P. Larson, *Nat. Biotechnol*., **21** (2003) 41-46.

[11] H. Mattoussi, J. M. Mauro, E. R. Goldman, G. P. Anderson, V. C. Sundar, F. V. Mikulec, M. G. Bawendi, *J. Am. Chem. Soc*., **122** (2000) 12142-12150.

[12] J. Aldana, Y. A. Wang, X. Peng, *J. Am. Chem. Soc*., **123** (2001) 8844-8850.

[13] D. M. Willard, L. L. Carillo, J. Jung, A. V. Orden, *Nano Lett*., **1** (2001) 469-474.

[14] G. P. Mitchell, C. A. Mirkin, R. L. Letsinger, *J. Am. Chem. Soc*., **121** (1999) 8122-8123.

[15] D.V. Talapin, A. L. Rogach, I. Mekis, S. Haubold, A. Kornowski, M. Haase, H. Weller, *Colloids Surf*., **202** (2002) 145-154.

[16] D. V. Talapin, A. L. Rogach, E. V. Shevchenko, A. Kornowski, M. Haase, H. Weller, *J. Am. Chem. Soc*., **124** (2002) 5782-5790.

[17] N. Gaponik, D. V. Talapin, A. L. Rogach, K. Hoppe, E. V. Shevchenko, A. Kornowksi, A. Eychmuller, H. Weller, *J. Phys. Chem*., **106** (2002) 7177-7185.

[18] A. L. Rogach, A. Kornowksi, M. Y. Gao, A. Eychmuller, H, Weller, *J. Phys. Chem. B*, **103** (1999) 3065-3069.

[19] M. Gao, C. Lesser, S. Kirstein, H. Mohwald, A. L. Rogach, H. Weller, *J. Appl. Phys*., **87** (2000) 2297-2302.

[20] A. L. Rogach, N. A. Kotov, D. S. Koktysh, J. W. Ostrander, G. A. Ragoisha, *Chem. Mater*., **12** (2000) 2721-2726.

[21] I. L. Radtchenko, G. B. Sukhorukov, N. Gaponik, A. Kornowksi, A. L. Rogach, H. Mohwald, *Adv. Mater.*, **13** (2001) 1684-1687.

[22] N. N. Mamedova, N. A. Kotov, A. L. Rogach, J. Studer, *Nanoletters*, **1** (2001) 281-286.

[23] D. V. Talapin, S. K. Poznyak, N. P. Gaponik, A. L. Rogach, A. Eychmuller, *Phys. E*, **14** (2002) 237-241.

[24] A. L. Rogach, L. Katsikas, A. Kornowksi, D. Su, A. Eychmuller, H. Weller, *Ber. Bunsen-Ges. Phys. Chem.*, **100** (1996) 1772-1778.

[25] M. Y. Gao, S. Kirsten, H. Mohwald, A. L. Rogach, A. Kornowski, A. Eychmuller and H. Weller, *J. Phys. Chem. B*, **102** (1998) 8360-8363.

[26] H. Bao, Y. Gong, Z. Li, M. Y. Gao, *Chem. Mater.*, **16** (2004) 3853-3859.

[27] H. Zhang, Z. Zhou, B. Yang, M. Y. Gao, *J. Phys. Chem. B*, **107** (2003) 8-13.

[28] H. Zhang, D. Wang, B. Yang, H. Mohwald, *J. Am. Chem. Soc.*, **128** (2006) 10171-10180.

[29] K. Zhao, J. Li, H. Wang, J. Zhuang, W. Wang, *J. Phys. Chem. C.*, **111** (2007) 5618-5621.

[30] A. L. Rogach, T. Franzl, T. A. Klar, J. Feldmann, N. Gaponik, V. Lesnyak, A. Shavel, A. Eychmuller, Y. P. Rakovich, J. F. Donegan, *J. Phys. Chem. C*, **111** (2007) 14628-14637.

[31] L. Zou, Z. Gu, N. Zhang, Y. Zhang, Z. Fang, W. Zhu, X. Zhong, *J. Mater. Chem.*, **18** (2008) 2807-2815.

[32] M. S. Abd El-sadek, J. R. Kumar, S. M. Badu, *Curr. Appl. Phys.*, **10** (2010) 317-322.

[33] M. Li, H. Zhou, H. Zhang, P. Sun, K. Yi, M. Wang, Z. Dong, S. Xu, *J. Lumin.* (2010), in press.

[34] S. O. Oluwafemi, N. Revaprasadu, A. J. Ramirez, *J. Cryst. Growth*., **310** (2008) 3230-3234.

[35] V. S. R. Rajasekhar Pullabhotla, N. Revaprasadu, *Mat. Lett*., **63** (2009) 2097-2099.

[36] S. Sapra, J. Nanda, D. D. Sarma, F. Abed El-Al, G. Hodes, *Chem. Commun*. **21** (2001) 2188-2189.

[37] A. Chatterjee, A. Priyam, S. K. Das, A. Saha, *J. Coll. Interf. Sci*., **294** (2001) 334-342.

[38] S. O. Oluwafemi, N. Revaprasadu, O. O. Adeyemi, *Colloids. Surfaces. B: Biointerface*., **79** (2010) 126-130.

[39] N. Gaponik, D. V. Talapin, A. L. Rogach, K. Hoppe, E. V. Shevchenko, A. Kornowski, A. Eychmuller, H. Weller, *J. Phys. Chem. B*, **106** (2002) 7177-7185.

[40] A. Shavelv, N. Gaponik, A. Eychmuller, *J. Phys. Chem. B*, **110** (2006) 19280-19284.

[41] J. Guo, W. Yang, C. Wang, *J. Phys. Chem. B*, **109** (2005) 17467-17473.

[42] K. Yu, S. Singh, N. Patrito, V. Chu, *Langmuir*., **20** (2004) 11161-11168.

[43] A. K. Singh, V. Viswanath, V. C. Janu, *J. Lumin.*, **129** (2009) 874-878.

[44] http://en.wikipedia.org/wiki/Absorbance, 19-02-2011.

[45] T. Rajh, O. I. Micic, A. J. Nozik, *J. Phys. Chem.*, **97** (1993) 11999-12003.

[46] H. B. Burgi, *Chim, Acta*., **57** (1974) 513-519.

[47] D. Hayes, O. L. Micic, M. T. Nenadovic, V. Swayambunathan, D. Meisel, J. *Phys. Chem.*, **93** (1989) 4603-4608.

[48] V. Swayambunathan, D. Hayes, K. H. Schmidt, Y. X. Liao, D. Meisel, *J. Am. Chem. Soc*., **112** (1990) 3831-3837.

[49] A. Santosh, B. K. C. Remant, N. Dharmaraj, N. Bhattarai, C. H. Kim, H. Y. Kim, *Spectrochimica. Acta Part A*, **63** (2006) 160-163.

[50] X. Hu, W. Cheng, T. Wang, E. Wang, S. Dong, *Nanotechnology*, **16** (2005) 2164-2169.

[51] J. L. Burt, C. Gutierrez-Wing, M. Miki-Yoshida, M. Jose-Yacaman, *Langmuir*, **20** (2004) 11178.

[52] M. Green, H. Harwood, C. Barrowman, P. Rahman, A. Eggeman, F. Festry, P. Dobson, T. Ng, *J. Mater. Chem.*, **17** (2007) 1989-1994.

[53] E. Ying, D. Li, S. Guo, S. Dong, J. Wang, *PLoS One.*, **3** (2008), p. e2222.

[54] H. Jiang, J. Jia, *J. Mater. Chem*., **18** (2008) 344-349.

[55] Y. Liu, J. Yu, *J. Colloid. Interface*. Sci., **333** (2009) 690-698.

[56] T. Wang, Z. Jin, Y. Shi, W. Li, J. Yang, *Crystal. Growth. Design*., **9** (2009) 5077-5082.

[57] S. Kumar, T. Nann, Chem. Commun., **19** (2003) 2478-2479.

[58] D. Kim, H. D. Jang, E. J. Kim, K. Koo, *Ultramicroscopy*, **108** (2008) 1278-1282.

[59] D. L. Pavia, G. M. Lampman, G. S. Kriz, *Introsuction to spectroscopy*, 3rd ed., USA, 2001.

[60] G. Li, M. J. Nogami, *Appl. Phys*., **75** (1994) 4276-4278.

[61] A. P. Alivisatos, *Science*, **271** (1996) 933-937.

[62] C. D. Lokhande, P. S. Patil, H. Tributsch, A. Ennaousi, *Solar Energy Mater*., **55** (1998) 379-393.

[63] V. J. Leppert, S. H. Risbud, M. J. Fendorf, *Philos. Mag. Lett*., **75** (1997) 29-33.

[64] Z. B. Shang, Y. Wang, W. J. Jin, *Talanta*, **78** (2009) 364-369.

[65] M.S. Abd El-sadek, S.M. Babu, *Physica*, *B*, **405** (2010) 3279–3283.

[66] Z. Tang, N. A. Kotov, M. Giersig, *Science*, **297** (2002) 237-239

CHAPTER FOUR

SUMMARY AND FUTURE WORK

4.0 *Summary*

The dissertation describes the synthesis of organically and water soluble CdTe nanoparticles synthesized by a hybrid solution based high temperature route. This synthetic method is simple and environmentally benign. The quality of the nanoparticles obtained is as good as the best particles obtained by routes requiring the use of hazardous starting materials and sophisticated equipment. The study reveals that key reaction parameters such as the cadmium source play important roles in the final morphology of the particles. According to initial reports on the growth mechanism of nanoparticles, the Ostwald ripening process was thought to be the dominant growth mechanism of particles in solution. In this work we propose that the particles grow by two different mechanisms as determined by the cadmium source. The high resolution transmission electron microscopy study provides evidence for these two mechanisms of growth.

The second part of the study describes the synthesis of water soluble CdTe nanoparticles capped by cysteine and triethylamine (TEA). The CdTe nanoparticles obtained were crystalline and displayed good optical properties rendering effective in biological applications. Reaction parameters such as capping agent, pH, reaction time and cadmium source do play an important role in the properties and morphology of the particles.

4.1 *Recommendations for Future Work*

The route is an effective one for the synthesis of tellurium-based nanoparticles. Future work on this route could include:

- Synthesis of other tellurium based nanoparticles e.g ZnTe, AgTe, SnTe and PdTe
- A detailed investigation into the growth mechanism of the particles.
- Use of other organic ligands e.g decaylamine and other water soluble ligands e.g starch, polyvinyl acetate (PVA) as capping groups.
- The application of CdTe in solar cells and biological labelling.

Overall the study opens up many avenues for further research into tellurium based nanoparticles.

.

SYNTHESIS AND SHAPE CONTROL OF FUNCTINALIZED CADMIUM TELLURIDE NANOPARTICLES

2010

Nhlakanipho Mntungwa